Extragalactic Background Light inhomogeneities and Lorentz-Invariance-Violation in gamma-gamma absorption and Compton scattering

Hassan Abdalla Hassan Hamad

iD orcid.org 0000-0002-0455-3791

Thesis submitted in fulfilment of the requirements for the degree *Doctor of Philosophy in Space Physics* at the North-West University

Promoter: Prof M Boettcher

Graduation May 2019

26598973

Acknowledgements

Abstract

Very-high-energy gamma ray photons (VHE; $E > 100$ GeV) from distant gamma ray objects (e.g. blazars) are expected to be absorbed by the diffuse extragalactic background light (EBL), which leads to a high-energy cut-off in a blazar's spectral energy distribution (SED). But recent observations of cosmological gamma ray sources, after correction for the standard EBL absorption, have been interpreted by some authors that the Universe is more transparent to VHE gamma rays than expected from our current knowledge of the EBL energy density and cosmological evolution. These unexpected VHE gamma ray signatures are currently one of the subjects of intensive research.

One of the suggested solutions to this problem is the hypothesis that a reduced EBL opacity results from the EBL energy density inhomogeneities in particular if the line of sight to a blazar is passing through a cosmic void (under-dense region) in intergalactic space.

In this thesis, we start by studying the effects of such inhomogeneities on the energy density of the EBL and the resulting gamma-gamma opacity, specifically, by investigating the effects of cosmic void along the line of sight to a distant blazar. First, we studied the possibility of one single void and then the possibility of multiple voids, by assuming an accumulation of voids (10 voids) of typical radii $R = 100 \, h^{-1}$ Mpc centred at a redshift of $z_v = 0.3$ along the line of sight to an object (for example, a blazar) located at redshift $z_v = 0.6$. We conclude that spectral hardening of the VHE gamma ray spectrum for blazars (e.g. PKS 1424+240), after correction for the EBL gamma ray attenuation, is most likely not an artifact of an over-estimation of the EBL absorption due to cosmic inhomogeneities.

In the second part of this thesis, we considered the impact of the Lorentz Invariance Violation (LIV) effect on the gamma-gamma opacity of the Universe to VHE gamma rays propagating from a distant object, compared with the possibility of multiple voids along the line of sight (LOS) to the same object, and we investigated the impact of the LIV effect on the Compton effect. Both subluminal and superluminal modifications of the dispersion relation of photons are considered. In the subluminal scenario, the LIV effects may result in a significant reduction due to the gamma-gamma absorption for photons with energies $\gtrsim 10$ TeV. However, the effect is not expected to be sufficient to explain the apparent spectral hardening of several observed VHE gamma ray blazars in the energy range from 100 GeV up to few TeVs, even when including effects of the EBL inhomogeneities in the distributions of matter and light in the intergalactic space. superluminal modifications of the dispersion relation of photons lead to a further enhancement of the EBL gamma-gamma absorption. We consider, for the first time, the influence of LIV on the Compton effect. We find that the modified Compton scattering process due to the LIV effect becomes relevant only for photons with energies, $E \gtrsim 1$ PeV. In the case of a superluminal modification of the photon dispersion relation, both the kinematic recoil effect and the Klein-Nishina suppression of the cross-section are reduced. However, we argue that the impact of LIV effect on the Compton scattering process is unlikely to be of astrophysical significance.

Keywords: High Energy Astrophysics, Gamma-Gamma Absorption, Extragalactic Background Light, Physics Beyond the Standard Model, Lorentz-Invariance Violation, Cosmology
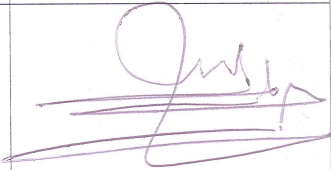
Preface

This thesis has been written according to **the article format style prescribed by North-West University**. Thus, the articles are in published format, written according to the author instructions of internationally accredited journals. As required by North-West University, in Table 1, contributions of authors for all articles/chapters as well as their assent for use as a part of this thesis are provided.

This thesis contains the following chapters:

- Chapter 1 and Chapter 2 : are introductory Chapters, the referencing style is written in the Astrophysical Journal (ApJ) format.

- Chapter 3: Article 1, published in the Astrophysical Journal.

- Chapter 4: Article 2, published in the Proceedings of the 4th Annual Conference on High Energy Astrophysics in Southern Africa (HEASA2016).

- Chapter 5: Article 3, published in the Proceedings of the 5th Annual Conference on High Energy Astrophysics in Southern Africa (HEASA2017), for the acceptance letter see Appendix 7.

- Chapter 6: Article 4, published in the Astrophysical Journal.

- Chapter 7: Is the Summary and Conclusions Chapter, the referencing style is written in the Astrophysical Journal (ApJ) format.

Table 1: Contributions of authors and assent of use as a part of this thesis.

Author	Article	Contribution	Assent
Hassan Abdalla	Article 1 - 4	Doing the calculations, developing the programming codes and writing the preliminary drafts.	
Markus Böttcher	Article 1 - 4	Designing the PhD project, providing intellectual input, and assisting in development of writing.	

Contents

Introduction

Gamma ray photons from distant astronomical objects with energies greater than the threshold energy for electron-positron pair creation are expected to be annihilated due to gamma-gamma absorption by Extragalactic Background Light (EBL). In particular, very-high-energy ($E > 100$ GeV) gamma rays from distant objects (e.g., blazars) are subject to gamma-gamma absorption by EBL, resulting in a high-energy cut-off in the gamma ray spectra of blazars. The probability of absorption depends on the distance of the object and the photon energy. Studies of EBL gamma-gamma absorption signatures have attracted further interest in high energy astrophysics and cosmology due to their potential to study the cluster environments of blazars (see e.g., Sushch & Böttcher 2015) and estimate cosmological parameters (see e.g., Dominguez & Prada 2013; Biteau & Williams 2015).

Recent observations of distant blazars, after correction for EBL absorption, have been interpreted by some authors (e.g., Furniss et al. 2013) to suggest that the Universe may be more transparent to VHE gamma rays than expected based on the existing EBL models. That is because for several blazars the VHE gamma ray spectra appear to be unexpectedly hard.

These unexpected VHE signatures are currently one of the the subjects of intensive research. To explain these spectral hardening signatures, there are several possible explanations that are proposed, for example the existence of exotic Axion Like Particles (ALPs) into which VHE gamma rays can oscillate in the presence of a magnetic field, thus enabling VHE gamma ray photons to avoid the absorption due to the EBL (e.g., Dominguez et al. 2011b); the hypothesis that the EBL energy density might be lower than expected from current EBL models (e.g., Furniss et al. 2013); the VHE gamma ray emission component due to interactions along the line of sight of extragalactic Ultrahigh-Energy Cosmic Rays (UHECRs) originating from the VHE gamma ray source (e.g., Essey & Kusenko 2010). In this thesis, we first studied the possibility of EBL inhomogeneity and then the possibility of Lorentz Invariant Violation (LIV). Before

the possible solution which we are trying to investigate in this thesis we start by introducing the necessary tools which are important as introduction in Chapter 1 and Chapter 2. Chapter 1 starts with the sources of the VHE gamma rays, how gamma ray photons can be detected using space telescopes and the ground-based gamma ray telescopes, and then a very brief introduction about EBL models, highlighting the model proposed by Razzaque et al. (2009) which will be used in Chapter 3 and Chapter 4 and the EBL model proposed by Finke et al. (2010) which will be used in Chapter 5 and Chapter 6. In the last Section of Chapter 1 (Section 1.3.3) we introduce the basic equation to calculate the optical depth of gamma-gamma absorption for VHE gamma ray photons coming from an objects located at cosmological distances (e.g. a blazar), showing that the EBL gamma-gamma absorption is quite significant for blazars observed at TeV energies, see Figure 1.3.4, at the end of Chapter 1.

To investigate the possibility of Lorentz Invariant Violation, the important tools needed to understand the foundation of LIV are the concept of symmetry in physics and how symmetry can be broken. Therefore in Chapter 2 the necessary tool for that is discussed from the philosophy and importance of symmetry in physics from both the classical and the quantum mechanics sides, how symmetry (e.g. Lorentz symmetry) can be broken and the possibility of new physics. In Chapter 3, we investigated the effect of EBL inhomogeneities and the resulting gamma-gamma opacity. Specifically, we considered the impact of a cosmic void along the line of sight to a distant source and investigate the resulting anisotropic and inhomogeneous EBL energy density and therefore, the EBL gamma-gamma opacity. The calculation is done for one single void and also using multiple voids along the line of sight, and more details on how an accumulation of 10 voids with typical radii can impact the EBL gamma-gamma absorption are presented in Chapter 4. In Chapter 5 the possibility of a Lorentz Invariance Violation (LIV) signature compared with the reduction of the EBL gamma-gamma absorption due to the existence of voids along the line of sight to distant VHE gamma ray sources, using the full EBL spectrum which is proposed by Finke et al. (2010), is presented.

The LIV effect using both subluminal and superluminal modifications of the photon dispersion relation and the influence of the LIV effect on the Compton scattering process are presented in Chapter 6. The summary and conclusions are presented in Chapter 7.

Throughout this thesis we assumed the ΛCDM cosmological model as the background framework which is generally the most acceptable model, even when we assumed inhomogeneity and anisotropy due to cosmic voids. Because the size of each individual void in consideration is much smaller than the scale which the cosmological principle may break down. The following cosmological parameters are assumed: the Hubble constant $H_0 = 70$ km s^{-1} Mpc^{-1}, the total matter density $\Omega_m = 0.3$, the cosmological constant density parameter $\Omega_\Lambda = 0.7$.

Extragalactic Background Light and Gamma Ray Attenuation

1.1 Gamma Ray Sources

gamma ray photons are mainly emitted by non-thermal mechanisms (e.g. Synchrotron emission, Compton scattering), tracing the most violent and energetic phenomena in our galaxy and beyond, such as superluminal jets powered by supermassive black holes (see for example, Böttcher et al. 2012), supernova explosions (e.g., H.E.S.S.Collaboration 2018), particle winds and shocks driven by neutron stars spinning on their axes and binary neutron star mergers such as the GW170817 event (e.g., Abbott et al. 2017; H.E.S.S.Collaboration 2017).

One of the most powerful known gamma ray sources is the jet of an active galactic nucleus (AGN). Radiation from AGNs is likely to be the result of the accretion of matter by a spinning supermassive black hole at the center of its host galaxy (see e.g., Maraschi 1992; Böttcher et al. 2012; Potter & Cotter 2012). There are numerous sub-classes of AGNs that have been classified based on their observed characteristics. The most powerful AGNs are classified as quasars (from Quasi-Stellar Objects or QSO, because they looked like stars in early telescopes). The blazars are AGNs with jets pointed toward the observer, in which radiation from the jets is enhanced by relativistic beaming. Their spectral energy distributions characterized by non-thermal emission extending from radio to gamma rays.

There are two fundamentally different approaches that have been proposed to explain the SEDs, referred to as hadronic and leptonic models. In leptonic models, the radiation output is due to the energy loss by electrons producing the synchrotron emission at lower energies and the high-energy component is expected to be due to upscattering soft seed photons by the same relativistic electrons (see e.g., Maraschi 1992; Potter & Cotter 2012; Böttcher et al. 2013). In hadronic models also protons are accelerated to ultra-relativistic energies, low-energy photons are still dominated by synchrotron emission from primary electrons, while the high-energy photons are dominated by π^0 decay, proton synchrotron emission and photo-pion production (for more details, see e.g., Böttcher et al. 2013).
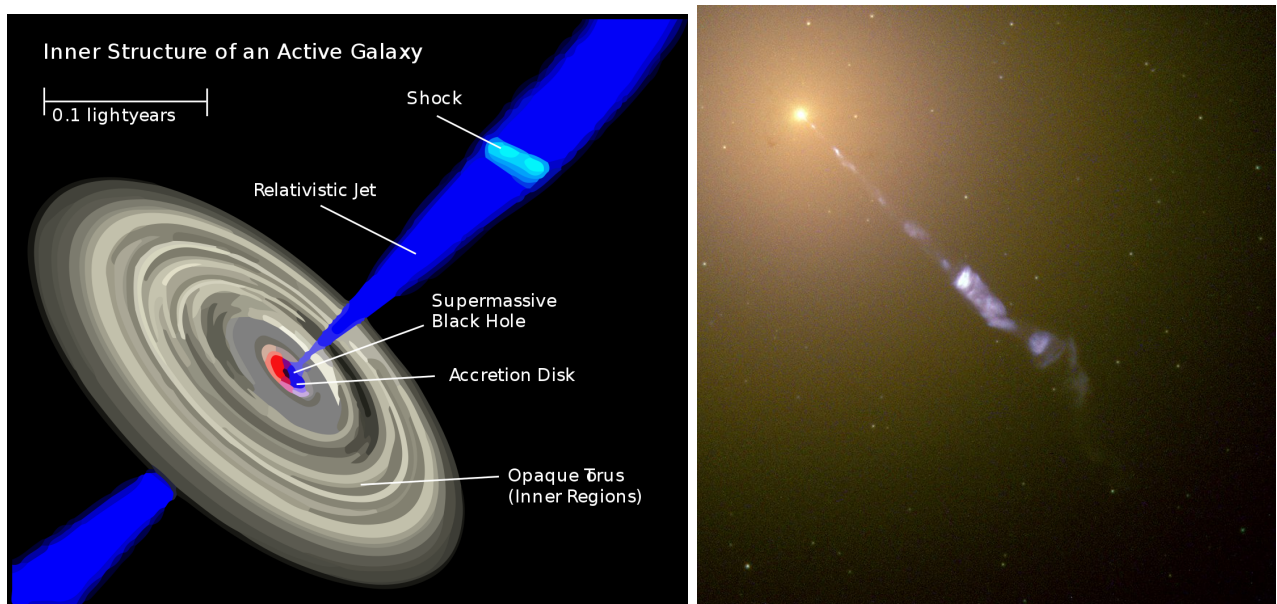
Figure 1.1.1: The left panel illustrates the inner structure of a galaxy with an active galactic nucleus and the right panel is an image taken by the Hubble Space Telescope of a 5000-light-year-long jet ejected from the active galaxy M87, the blue synchrotron radiation contrasts with the yellow starlight from the host galaxy.
credit: wikipedia.org https://en.wikipedia.org/wiki/Active_galactic_nucleus.

1.2 The Detection of Gamma Rays

There are several challenges associated with gamma ray observations. The first challenge is that the atmosphere is optically thick for short wavelengths, therefore it is difficult to observe gamma rays from the surface of the Earth. The second challenge is that there are a small number of gamma ray photons compared to the optical photons. Due to these problems, gamma ray photons can be detected using space telescopes such as Fermi gamma ray Space Telescope or

indirectly by observing the Cherenkov radiation that occurs due to electromagnetic cascading using ground-based telescopes.

1.2.1   Fermi Gamma Ray Space Telescope

The Fermi gamma ray Space Telescope (FGST) is a powerful space observatory it is a high-energy gamma ray telescope (covering the energies from below 20 MeV to around 300 GeV) and launched into orbit on June 11, 2008 (Atwood et al. 2009). Its main instruments are the gamma ray Burst Monitor (GBM) and the Large Area Telescope, which is called Fermi LAT, see Figure (1.2.1). The LAT detector measures the tracks of the electrons and positrons that result when incident gamma rays undergoes pair creations. The scientific objectives addressed by the Fermi LAT include understanding the mechanisms of particle acceleration operating in the sources, determining the nature of the unidentified sources and the origins of the diffuse photons revealed by Energetic gamma ray Experiment Telescope (EGRET), understanding the high-energy behaviour of gamma ray Bursts (GRBs) and transients and using high-energy gamma rays to probe the physics of the early Universe. More details about these objectives and technical instrument details can be found in the Collaboration paper (Atwood et al. 2009).

1.2.2   Ground-based Gamma Ray Telescopes

Ground-based gamma ray astrophysics effectively began in 1989, with the first detection of TeV photons from Crab Nebula, by using the 10m Cherenkov telescope of the Whipple Observatory (Weekes et al. 1989). The typical effective collection area of the single Cherenkov Telescope (CT) is 100000 m^2, which is larger around five orders of magnitude than what can be realistically achieved via direct detection in space (Hinton 2009). Also one of the advantages of ground-based gamma ray telescopes is their high angular resolution $< 2°$ (more details can be found in Weekes et al. 1989).
As mentioned, gamma ray photons cannot be observed directly from the ground when they reach the Earth's atmosphere, gamma ray photons collide with atoms and molecules at the Earth's atmosphere and initiate electromagnetic cascades via the electron-positron pair creation processes and subsequent bremsstrahlung. The gamma ray shower detection at ground level is illustrated in Figure (1.2.2) (for more details see e.g., Weekes et al. 1989; Mangano 2017).
Ground-based gamma ray observations have greatly progressed during the last few decades
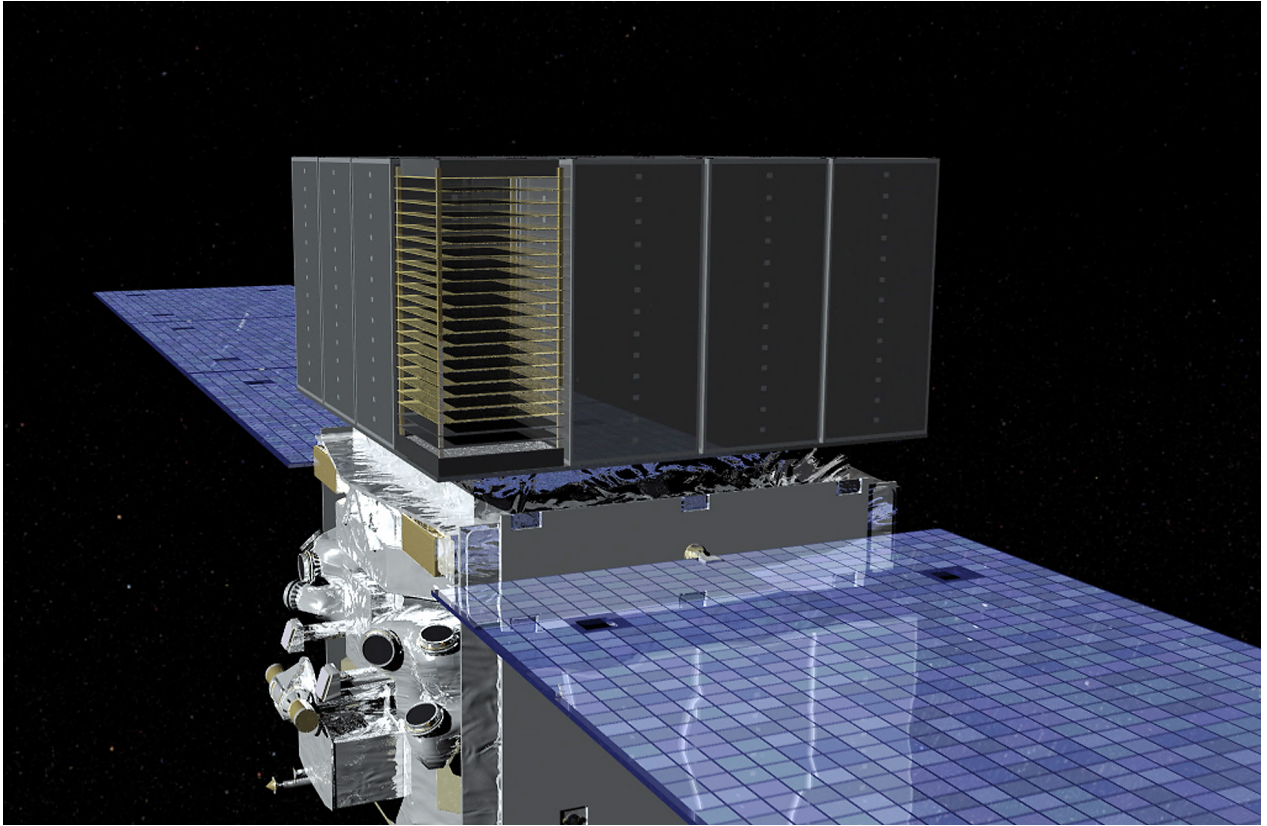
Figure 1.2.1: Artist's view of the Fermi LAT satellite detector, credit: Fermi gamma ray Space Telescope website, [www.nasa.gov/content/fermi/images]. For more details regarding to the Scintillator crystal detector elements and the tracker design principles see Atwood et al. (2009)

through the use of imaging atmospheric Cherenkov telescopes (IACTs) such as High Energy Stereoscopic System H.E.S.S. (see Figure 1.2.3), Major Atmospheric Gamma Imaging Cherenkov Telescopes MAGIC (see Figure 1.2.6) and Very Energetic Radiation Imaging Telescope Array System VERITAS (see Figure 1.2.4).

Furthermore, there is now an international project to build the largest high-energy gamma ray observatory in the world called the Cherenkov Telescope Array (CTA), which is expected to be a major global observatory for VHE gamma rays astrophysics over the next decade and beyond. This project will consist of two arrays of IACTs, a Cherenkov Telescope array in the Northern Hemisphere with emphasis on the study of extragalactic sources at the lowest possible energies (from 20 GeV up to around 20 TeV), and a second Cherenkov Telescope array in the Southern Hemisphere covering VHE gamma rays (from 100 GeV up to around 300 TeV).

The CTA will be around ten times more sensitive and has an unprecedented accuracy compared to the current telescopes such as MAGIC, H.E.S.S., and VERITAS in its detection of high-energy gamma rays. More detailed information for CTA Science can be found in Acharya et al. (2017).
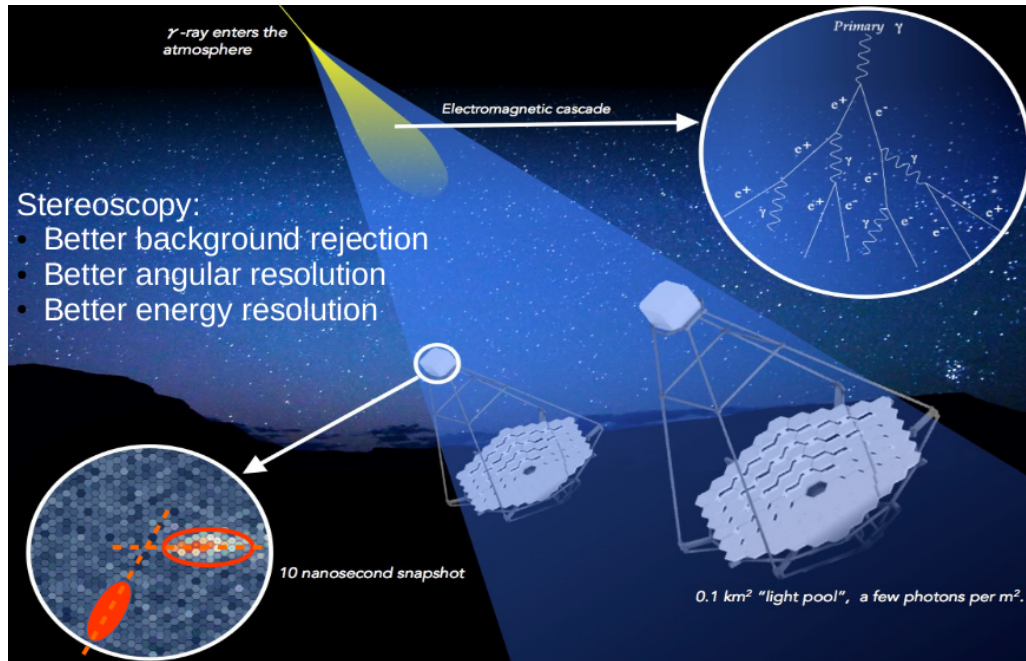
Figure 1.2.2: Schematic drawing of the imaging atmospheric Cherenkov technique. A telescope located within the Cherenkov light pool can record an image of the primary gamma ray indirectly. When a gamma ray interacts with an atmospheric nucleus an electron-positron pair is usually produced and each one of the pair can interact with other atoms generating a cascade of particles. Some of the particles travel at ultra-relativistic speed and emit Cherenkov light. Therefore, the optical mirrors of the telescopes reflect the collected Cherenkov light into the camera, which contains photomultiplier tubes (PMTs). The final shower image can be recorded as shown in the bottom left of this figure. The simultaneous observation of a cascade shower with several telescopes such as H.E.S.S. (called Stereoscopic) under different viewing angles increases substantially angular and energy resolution. This figure is taken from Mangano (2017).

Figure 1.2.3: H.E.S.S. is located in Namibia, has five telescopes, four with a mirror 12 m in diameter are called Phase I and went into operation in 2002, and one larger telescope with a 28 m mirror, constructed in the centre of the array. This current system, called H.E.S.S. II, saw its first light on 26 July 2012 [credit: webpages of H.E.S.S., https://www.mpi-hd.mpg.de/hfm/HESS/].

Figure 1.2.4: VERITAS is an array of four telescopes with a mirror 12 m in diameter each, located in Mount Hopkins, Arizona, US. The first light celebration for the full 4 telescope array was on April 27-28, 2007 [credit: webpages of VERITAS https://veritas.sao.arizona.edu/].
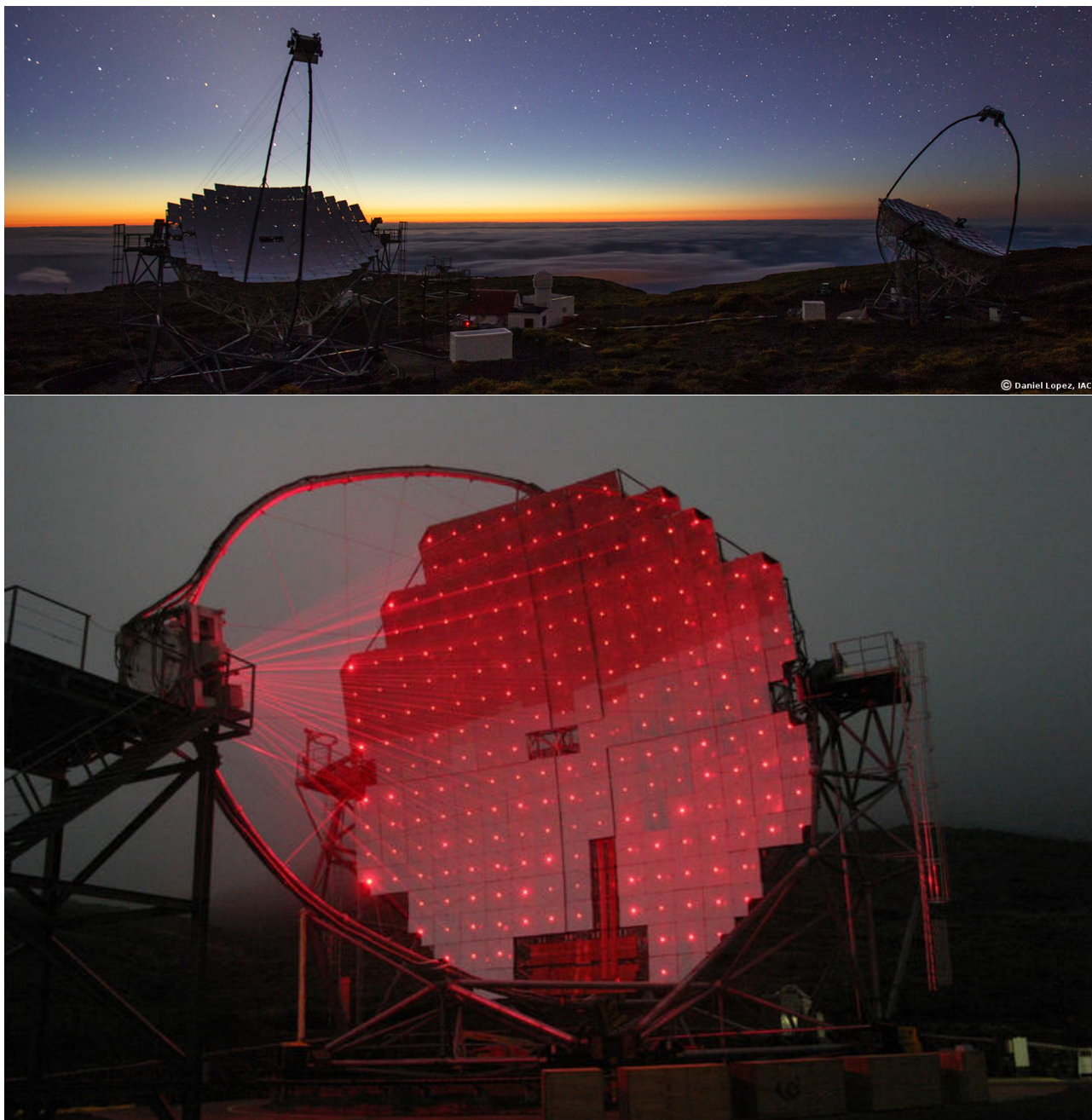
Figure 1.2.5: MAGIC is a system of two telescopes with a mirror 12 m in diameter each, located in La Palma, one of the Canary Islands, at about 2200 m above sea level, bottom panel, during foggy nights, the laser reference beams of MAGIC's active control could be seen [credit: webpages of MAGIC https://wwwmagic.mpp.mpg.de/].
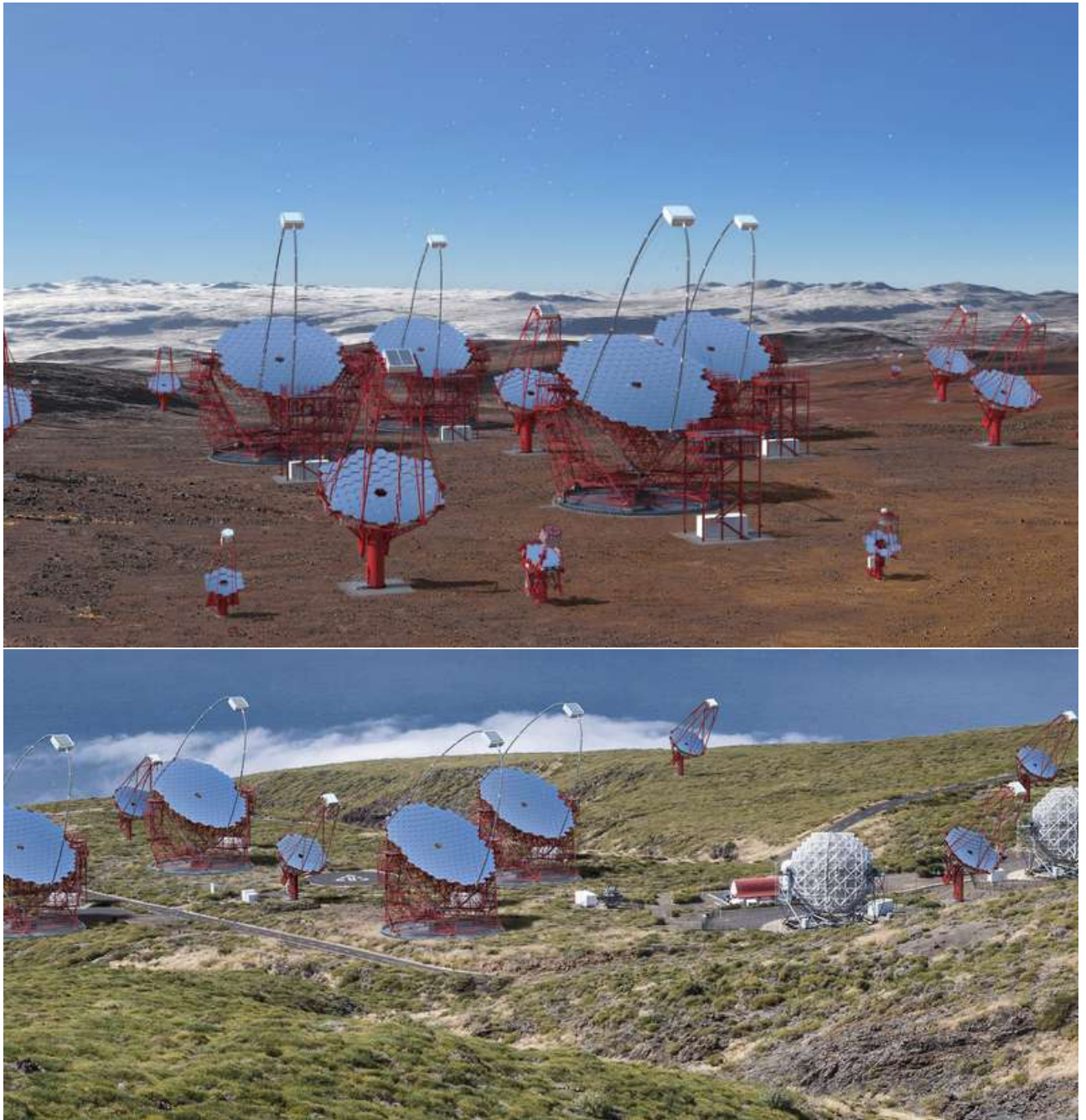
Figure 1.2.6: Artist's view of the CTA telescopes, the top panel is an image of CTA's Southern Hemisphere Site and the bottom panel is an image of CTA's Northern Hemisphere Site Credit: Gabriel Pérez Diaz, IAC, SMM [credit: webpages of CTA https://phys.org/news/2017-09-cherenkov-telescope-array-science-case.html].

High Altitude Water Cherenkov Observatory

The High Altitude Water Cherenkov (HAWC) observatory is an instrument for the detection of high-energy gamma rays and cosmic-rays (from 100 GeV to 100 TeV), located on the flanks of the Sierra Negra volcano in Mexico at an altitude of 4100 meters. HAWC is a Water Cherenkov shower detector array for the observation of TeV gamma rays.

Figure 1.2.7: The HAWC was completed in 2015, and consists of an array of 300 water Cherenkov detectors; each tank contains circa 188,000 liters of water and four photomulitplier tubes (PMTs). In the right panel is a simulation of a 1 GeV muon (red line) passing through one detector and emitting Cherenkov light (green lines), for more details see Mostafa (2014) [credit: webpages of HAWC https://www.hawc-observatory.org/].

1.3 Extragalacitc Background Light and Gamma-Gamma Absorption

The Extragalactic Background Light (EBL) can be defined as the accumulated photons (diffused light) from the era of the decoupling until the present day. In other words, the EBL is the integrated light from all extragalactic sources. In this definition the solar system as well as the high-energy background radiations such as X-rays and gamma rays and the low-energy foreground photons from the Milky Way are excluded. The direct measurement of the EBL is very difficult due to the contribution of zodiacal light (Hauser & Dwek 2001).

There are several studies of the EBL focusing on the predicted gamma-gamma opacity imprints and employing a variety of empirical and theoretical methods (e.g., Stecker 1969; Aharonian et al. 2006; Franceschini et al. 2008; Razzaque et al. 2009; Finke et al. 2010; Dominguez et al. 2011a; Gilmore et al. 2012). All the cited works agree that the Universe should be opaque

to VHE gamma ray photons from extragalactic sources at high redshift ($z \gtrsim 1$). All models have been developed to derive an overall EBL spectrum based on the knowledge of the star formation rate (SFR) and the evolution of the galaxies incorporated with the observational constraints.

In this chapter we will highlight the model which was proposed by Razzaque et al. (2009) and its extension Finke et al. (2010), because we will use these two models in the following chapters.

1.3.1 Razzaque et al. EBL Model

The Razzaque et al. (2009) EBL model aims to calculate the contribution of the stellar component only for the EBL spectrum. In this model the re-emission in the infra-red of starlight absorbed by dust and the contributions from AGNs and quasars are ignored. Their goal was to build a model of the EBL starlight component of the spectrum (from 0.1 to 10 eV only) directly from the stellar thermal surface radiation. Also, post-main-sequence stars are ignored in this model because their lifetime is very short compared to the main-sequence lifetime. Therefore, their contribution to the UV-optical wave bands is expected to be not significant. This model is built as follows to calculate the emitted number of photons from a star over cosmic time. The relationship between the cosmic time and redshift can be written as

$$(\frac{dt}{dz})^{-1} = -H_0(1+z)\sqrt{(\Omega_m(1+z)^3 + \Omega_\Lambda}, \tag{1.3.1}$$

H_0 is the Hubble constant, Ω_m, Ω_Λ are dimensionless matter and vacuum en- ergy densities. A lifetime of the star t_* with mass M from its birth at red-shift z_b to the red-shift $z_d(M)$ which it had evolved off the main sequence, can be written as

$$t_* = \int_{z_d(M)}^{z_b} dz \left| \frac{dt}{dz} \right|. \tag{1.3.2}$$

By inverting Equation (1.3.2), $z_d(M, z)$ can be written as

$$z_d(M, z) = -1 + \left(-\left(\frac{\Omega_\Lambda}{\Omega_m}\right) \operatorname{sech}\left[\frac{3}{2}H_0t_* \tanh^{-1}\sqrt{1 + \frac{\Omega_m}{\Omega_\Lambda}(1+z)^3} \right]^2 \right)^{\frac{1}{3}}. \tag{1.3.3}$$

The lifetime t_* of the star can be calculated as

$$t_* = t_\odot \left(\frac{M}{M_\odot}\right)\left(\frac{L_\odot}{L}\right), \tag{1.3.4}$$

where L, M are the luminosity and mass of the main sequence star respectively and $L_{\odot}$, $M_{\odot}$ and $t_{\odot}$ are the solar luminosity, solar mass and lifetime respectively.

The number of stars formed at a redshift z depends on the star formation rate (SFR) and the initial mass function (IMF). In Razzaque et al. (2009) a universal IMF which is normalized between mass from $M_{min} = 0.1 M_{\odot}$ to $M_{max} = 120 M_{\odot}$ is assumed as $\int_{M_{min}}^{M_{max}} dM \xi(M) M$. The mass distribution $\xi(M)$ of a given stellar population is represented by the IMF which is described by the functional form $\xi(M) = M^{-k}$, where k depends to the stellar masses. The IMF is illustrated in Figure 1.3.2, more details can be found in (Razzaque et al. 2009).

The function for the star formation model from Cole (2001) is used,

$$\Psi(z) = \frac{h(a + bz)}{[1 + (z/c)^d]}, \tag{1.3.5}$$

where h,a,b,c,d is the dimensionless parameters depend on the model (for more details, see e.g., Cole 2001). In this work we will use a model which corresponds to the Salpeter B IMF model. So, the parameters for this model are $a = 0.0170$, $b = 0.13$, $c = 3.3$, and $d = 5.3$ (see Figure 1.3.2).

Now, the EBL energy density can be calculated (for more details see Razzaque et al., 2009)

$$\begin{aligned}
\frac{dN(\epsilon, z)}{d\Omega d\epsilon dV} &= \int_{z=z_i}^{\infty} d\tilde{z} \left| \frac{dt}{d\tilde{z}} \right| \Psi(\tilde{z}) \int_{M_{min}}^{M_{max}} dM \left(\frac{dN}{dM} \right) \\
&\times \int_{max\{z_d(M,z')\}}^{\tilde{z}} dz' \left| \frac{dt}{dz'} \right| f_{esc}(\epsilon') \frac{dN(\epsilon' M)}{d\epsilon' dt} (1 + z'),
\end{aligned} \tag{1.3.6}$$

where $f_{esc}(\epsilon')$ is the escape fraction of photons from the host galaxy and $\frac{dN(\epsilon' M)}{d\epsilon' dt}$ is the total number of photons emitted per unit energy and time by a star with mass M. To calculate the EBL energy density in co-moving cordinate, the energy and volume can be transformed as $\epsilon_1 = \epsilon(1 + z_1)$ and $V_1 = V/(1 + z1)^3$ respectively, then by using Equation (1.3.6), the EBL energy density can be written as (Razzaque et al., 2009)

$$\epsilon_1 \mu_1 = (1 + z_1)^4 \, \epsilon^2 \, \frac{dN(\epsilon, z = z_1)}{d\epsilon \, dV}. \tag{1.3.7}$$

This model can be used to calculate the opacity of the Universe for gamma ray photons with energy up to around 300 GeV, which is relevant for the high-energy data from the FGST and the Atmospheric (or Air) Cherenkov Telescopes, but the gamma-gamma opacity calculation using this model is insufficient for photons with energy around 500 GeV or higher (Razzaque et al. 2009).
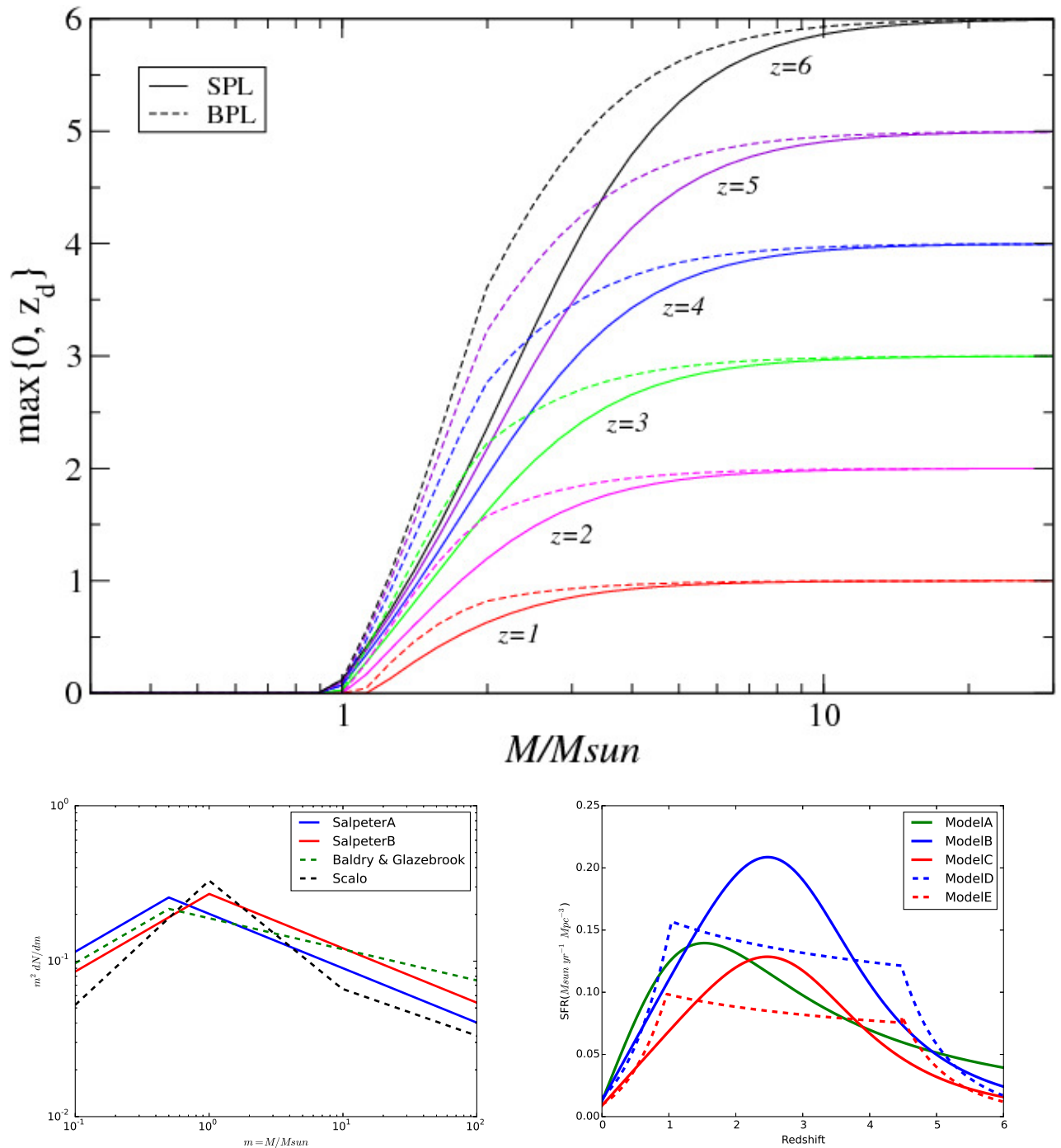
Figure 1.3.1: The top panel is an illustration of $\max\{0, z_d\}$ versus the masses in solar units (see equation 1.3.4). The solid-lines represent the lifet-time of the main-sequence stars following the Single-Power-Law (SPL) and the dashed-lines represent results for the Broken-Power-Law (BPL). The bottom left panel represents the four different IMF models and the bottom right panel shows five different SFR models. These three plots are reproduced from Razzaque et al. (2009) in which more details can be found.
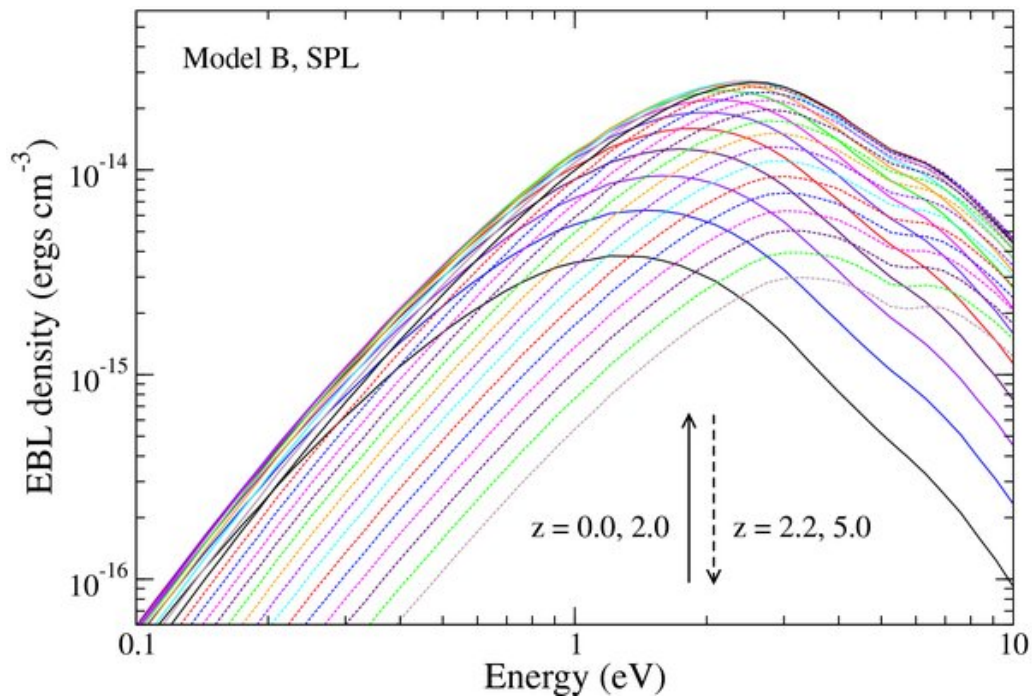
Figure 1.3.2: Evolution of the comoving EBL energy density as calculated by Equation (1.3.7). The curves are plotted for $z = 0 - 5$ with 0.2 interval. The EBL density increases up to redshift $z = 2.2$ and then decreases, as indicated by the solid and dashed arrows, this due to the evolution of SFR with red-shift (see Figure 1.3.1). This figure is taken from Razzaque et al. (2009).

To calculate the opacity for VHE gamma ray photons with energy higher than around 500 GeV the full EBL spectrum from far infra-red to optical-ultraviolet is needed because such VHE gamma ray photons could interact with EBL photons in the mid- to far-IR, which has been ignored in Razzaque et al. (2009). The possible interaction energies between the VHE gamma ray photons and the diffused EBL photons can be deduced from the gamma-gamma pair-production threshold formula (1.3.10), see the black solid line in Figure 4, Chapter 5.

1.3.2   Finke et al. EBL Model

In Razzaque et al. (2009), the EBL model in the optical through ultraviolet has been developed by considering the SFR and IMF treating stars on their main sequence lifetime as blackbodies. This model is extended by Finke et al. (2010), to include post-main-sequence stars and re-processing of star-light by dust. In Razzaque et al. (2009) only the escape fraction $f_{esc}(\epsilon^{'})$ of photons from the host galaxy is considered (see Equation 1.3.6) but the fraction of photons which does not escape $1 - f_{esc}(\epsilon^{'})$ is ignored. By setting the luminosity density from the fraction of absorbed starlight $(1 - f_{esc}(\epsilon^{'}))$ equal to the luminosity density from dust emission, the infrared emission is calculated in the Finke et al. EBL model (for more details see, Finke et al. 2010). The full EBL spectrum from UV through far-IR, from direct stellar radiation and stellar radiation which is absorbed and re-radiated by dust is presented in Figure 1.3.3.
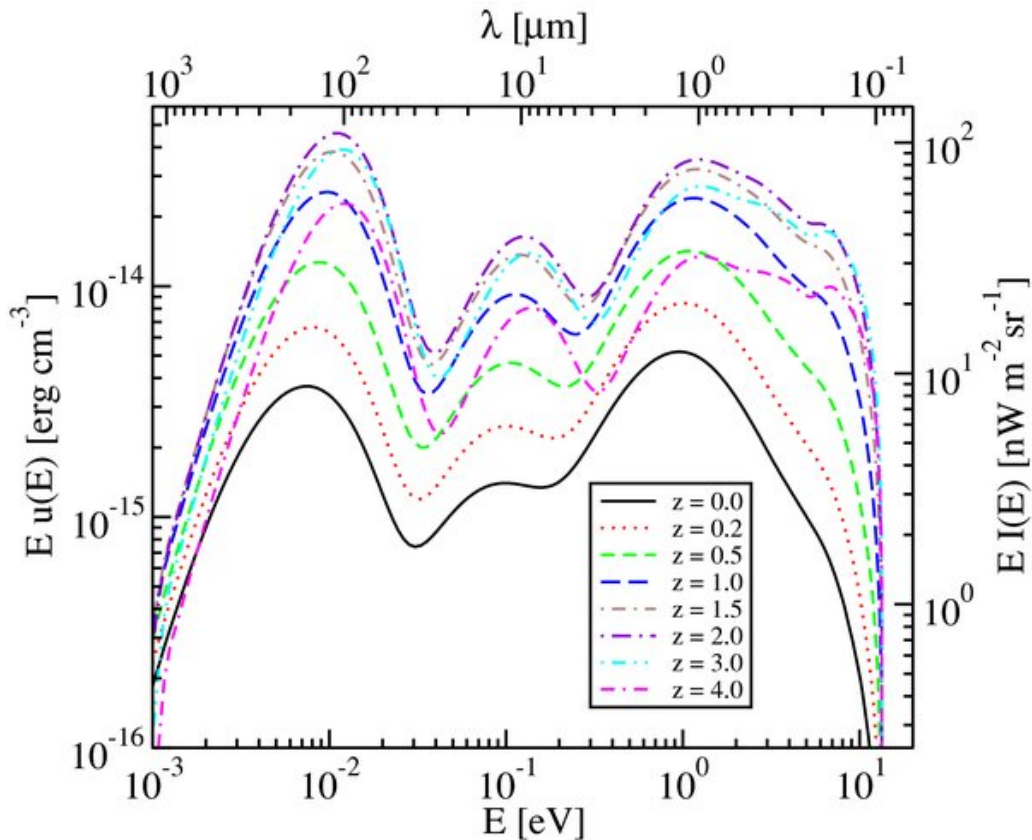
Figure 1.3.3: The EBL energy density as a function of photon energy, for different redshifts. This figure is taken from Finke et al. (2010).

1.3.3 Absorption of Gamma Rays

The optical depth $\tau_{\gamma\gamma}(E, z)$ of gamma-gamma absorption for VHE gamma ray photons coming from sources at redshift z_s due to their interaction with the EBL can be written as Gould & Schréder (1967)

$$\tau_{\gamma\gamma}(E, z) = c \int_0^{z_s} dz_1 \left| \frac{dt}{dz_1} \right| \times \int_0^\infty d\epsilon_1 \int_{-1}^1 2\pi \ d\mu \ \frac{\mu_{\epsilon_1}}{\epsilon_1} \ (1 - \mu)\sigma_{\gamma\gamma}(s), \qquad (1.3.8)$$

where $\mu = \cos(\theta)$ and μ_{ϵ_1} is the EBL energy density and $\sigma_{\gamma\gamma}(s)$ is the gamma-gamma pair-production cross-section, which can be written as

$$\sigma_{\gamma\gamma}(s) = \frac{1}{2}\pi r_e^2 (1 - \beta_{cm}) \left[(3 - \beta_{cm}^4) \ln \left(\frac{1 + \beta_{cm}}{1 - \beta_{cm}} \right) - 2\beta_{cm}(2 - \beta_{cm}^2) \right]$$

where r_e is the clasical electron radius and $(\beta_{cm} = (1 - \frac{1}{s})^{1/2})$ is the electron-positron velocity in the centre of momentum system, $s = \frac{s_0}{2}(1 - cos\theta)$, is the centre of mass frame and $s_0 = \frac{\epsilon_1 E}{m^2 c^4}$. We introduce the dimensionless function $\bar{\varphi}$ defined by Gould & Schréder (1967) as

$$\bar{\varphi}[s_0(\epsilon)] = \int_1^{s_0(\epsilon)} s\bar{\sigma}(s)ds,$$

where $\bar{\sigma}(s) = \frac{2\sigma(s)}{\pi r_2^2}$ and $s_0(\epsilon) = E(1 + z)\epsilon/m_e^2 c^4$.
Then Equation (1.3.9) can be written as (see e.g., Razzaque et al. 2009)

$$\tau_{\gamma\gamma}(E, z) = c \ \pi r_e^2 \left(\frac{m_e^2 c^4}{E} \right)^2 \int_0^{z_s} \frac{dz_1}{(1 + z_1)^2} \left| \frac{dt}{dz_1} \right| \times \int_{\epsilon_{th}}^\infty d\epsilon_1 \ \frac{\mu_{\epsilon_1}}{\epsilon_1^3} \ \bar{\varphi}[s_0(\epsilon)], \qquad (1.3.9)$$

where m_e is the electron rest mass and ϵ_{th} is the threshold energy for electron-positron pair-production can be written as

$$\epsilon_{th} = \frac{m_e^2 c^4}{E(1 + z_1)}. \qquad (1.3.10)$$

From the gamma-gamma opacity $\tau_{\gamma\gamma}(E, z)$, the attenuation for the intrinsic photon flux F_ν^{int} can be written as

$$F_\nu^{obs} = F_\nu^{int} e^{-\tau_{\gamma\gamma}(E,z)}, \qquad (1.3.11)$$

where F_ν^{obs} is the observed spectrum.
For different sources, the νF_ν spectra before and after de-absorption for each source using the Finke et al. EBL model are plotted in the top panels of Figure 1.3.4. The Universe becomes optically thick for gamma ray photons, defined where $\tau_{\gamma\gamma}(E, z) = 1$, see the bottom panel of Figure 1.3.4. As we can see from Figure 1.3.4, the absorption is quite significant for many/most blazars observed at TeV energies with CTs.
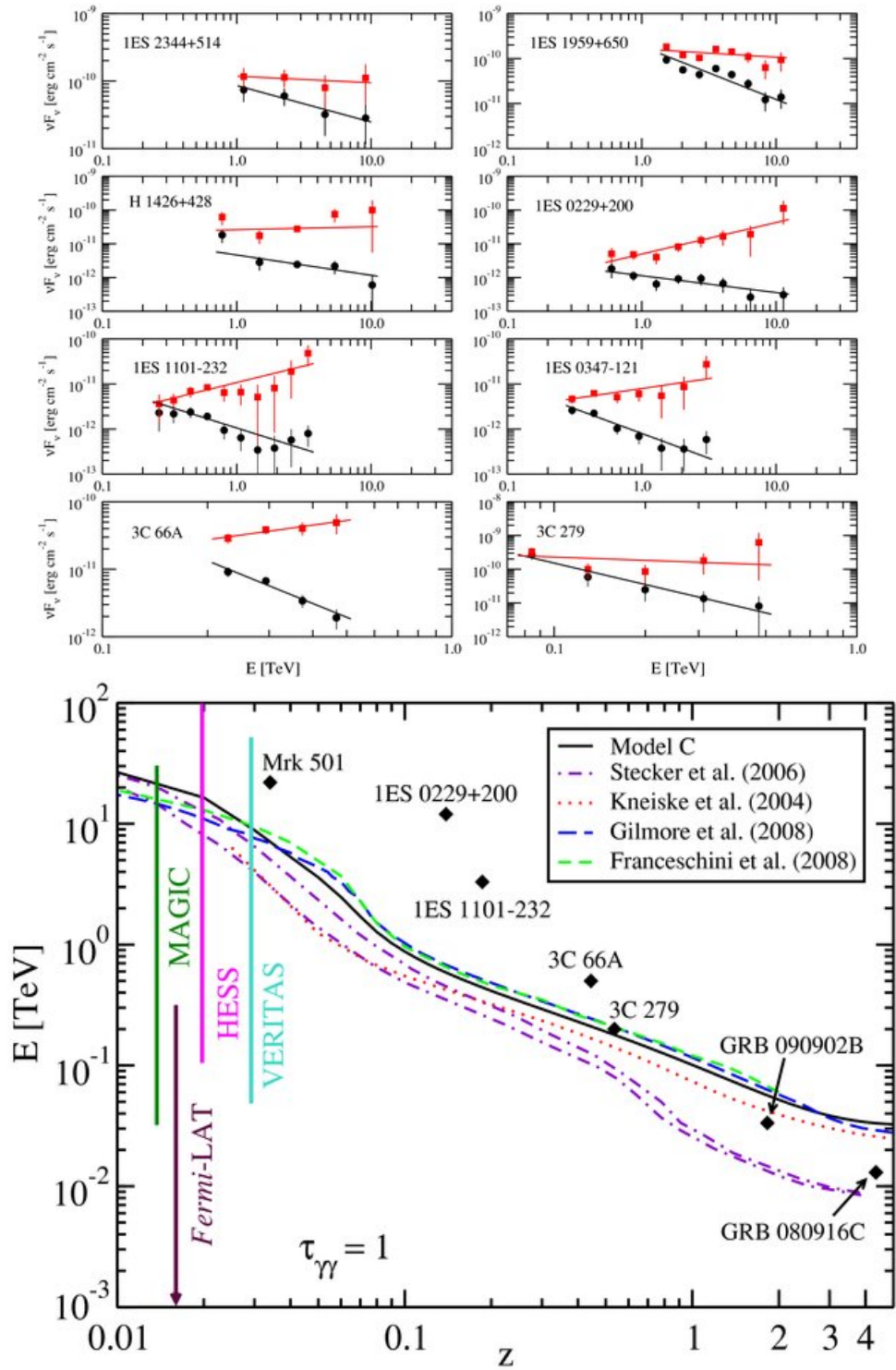
Figure 1.3.4: TeV blazar spectra observed indicated by circles and deabsorbed indicated by squares are ploted in the top panels. $\tau_{\gamma\gamma}(E, z) = 1$ for several EBL models as indicated in the bottom panel. These Figures are taken from Finke et al. (2010).

References

Abbott, B. P., Abbott, R., Abbott, T. D., Acernese, F., Ackley, K., et al. 2017, ApJ, 848, 2, arXiv: 1710.05834

Aharonian, F., Akhperjanian, A. G., Bazer-Bachi, A. R., et al. 2006, Nature, 440, 1018

H.E.S.S.Collaboration: Abdalla, H., Abramowski, A. & Aharonian, F., et al., 2018, Astron. Astrophys., 612, A5, arXiv: 1609.00600

H.E.S.S.Collaboration: Abdalla, H., Abramowski, A. & Aharonian, F., et al., 2017, ApJ, 850, L22, arXiv: 1710.05862

Acharya, B. S., Agudo, I., Samarai, I. A., Alfaro, R., Alfaro, J., Alispach, C., Alves Batista, R. & Amans, J.P., et al., 2017, Cherenkov Telescope Array Consortium, arXiv:1709.07997

Atwood, W. B., Abdo, A.A., Ackermann, M., and Althouse, W. & Anderson, B. et al., 2009, ApJ, 697, 1071, arXiv: 0902.1089

Biteau A. & Williams D. A. 2015, ApJ, 812, 1

Böttcher, M., Harris, D., E. & Krawczynski, H., 2012, Relativistic Jets from Active Galactic Nuclei, ISBN: 978-3-527-41037-8

Böttcher, M., Reimer, A., Sweeney, K., & Prakash,A., 2013, ApJ, 768, 54, arXiv: 1304.0605

Cole, S., et al. 2001, MNRAS, 326, 255

Dominguez, A., Primack, J. R., Rosario, D. J., et al., 2011a, MNRAS, 410, 2556

Dominguez, A., Sánchez-Conde, M. A., & Prada, F., 2011b, J. Cosmol. Astropart. Phys., 11, 020

Dominguez, A. & Prada, F., 2013, ApJ, 771, L34

Essey, W. & Kusenko A., 2010, ApJ, 33, 81

Finke, J. D., Razzaque, S. & Dermer, C. D., 2010, ApJ, 712, 238

Franceschini, A., Rodigheiro, G., & Vaccari, M., 2008, A&A, 487, 837

Furniss A., et al., 2013, ApJ, 768, L31

Furniss A., Stutter, P. M., Primack, J. R., & Dominguez, A., 2015, MNRAS, 446, 2267

Gilmore, R. C., Sommerville, R. S., Primack, J. R., & Dominguez, A., 2012, MNRAS, 422, 3189

Gould, R. J. & Schréder, G. P. 1967, Phys. Rev., 155, 1408

Hauser, M. G. & Dwek, E. 2001, ARA&A„ 39, 249

Hinton, J., 2009, New J. Phys., 11,055005, arXiv: 0803.1609

Mangano, S., For the collaboration, Proceedings, 52nd Rencontres de Moriond on Very High Energy Phenomena in the Universe: La Thuile, Italy, March 18-25, 2017, 111-122, arXiv: 1705.07805

Maraschi, L., Celotti, A., & Ghisellini, G., 1992, ApJ, 397, L5

Mostafa, Miguel A. 2014, Braz. J. Phys., 44, 571, arXiv: 1310.7237

Potter, W. J. & Cotter, G. 2012, MNRAS, 423, 756

Razzaque S., Demer, C. D., & Finke, J. D., 2009, ApJ, 697, 483

Stecker, F. W. 1969, ApJ, 157, 507

Stecker, F. W., de Jager, O. C., & Salamon, M. H., 1992, ApJ, 390, L49

Sushch, I. & Böttcher, M. 2015, A & A, 573, A47

Weekes, T. C., Cawley, M. F., Fegan, D. J., Gibbs, K. G., & Hillas, A. M., et al., 1989, ApJ, 342, 379

Brief Overview of Symmetry and Symmetry Breaking

2.1 Symmetry

> It is increasingly clear that the symmetry group of nature is the deepest thing that we understand about nature today
>
> *Steven Weinberg*

The physical or mathematical feature (e.g. quantity) of a system that is preserved or remains unchanged under some transformation is called symmetry. Since the sixth century BC, the days of natural philosophy (during the time of the ancient Greek philosophers such as Pythagoras), symmetry has provided insight into the laws of physics and the nature of the cosmos. The principles of symmetry played only a very small explicit role until the twentieth century. The conservation laws, especially those of energy and momentum were regarded as a fundamental importance and considered to be consequences of the dynamic laws of nature rather than as consequences of the symmetries. For example, the Maxwell's equations formulated in 1865 embodied both Lorentz symmetry and gauge invariance (symmetry). Nonetheless, these symmetries were not fully appreciated for over 40 years (Gross 1996).

Nowadays, the concepts of symmetry are regarded as the most fundamental part and play a central role in our description of nature. There are two different types of symmetries which generally can be classified into *discrete symmetries* and *continuous symmetries*. Continuous symmetries can be described by *Lie groups*, while discrete symmetries are described by *finite groups*.

2.1.1 Symmetries in Classical Mechanics

The grand theme of symmetries in classical mechanics is simplifying a mechanical problem by exploiting a symmetry to reduce the number of variables. According to *Noether's theorem* there is a very deep connection between symmetries and conservation laws. Noether's theorem states that *every differentiable symmetry of the action of a physical system has a corresponding conservation law.*

The action (S) of a physical system is the integral over time (t) of a Lagrangian (L), from which the system's behaviour can be calculated by using the principle of least action.

The Lagrangian L is the difference between a kinetic energy T and a potential energy V for a system, which can be expressed by using generalised coordinates $q(t) = (q(t)_1, q(t)_2, ..., q(t)_N)$ as :

$$L(\dot{q}, q, t) = T(\dot{q}, q, t) - V(q, t), \quad \textit{Note: for simplicity we set } q(t) \equiv q, \quad (2.1.1)$$

where $\dot{q} \equiv dq/dt$. The principle of least action (or also called the principle of stationary action) is a variational principle that can be applied to the action of a mechanical system and can be used to obtain the equations of motion for that system.

The action of the mechanical system S can be defined as the integral of the Lagrangian L between two instants of time, the initial time $t = t_i$ and final time $t = t_f$ as

$$S = \int_{t_i}^{t_f} dt \ L(\dot{q}, q, t). \quad (2.1.2)$$

By using the extremum (or action) principle, it required that the first-order change for the action δS must be zero, the equations of motion of the system can be written as follows,

$$\frac{d}{dt}\left(\frac{\partial L}{\partial \dot{q}}\right) - \frac{\partial L}{\partial q} = 0. \quad (2.1.3)$$

As one can see from Equation (2.1.3), if the Lagrangian is independent of a specific coordinate or several coordinates q_m (called cyclic coordinates) the second term is zero. Therefore, from

Equation ([2.1.3](#)) we can deduce,

$$\frac{\partial L}{\partial \dot{q_m}} = const.$$

Thus, for each cyclic coordinate q_m, there is a constant of motion associated with the coordinate q_m. Using cyclic coordinates is very important to calculate the conserved quantities in physics; for example if we assume a Lagrangian $L = m/2(\dot{x}^2 + \dot{y}^2) + cx$, clearly we can notice that the motion is in x-y plane, but our potential term cx is independent of the y coordinate. Therefore, the momentum in the y direction is conserved, and by considering a coordinate transformation which can describe a continuous set of translations in the cyclic coordinate,

$$q \rightarrow q' = q_m + a,$$

where a is a continuously varied parameter. However, the coordinate is cyclic, the Lagrangian is invariant under these translations. Symmetries of the equations of motion can be used to derive new solutions.

2.1.2   Symmetries in Quantum Mechanics

Symmetries in quantum mechanics are extremely powerful tools. In quantum mechanics the physical states for given vectors (e.g. $|\phi\rangle$, $|\psi\rangle$, $|\chi\rangle$ ... etc) for the systems are represented in the Hilbert space $\mathcal{H}$ by rays $\mathcal{R}$ rather than vectors. By rays $\mathcal{R}$ we mean classes of equivalence of vectors which satisfy the condition $|\psi\rangle \simeq |\psi\prime\rangle$ if they differ from one another by a phase factor $|\psi\rangle = e^{i\theta} |\psi\prime\rangle$. The observables (let us call it A) are represented by linear Hermitian operators. Hermitian means that which satisfies $A = A^+$, where for any linear operator A, the adjoint A^+ is defined by the relation

$$\langle \phi | A^+ \psi \rangle = \langle A\phi | \psi \rangle = \langle \phi | A\psi \rangle^* . \tag{2.1.4}$$

The physical information which can be extracted from the quantum mechanical systems is the probability $\mathbf{P}$. Suppose that we have a physical system represented by rays $(\mathcal{R}_1, \mathcal{R}_2, ...\mathcal{R}_n)$, if we assumed that $\mathcal{R} = |\psi\rangle$ and $\mathcal{R}_n = |\psi_n\rangle$, the state represented by $\mathcal{R}_n$ is given by

$$P(\mathcal{R} \rightarrow \mathcal{R}_n) = |\langle \psi | \psi_n \rangle|^2. \tag{2.1.5}$$

Symmetries in quantum mechanics are changes of the system which preserve probabilities of all possible measurements or in other words *"the probabilities measured by one observer O must be the same as the probabilities measured by another observer O' "*, that means,

$$P(\mathcal{R} \rightarrow \mathcal{R}_n) = P(\mathcal{R}' \rightarrow \mathcal{R}'_n); \quad |\langle \psi | \psi_n \rangle|^2 = |\langle \psi' | \psi'_n \rangle|^2.$$

Wigner's Symmetry representation theorem is considered to be a cornerstone of the mathematical formulation of quantum mechanics, which states that:

Theorem 1. *The Hilbert space operators corresponding to symmetry transformations can be of two types only: either they are unitary and linear operators U,*

$$\langle U\phi | U\psi \rangle = \langle \phi | \psi \rangle \quad ; \quad \forall \ |\phi\rangle, |\psi\rangle \ \in \ \mathcal{H},$$

$$U(\alpha \, |\phi\rangle + \beta \, |\psi\rangle) = \alpha U \, |\phi\rangle + \beta U \, |\psi\rangle \quad ; \quad \forall \ |\phi\rangle, |\psi\rangle \ \in \ \mathcal{H} \ , \ \forall \alpha, \beta \ \in \ \mathbb{C},$$

or antiunitary and antilinear operators A

$$\langle A\phi | A\psi \rangle = \langle \phi | \psi \rangle^* \quad ; \quad \forall \ |\phi\rangle, |\psi\rangle \ \in \ \mathcal{H},$$

$$A(\alpha \, |\phi\rangle + \beta \, |\psi\rangle) = \alpha^* A \, |\phi\rangle + \beta^* A \, |\psi\rangle \quad ; \quad \forall \ |\phi\rangle, |\psi\rangle \in \mathcal{H} \ , \ \forall \ \alpha, \beta \ \in \ \mathbb{C}.$$

The complete proof for Wigner's theorem (1) can be found in Weinberg (1995), which is presented at the end of Chapter 1 (Appendix A). From Wigner's theorem (1) one of the observations which one can make, is that the identity operator $U = I$ is unitary and linear. The important consequence from this trivial observation is that *(any set of transformations that are continuously connected to the identity I must correspond to operators that are unitary and linear.)*

There are many continuous symmetries in physics (e.g. rotation), and by continuous we mean that we can connect the associated unitary operator U with the identity I by a continuous change in some parameters, such as the continuous change in angle for the rotation group.

The set of symmetry transformations has certain properties that define it as a group G. If T_1 is a transformation that takes rays $R \longrightarrow R'$ and T_2 is transformation that takes $R' \longrightarrow R''$, another transformation $T = T_2 \circ T_1$, that can take $R \longrightarrow R''$ can be defined by using an operator acting into Hilbert space $\mathcal{H}$. For illustration, see Figure 2.1.1.

To reflect the structure of this group of transformations which is illustrated in Figure 2.1.1, we can consider a unitary representation such as $T \to U(T)$ by using the fact that if we take any transformation T we will get some unitary operator $U(T)$, similarly T_1 and T_2 can be mapped into $U(T_1)$ and $U(T_2)$ respectively. Since these operators $(U(T_1), U(T_2), U(T))$ act on vectors $|\psi\rangle$, these vectors can differ only by a phase factor $e^{\phi_n(T2\circ T1)}$, and we can write (see also Weinberg 1995; Das & Okubo 2014),

$$U(T_2)U(T_1) \, |\psi_n\rangle = e^{\phi_n(T2\circ T1)} U(T_2 \circ T_1) \, |\psi_n\rangle . \qquad (2.1.6)$$

By using the linearity of the operator $U(T)$, we can show that the face factor $e^{\phi_n(T2\circ T1)}$ is independent of the state $|\psi\rangle$ (for example see Das & Okubo 2014). Therefore, from (2.1.6) we
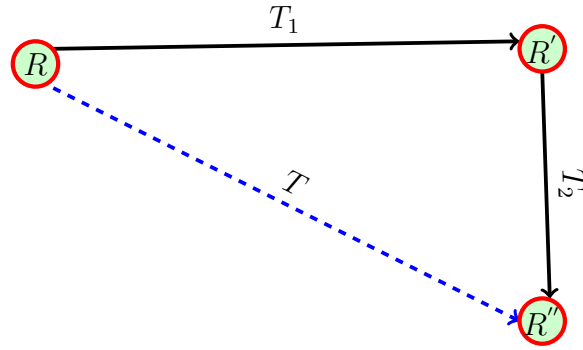
Figure 2.1.1: This is an illustration representing a set of symmetry transformations $T_1 :$ $R \longrightarrow R'$ and $T_2 : R' \longrightarrow R''$ defined in a group G, another transformation $T = T_2 \circ T_1$ in the group G can be defined such that $T : R \longrightarrow R''$.

can write an operator statement as

$$U(T_2)U(T_1) = e^{\phi_n(T2 \circ T1)}U(T_2 \circ T_1). \tag{2.1.7}$$

If $\phi_n = 0$, the operator $(2.1.7)$ is called a *unitary representation of the group of transformations*, but for $\phi_n \neq 0$, it is called a *projective representation* (Weinberg 1995).

Any group of symmetric transformation which is continuously connected to the identity I is called *continuous symmetry*. A Lie group is the most common type of continuous group and has special importance in physics. The basic idea of a Lie group representations is that we need to study the properties of *infinitesimal* transformations characterized by parameters *infinitesimally close to the identity $U = I$*.

Now, consider a set of elements as a group of transformation $T(\phi)$ which depends on a number of real continuous parameters $\phi = \phi^1, \phi^2, ... \phi^m$, each element of the group connected to the identity by a path within the group. If we take $T(\phi_1)$ and $T(\phi_2)$, we can use the group multiplication as

$$T(\phi_1) \, T(\phi_2) = T(g(\phi_1, \phi_2)), \tag{2.1.8}$$

where $g(\phi_1, \phi_2)$ is a composition function defined as a set of numbers depending on ϕ_1 and ϕ_2. We assume that $\phi = 0$ corresponds to the identity transformation, that means $T(0) = 1$, and therefore $g(\phi_1, 0) = \phi_1$, $g(0, \phi_2) = \phi_2$ and $g(0, 0) = 0$.

The trick to understand the structure of such group is to consider infinitesimal transformation. Let us assume ϕ is infinitesimal, then the unitary operator $U(T(\phi))$ can be expanded around the identity as

$$U(T(\phi)) = 1 + i\phi^a t_a. \tag{2.1.9}$$

Note that we kept only the first order and ignored other terms, because ϕ is infinitesimally small and our constraint is that the operator U has to be unitary. Therefore $U^+U = 1$, then

using (2.1.9) we can write

$$(1 - i\phi^a t_a^+)(1 + i\phi^a t_a) = 1 - i\phi^a(t_a^+ - t_a) = 1. \tag{2.1.10}$$

From (2.1.10), clearly we can see that $t_a = t_a^+$, which means the generator t_a is Hermitian.

To study more deeply the structure of the group, let us consider ϕ is only small but not infinitesimally small as before (which means, we can keep up to the quadratic terms) in the Taylor expansion,

$$U(T(\phi)) = 1 + i\phi^a t_a + \frac{1}{2}\phi^a\phi^b t_{ab}, \tag{2.1.11}$$

where the operator t_{ab} is symmetric $(t_{ab} = t_{ba})$.

Suppose that $U(T(\phi))$ provides a unitary representation of this group of transformations. Therefore, by using (2.1.8) we can write

$$U(T(\phi_1))\, U(T(\phi_2)) = U(T(g(\phi_1, \phi_2))). \tag{2.1.12}$$

Now, using the Taylor expansion we can expand the function $g(\phi_1, \phi_2)$ around the identity (which means around $\phi_1 = \phi_2 = 0$) up to the second order to obtain,

$$g^a(\phi_1, \phi_2) = A^a + B^a{}_b\phi_1^b + C^a{}_b\phi_2^b + D^a{}_{bc}\phi_1^b\phi_2^c + E^a{}_{bc}\phi_1^b\phi_1^c + F^a{}_{bc}\phi_2^b\phi_2^c. \tag{2.1.13}$$

According to the arguments which we discussed after Equation (2.1.8) such that $g(\phi_1, 0) = \phi_1$, $g(0, \phi_2) = \phi_2$ and $g(0, 0) = 0$, we can see that $A^a = 0$, $B^a{}_b = C^a{}_b = \delta^a_b$ and $E^a{}_{bc} = 0 = F^a{}_{bc}$. Therefore, Equation (2.1.13) can be written as

$$g^a(\phi_1, \phi_2) = \phi_1^a + \phi_2^a + D^a{}_{bc}\phi_1^b\phi_2^c. \tag{2.1.14}$$

By using the Taylor expansion and keeping up to the quadratic terms for both sides of the Equation (2.1.12), we can write

$$(1 + i\phi_1^a t_a + \frac{1}{2}\phi_1^a\phi_1^b t_{ab})\, (1 + i\phi_2^a t_a + \frac{1}{2}\phi_2^a\phi_2^b t_{ab}) = 1 - ig^a(\phi_1, \phi_2)t_a + \frac{1}{2}g^a(\phi_1, \phi_2)g^b(\phi_1, \phi_2)t_{ab}. \tag{2.1.15}$$

From Equation (2.1.14), substituting for $g^a(\phi_1, \phi_2)$ and $g^b(\phi_1, \phi_2)$ in the right-hand side of Equation (2.1.15) with a little algebra, we get

$$-t_a t_b = iD^c{}_{ab}t_c + t_{ab}. \tag{2.1.16}$$

By using the fact that t_{ab} is symmetric, Equation (2.1.16) can be written as

$$-t_b t_a = iD^c{}_{ba}t_c + t_{ab}, \tag{2.1.17}$$

and by multiplying Equation (2.1.16) by (-1) and adding it with Equation (2.1.17), we can write

$$t_a t_b - t_b t_a = i(D^c_{\ ba} - D^c_{\ ab})t_c. \tag{2.1.18}$$

We can write $(D^c_{\ ba} - D^c_{\ ab}) \equiv f^c_{\ ab}$, note that $f^c_{\ ab} = -f^c_{\ ba}$. Therefore, Equation (2.1.18) can be written as

$$[t_a - t_b] = i f^c_{\ ab} t_c, \tag{2.1.19}$$

where $[t_a - t_b]$ is called a commutator and $f^c_{\ ab}$ is called the structure constant.

2.1.3   Lorentz Symmetry

In Lorentz transformations, the distance between two events in the direction of motion and time interval could be different in different frames of reference, which can be expressed as

$$\begin{aligned}
ct' &= \gamma\,(ct - \beta x), \\
x' &= \gamma\,(x - \beta ct), \\
y' &= y, \\
z' &= z,
\end{aligned} \tag{2.1.20}$$

where $\gamma \equiv \frac{1}{\sqrt{1 - \frac{v^2}{c^2}}}$, $\beta \equiv \frac{v}{c}$, and (t', x', y', z') and (t, x, y, z) represent an event's coordinates in two frames with relative velocity in x-direction v. Also, Equation (2.1.20) can be written in matrix format, in the form of $x'^\mu = \Lambda^\mu_\nu x^\nu$, where $\mu = 0, 1, 2, 3$ and the Lorentz transformation matrix Λ^μ_ν can be written as

$$\Lambda^\mu_\nu = \begin{pmatrix} \gamma & -\gamma\beta & 0 & 0 \\ -\gamma\beta & \gamma & 0 & 0 \\ 0 & 0 & 1 & 0 \\ 0 & 0 & 0 & 1 \end{pmatrix}. \tag{2.1.21}$$

In the special theory of relativity, the space-time interval ds^2 is an invariant under Lorentz transformations, as all observers who measure time and distance carefully will find the same *space-time* interval between any two events. Mathematically the interval between any two events can be described by

$$ds^2 = \eta_{\mu\nu} dx^\mu dx^\nu, \tag{2.1.22}$$

where $\eta_{\mu\nu}$ can be written as

$$\eta_{\mu\nu} = \begin{pmatrix} 1 & 0 & 0 & 0 \\ 0 & -1 & 0 & 0 \\ 0 & 0 & -1 & 0 \\ 0 & 0 & 0 & -1 \end{pmatrix}. \tag{2.1.23}$$

By using Equation (2.1.22), we can write

$$ds^2 = \eta_{\mu\nu}dx^\mu dx^\nu = \eta_{\alpha\beta}dx'^\alpha dx'^\beta = \eta_{\alpha\beta}\Lambda^\alpha{}_\mu dx^\mu \Lambda^\alpha{}_\nu dx^\nu = (\eta_{\alpha\beta}\Lambda^\alpha{}_\mu \Lambda^\alpha{}_\nu)dx^\mu dx^\nu. \tag{2.1.24}$$

Since x^μ and x^ν are arbitrary, and $\eta_{\alpha\beta}$ is symmetric, this implies,

$$\eta_{\mu\nu} = \eta_{\alpha\beta}\Lambda^\alpha{}_\mu \Lambda^\beta{}_\nu. \tag{2.1.25}$$

Also in Minkowski space-time, from the four-momentum $P = (E/c, p)$ and using the fact that $P.P$ is an invariant quantity, we can derive the dispersion relation as

$$E^2 = p^2 c^2 + m_0^2 c^4, \tag{2.1.26}$$

where, m_0 is the rest mass of the particle (note: for the photon $m_0 = 0$), E and p are the energy and momentum of the particle respectively.

2.1.4 Inhomogeneous Lorentz Group (Poincaré Group)

The inhomogeneous Lorentz group, commonly called the Poincaré group, has ten parameters, four for space-time translations a, and six for homogeneous Lorentz transformations Λ. Therefore, if we have a space-time point x^μ the Poincaré transformation can be defined as

$$x'^\mu \equiv \Lambda^\mu{}_\nu x^\nu + a^\mu. \tag{2.1.27}$$

Sometimes we can use an index-free notation $(x' \mapsto \Lambda x + a)$. This transformation forms a group (Λ, a), which is called the Poincaré group. To study the composition law for the finite transformation, let us start with the vector x and make a transformation $(\Lambda_1 a_1)$ to x', as follows,

$$x \xrightarrow{\Lambda_1 a_1} \Lambda_1 x_1 + a_1 = x'. \tag{2.1.28}$$

Now we can do the same for the transformation to x'' by using $(\Lambda_2 a_2)$, and substituting for x' as

$$x' \xrightarrow{\Lambda_2 a_2} \Lambda_2 x' + a_2 = \Lambda_2(\Lambda_1 x_1 + a_1) + a_2 = \Lambda_2 \Lambda_1 x_1 + \Lambda_2 a_1 + a_2 = x''. \tag{2.1.29}$$

Therefore, the group composition law can be written as

$$(\Lambda_2, a_2) \circ (\Lambda_1, a_1) = (\Lambda_2 \Lambda_1, \Lambda_2 a_1 + a_2). \tag{2.1.30}$$

The term $\Lambda_2 a_1$ reflects the fact that if we do the second Lorentz transformation basically act on the first translations, which makes sense!

Instead of two successive transformations (finite transformation) which we derived in (2.1.30), let us see what happens in the case of infinitesimal transformation. The infinitesimal transformation for the translations is very trivial and can happen just by choosing a very small vector ϵ^μ, and for the Lorentz transformation we could write

$$\Lambda^\mu_\nu = \delta^\mu_\nu + w^\mu_\nu, \tag{2.1.31}$$

where w^μ_ν is an infinitesimal transformation and δ^μ_ν is the Kronecker delta which is equal to 1 for $\mu = \nu$ and otherwise is equal to zero. To study the properties of w^μ_ν, by using Equation (2.1.25), we can write

$$\eta_{\rho\sigma} = \eta_{\mu\nu} \Lambda^\mu_{\ \rho} \Lambda^\nu_{\ \sigma} = \eta_{\mu\nu} (\delta^\mu_{\ \rho} + w^\mu_{\ \rho})(\delta^\nu_{\ \sigma} + {}^\nu_{\ \sigma}) = \eta_{\rho\sigma} + w_{\sigma\rho} + w_{\rho\sigma}. \tag{2.1.32}$$

Note that this is an infinitesimal transformation, therefore we kept the linear terms only. From Equation (2.1.32) clearly we see that, $w_{\sigma\rho} = -w_{\rho\sigma}$. Therefore, $w_{\sigma\rho}$ is an antisymmetric second-rank tensor in four dimensions and has 6 independent components.

To study the structure of the Poincaré group, first we can start by representing the Poincaré group (Λ, a) as an operator acting on the Hilbert space $\mathcal{H}$. As we discussed in the beginning of this chapter (see Section 2.1.2) the most suitable operator in this case is the unitary operator $U(\Lambda, a)$. Therefore, we can write

$$|\psi\rangle = U(\Lambda, a) |\psi\rangle, \tag{2.1.33}$$

and the Poincaré group representation, from Equation (2.1.30) can be written as

$$U(\Lambda_2, a_2) \circ U(\Lambda_1, a_1) = U(\Lambda_2 \Lambda_1, \Lambda_2 a_1 + a_2). \tag{2.1.34}$$

As we did at the beginning of this chapter (see, Section 2.1.2), for an infinitesimal transformation, the unitary operator for the Poincaré group (which can be written as, $U(1 + w, \epsilon)$) must then equal 1 plus terms linear in ϵ and w as (see e.g. Weinberg 1995)

$$U(1 + w, \epsilon) = 1 + \frac{1}{2} i w_{\rho\sigma} J^{\rho\sigma} - i\epsilon_\rho P^\rho, \tag{2.1.35}$$

where $J^{\rho\sigma}$ and P^ρ are the generators of the *Poincaré algebra*, and they should be Hermitian because $U(1+w, \epsilon)$ is unitary. Since $w_{\rho\sigma}$ is antisymmetric (see Equation (2.1.32)), we can take the operator $J^{\rho\sigma}$ to be antisymmetric as well: $J^{\rho\sigma} = -J^{\sigma\rho}$. On the other hand, from the fact that $U(1+w, \epsilon)$ is unitary and linear, the same as (2.1.35) we can expand $U(1+w, \epsilon)$ as

$$U^{-1}(1+w, \epsilon) = U^+(1+w, \epsilon) = 1 - \frac{1}{2}iw_{\rho\sigma}J^{\rho\sigma} + i\epsilon_\rho P^\rho. \tag{2.1.36}$$

Now, we are going to find out how J and P behave under a Poincaré transformation. If we have an operator O, acting on $\langle\phi|$ and $|\psi\rangle$, to study how the operator O looks from an another observer O', we can use the following trick!

$$\langle\phi|O|\psi\rangle = \langle\phi|U^+UOU^+U|\psi\rangle = \langle U\phi|UOU^+|U\psi\rangle = \langle U\phi|O'|U\psi\rangle. \tag{2.1.37}$$

By using the same trick which we used in (2.1.37), and using Equations (2.1.36) and (2.1.37) with some algebra (also, see e.g. Weinberg 1995), we can write

$$\begin{aligned} U(\Lambda, a)\, U(1+w, \epsilon)\, U^{-1}(\Lambda, a) &= U(\Lambda, a)\, (1 + \frac{1}{2}iw_{\rho\sigma}J^{\rho\sigma} - i\epsilon_\rho P^\rho)\, U^{-1}(\Lambda, a) \\ &= U(1 + \Lambda w\Lambda^{-1}, \Lambda\epsilon - \Lambda w\Lambda^{-1}a). \end{aligned} \tag{2.1.38}$$

Consequently, we can write

$$U(\Lambda, a)\, J^{\mu\nu}\, U^{+1}(\Lambda, a) = \Lambda_\rho{}^\mu\Lambda_\sigma{}^\nu\, (J^{\rho\sigma} - a^\rho P^\sigma + a^\sigma P^\rho), \tag{2.1.39}$$

and

$$U(\Lambda, a)\, P^\mu\, U^{+1}(\Lambda, a) = \Lambda_\rho{}^\mu P^\rho. \tag{2.1.40}$$

In order to get the Poincaré algebra, one could take Λ and a in Equation (2.1.39) and (2.1.40) to be infinitesimal ($\Lambda \mapsto 1+\tilde{w}$, $a \mapsto \tilde{\epsilon}$), through substituting in (2.1.39) and (2.1.40), and doing some algebra (also, see e.g. Weinberg 1995), the commutation rules can be written as

$$\begin{aligned} i[J^{\mu\nu}, J^{\rho\sigma}] &= \eta^{\nu\rho}J^{\mu\sigma} - \eta^{\mu\rho}J^{\nu\sigma} - \eta^{\sigma\mu}J^{\rho\nu} + \eta^{\sigma\nu}J^{\rho\mu}, \\ i[P^\mu, J^{\rho\sigma}] &= \eta^{\mu\rho}P^\sigma - \eta^{\nu\sigma}P^\rho, \\ [P^\mu, P^\rho] &= 0. \end{aligned} \tag{2.1.41}$$

In order to give physical meaning to the generators J and P, one could start by the simple abelian sub-group (such as translation only, in the Poincaré group). By abelian we mean non-commutative (see previous sections). We can assume that we have an element in the group $U(1, a)$ and $U(1, b)$, by applying the group multiplication, from Equation (2.1.34), we can notice

that this is just a translation, which is can be written as

$$U(1, a) \circ U(1, b) = U(1, a + b). \tag{2.1.42}$$

From Equation (2.1.42), if $a = b$, we can write

$$U(1, a) \circ U(1, b) = U(1, 2a). \tag{2.1.43}$$

Using Equation (2.1.43), we can do a little trick by writing any finite element in the group as

$$U(1, a) = U(1, \frac{a}{N})^N, \tag{2.1.44}$$

which means that we are doing small translations N times.

Now, we can consider an infinitesimal transformation, using Equation (2.1.35) after setting $w = 0$, because we are considering the translation only. Therefore Equation (2.1.44) can be written as

$$U(1, a) = \lim_{N \to \infty} U(1, \frac{a}{N})^N = \lim_{N \to \infty} (1 - i\frac{a_\mu}{N} P^\mu)^N = e^{-ia_\mu P^\mu}. \tag{2.1.45}$$

Now, let us consider $a^\mu = \{t, 0, 0, 0\}$; we can see that this corresponds to an operator e^{-itP^0}. Therefore, from the foundation of quantum mechanics and by setting the Planck constant $h = 1$, clearly we can see that the zero component P^0 has to be identified with the Hamiltonian H. If P^0 is the Hamiltonian, the other three components P^1, P^2, P^3 can be identified with the momentum operator P and the angular momentum operator J can be identified as J^{23}, J^{31}, J^{12}, (for more details, e.g. Weinberg 1995).

In physics, the operators that commute with all elements of the algebra are called Casimir operators, while one of the easy examples for a Casimir operator of the Poincaré group is $P^2 \equiv P_\mu P^\mu$.

A single particle has a unique value,

$$P^2 \equiv P_\mu P^\mu = M^2, \tag{2.1.46}$$

where M is the rest mass of the particle. Also in the Poincaré group there is another Casimir operator W^2, which can be obtained by defining a vector (see e.g. Das & Okubo 2014; Weinberg 1995)

$$W^\mu \equiv \epsilon^{\mu\nu\sigma\rho} P_\nu J_{\sigma\rho}, \tag{2.1.47}$$

where $\epsilon^{\mu\nu\sigma\rho}$ is an antisymmetric (Levi-Civita) and W^μ is a four-dimensional vector called Pauli-Ljubanski vector.

The quantity $W^2 = M_\mu M^\mu$ is Lorentz invariant and hence commutes with all generators, which

describes the spin of the particle and M_μ is the generators of rotation transformation (for more details see, e.g., Weinberg 1995).

2.2 Lorentz Symmetry Violation

Lorentz symmetry (invariance) is considered to be one of the pillars of modern physics and a fundamental symmetry in Quantum Field Theory (QFT). During the last few decades, there have been many theoretical suggestions that a Lorentz symmetry may not be an exact symmetry at all energies. Due to the importance of this research topic, there are several papers on studying the Lorentz invariant violation (see for example Colladay & Kostelecký 1998; Carroll et al. 2001; Hinchliffe et al. 2004). Moreover, various approaches have been used for violating Lorentz symmetry such as string theory (see for example Fujikawa 1984), Lorentz violation in supersymmetric field theories (see for example Nibbelink & Pospelov 2005), assuming preferred reference frames a revival of the old aether idea (see e.g. Jacobson & Mattingly 2004) and non-commutative field theory (see for example Carroll et al. 2001; Hinchliffe et al. 2004; Borowiec et al. 2010). In this thesis we are not going to dive into the details of all possibilities, just we will use the tools which have been developed in the previous section to see how a Lorentz symmetry can be broken by using non-commutative geometry, again diving into the technical details of the non-commutative algebra is beyond the scope of this work (more details can be found in Carroll et al. 2001; Hinchliffe et al. 2004). In Section 2.2.2, we will highlight the consequences of the Lorentz Invariance Violation (LIV) effect, the possibility of unfamiliar physics and possible future observations.

2.2.1 Non-Commutative Geometry

The difference between classical and quantum mechanics is that the algebra of the observables in classical systems can be described by commutative algebras but in quantum mechanics, the algebra of observables (such as the position x, and the momentum p) is non-commutative:

$$[x, p] = i\hbar. \tag{2.2.1}$$

By non-commutative, we mean that the commutator is not equal zero (see Equation 2.1.19 in Section 2.1.2 in this chapter). The earliest published work regarding the coordinates that may not commute is the work of Snyder (1947), who acknowledges Heisenberg's principle (mathematically described by equation 2.2.1). One of the consequences of non-commutative geometry

is the Lorentz symmetry breaking, which could lead to interesting new phenomenological possibilities (e.g., Carroll et al. 2001) and also to alternative or new theories that lie beyond standard-model physics (e.g., Colladay 1997). Generally, the non-commutative space-time can be defined as a deformation of ordinary space-time in which the space-time coordinates x_μ can be represented by non-commutative Hermitian operators $\hat{x}_\mu$ (for more details see Carroll et al. 2001; Hinchliffe et al. 2004):

$$[\hat{x}_\mu, \hat{x}_\nu] = i\lambda_P^2 \theta_{\mu\nu}, \qquad (2.2.2)$$

where λ_P is the Plank length and $\theta_{\mu\nu}$ is an antisymmetric tensor. Note that for $\theta_{\mu\nu} \to 0$ the standard commutation relation is recovered. Also one could prove that Equation (2.2.2) is not an invariant under the action of the Poincaré group ($\hat{x}_\mu \mapsto \hat{x}'_\mu \equiv \Lambda_\mu^\alpha \hat{x}_\alpha + a_\mu$) as follows:

$$[\hat{x}'_\mu, \hat{x}'_\nu] = i\lambda_P^2 \Lambda_\mu^\alpha \Lambda_\nu^\beta \ \theta_{\alpha\beta} \neq [\hat{x}_\mu, \hat{x}_\nu]. \qquad (2.2.3)$$

If we impose

$$[\hat{x}'_\mu, \hat{x}'_\nu] = i\lambda_P^2 \theta_{\mu\nu} = [\hat{x}_\mu, \hat{x}_\nu], \qquad (2.2.4)$$

this group is no longer the Poincaré group, but a deformed version of it (for more details see Martinetti 2015), called $\theta-Poincaré\ group$. From Equation (2.2.4) one can note that this group is characterized by a non-trivial commutation relation for the translation, as follows:

$$[a_\mu, a_\nu] = i\theta_{\mu\nu} - i\theta_{\alpha\beta}\Lambda_\mu^\alpha \Lambda_\nu^\beta. \qquad (2.2.5)$$

By considering the boost N_i, the rotations M_i and the momentum P_μ, the deformed commutation relations can be written as (Majid & Ruegg 1994)

$$\begin{aligned}
[P_\mu, P_\nu] &= 0, \\
[M_i, P_0] &= 0, \\
[M_i, P_j] &= i\epsilon_{ijk}P_k, \\
[M_i, M_j] &= i\epsilon_{ijk}M_k, \\
[M_i, N_j] &= i\epsilon_{ijk}N_k, \\
[N_i, N_j] &= -i\epsilon_{ijk}M_k, \\
[N_i, P_j] &= i\delta_{ij}\left(\frac{\kappa}{2}(1 - e^{-2P_0/\kappa}) + \frac{1}{2\kappa}\overrightarrow{P}^2\right) - i\frac{1}{\kappa}P_iP_j, \\
[N_i, P_0] &= iP_i,
\end{aligned} \qquad (2.2.6)$$

where ϵ_{ijk} is an antisymmetric tensor, κ is constant, i, j = 1, 2, 3.

Using the deformed commutation relations (2.2.6) with some algebra (for more details see,

Majid & Ruegg 1994; Kosinski et al. 1995), the Casimir for this algebra has the form

$$M^2 = \frac{P_0^2 - \overrightarrow{P}^2}{1 - \frac{P_0}{\kappa}}. \tag{2.2.7}$$

Equation (2.2.7), can be written as

$$P_0^2 = \overrightarrow{P}^2 + M^2 \left(1 - \frac{P_0}{\kappa}\right). \tag{2.2.8}$$

As has been explained from Equation (2.1.45), P_0 is the representative Hamiltonian (energy) of the particle and $\overrightarrow{P}$ is the momentum of the particle and M is the rest mass energy for the particle (see equation 2.1.46).

The deformed Casimir relation (2.2.8), could lead to a modification of the dispersion relation as follows (see, e.g., Carroll et al. 2001; Martinetti 2015)

$$E^2 = p^2 c^2 + m^2 c^4 \left(1 + \xi \frac{E}{E_P} + \ ...\ \right), \tag{2.2.9}$$

where E_P is the Planck energy scale, c the conventional speed of light in vacuum and ξ is dimensionless parameter. Also, there are several other approaches by considering non-commutative algebra such as *k-Poincaré deformation*, which lead to modification for the commutation rules (2.1.41) and therefore one can expect non-negligible deformation for the dispersion relation. For example, detailed calculation by using $k-$deformed Minkowski spacetime provided with non-commutative coordinates can be found in Borowiec et al. (2010).

2.2.2   Time-Lag due to the Lorentz Invariance Violation Effect

The speed of light c in a refractive medium depends on its wavelength (frequency) as a shorter wavelength (higher frequency) is expected to propagate more slowly than a longer wavelength (lower frequency) counterpart. This effect is due to the sensitivity of photons to the microscopic structure of the refractive medium of the materials. Several quantum gravity (QG) theories predict that VHE gamma ray photons could be sensitive to the microscopic structure of spacetime, that can lead to the Lorentz invariance violation. Therefore, gamma rays with higher energy are expected to propagate more slowly compared to their lower-energy counterparts (e.g., Amelino et al. 1998; Bolmont 2016; Tavecchio & Bonnoli 2016; Lorentz & Brun 2017). This would lead to an energy-dependent refractive index for light in vacuum (see, e.g., Bolmont 2016). The deviation from Lorentz symmetry can be measured by comparing the arrival time of photons at different energies originating from the same astrophysical source (see, e.g., Amelino

et al. 1998; Bolmont 2016; Lorentz & Brun 2017). For more general cases both subluminal and superluminal modifications of the photon dispersion relation can be considered, subluminal meaning that decreasing photon speed with decreasing wavelength and superluminal means increasing photon speed with decreasing wavelength. Using Equation (2.2.9), we can write the modified dispersion relation for the photons and electrons as (see also., Bolmont 2016):

$$E^2 = p^2c^2 + m^2c^4 + SE^2 \left(\frac{E}{E_{LIV}}\right)^n, \tag{2.2.10}$$

where $S = -1$ represents a subluminal scenario, and $S = +1$ represents the superluminal case. The characteristic energy E_{LIV} is parameterized as a fraction of the Planck energy, $E_{\text{LIV}} = E_P/\xi_n$, where the order of the leading correction n and the dimensionless parameter ξ_n depend on the theoretical framework particle type (see e.g., Amelino et al. 1998; Bolmont 2016; Tavecchio & Bonnoli 2016). A value of $E_{LIV} \sim E_P$ (i.e., $\xi_1 = 1$) has been considered to be the physically best motivated choice (see, e.g., Liberati & Maccione 2009; Fairbairn et al. 2014; Tavecchio & Bonnoli 2016), which is also consistent with the results of (Biteau & Williams 2015) that constrained $E_{LIV} > 0.65\ E_P$. For photons, Equation (2.2.10) can be written as:

$$E^2 = p^2c^2 + S\frac{E^3}{E_{LIV}}. \tag{2.2.11}$$

Note that we consider only the leading correction $n = 1$ case. From Equatin (2.2.11) we can calculate the speed $v = dE/dp$ as:

$$2EdE/dp \ - \ 3S\frac{E^2}{E_{LIV}}dE/dp \ = \ 2pc^2, \tag{2.2.12}$$

therefore,

$$v = dE/dp = \frac{pc^2}{E(1 - \frac{3}{2}\frac{S\ E}{E_{LIV}})}. \tag{2.2.13}$$

From Equation (2.2.11) we can substitute for p, by $p = \frac{E}{c}\sqrt{(1 - S\frac{E}{E_{LIV}})}$ to get

$$v = dE/dp = c\ \left(\frac{\sqrt{(1 - S\frac{E}{E_{LIV}})}}{(1 - \frac{3SE}{2E_{LIV}})}\right) \approx c\ \left(\frac{(1 - S\frac{E}{2E_{LIV}})}{(1 - \frac{3SE}{2E_{LIV}})}\right). \tag{2.2.14}$$

By setting $x = S\frac{E}{E_{LIV}}$ and using a binomial approximation, Equation (2.2.14) can be written as

$$\frac{1 - x/2}{1 - 3x/2} = (1 - x/2)(1 - 3x/2)^{-1} = (1 - x/2)(1 + 3x/2) = 1 - x/2 + 3x/2 + (3/4)x^2.$$

Therefore, by neglecting the last term, because it is second order and x is small, we can write

$$v \approx c \left(1 + S \frac{E}{E_{LIV}} \right).$$

(2.2.15)

From Equation (2.2.15) we can see that the photon speed in the case of a subluminal scenario ($S = -1$) is decreasing with increasing energy and the other way around in the case of a superluminal scenario.

The time lag between two photons when they reach earth depends on the red-shift of the source and on cosmological parameters. We can consider two photons with energies E_h for the high energy photon and E_l for the low energy photon, measured at redshift $z = 0$. By using the ΛCDM model one can calculate the corresponding co-moving distance for each photon. The time-lag over energy difference Δt_n can be written as (for more details see Bolmont 2016):

$$\Delta t_n = S \, \frac{n+1}{2} \, \frac{E_h^n - E_l^n}{E_{LIV}} \int_0^z \frac{(1 + z')^n}{H(z')} dz',$$

(2.2.16)

where $H(z') = H_0 \sqrt{[\Omega_m (1 + z')^3 + \Omega_\Lambda]}$. Recently, there have been several attempts for different VHE gamma ray sources such as Mrk 501 to constrain the LIV scale E_{LIV}, (for details see e.g., Bolmont 2016).

2.2.3 Lorentz Invariance Violation and Photon Stability

According to the standard quantum electrodynamics the following interaction is forbidden,

$$\gamma \rightarrow e^+ + e^-.$$

Before trying frameworks different from the standard quantum electrodynamics (QED), we are going to prove why the above process is not possible according to the standard QED. The four momentum $\underline{P}_{ph}$ for a photon can be written as

$$\underline{P}_{ph} = \frac{E_{ph}}{c} \begin{pmatrix} 1 \\ \hat{k} \end{pmatrix},$$

(2.2.17)

where E_{ph} is the energy of the photon. The four momentum $\underline{P}_e \pm$ of the electron-positron pair,

$$\underline{P}_e \pm = \gamma_{e\pm} m_e c \begin{pmatrix} 1 \\ \beta_{e\pm} \end{pmatrix}.$$

(2.2.18)

By writing the law of conservation and square both sides, we can write

$$\left(\underline{P}_{ph} \right)^2 = \left(\underline{P}_{e+} + \underline{P}_{e-} \right)^2 \implies \left(\underline{P}_{ph} \right)^2 = \underline{P}_{e+}^2 + \underline{P}_{e-}^2 + 2\underline{P}_{e+}\underline{P}_{e-}.$$

(2.2.19)

For the photon, by using (2.2.17) we can write

$$\left(\underline{P}_{ph}\right)^2 = \frac{E_{ph}^2}{c^2}(1 - \hat{k}.\hat{k}) = \frac{E_{ph}^2}{c^2}(1 - 1) = 0. \qquad (2.2.20)$$

Also from (2.2.18) and (2.2.19) for the electron-positron pair we can get

$$\underline{P}_{e+}^2 + \underline{P}_{e-}^2 + 2\underline{P}_{e+}\underline{P}_{e-} = (m_e c)^2 + (m_e c)^2 + 2(m_e c)^2 = 4(m_e c)^2. \qquad (2.2.21)$$

The energy and momentum should be simultaneously conserved, but clearly we can notice from (2.2.20) and (2.2.21) that in this case it is not. That means that, a single photon **cannot** produce an electron-positron pair without interacting with another photon, according to standard QED.

Now we are going to consider the Lorentz invariance violation to calculate the photon energy and momentum. If we consider the modified dispersion (2.2.9), the four-momentum for the photons, can be written as

$$p_\gamma.p_\gamma = \frac{E_\gamma^2}{c^2} - p_\gamma^2 = \frac{1}{c^2}\left(p_\gamma^2 c^2 - S\frac{E_\gamma^3}{E_{LIV}}\right) - p_\gamma^2 = -S\frac{E_\gamma^3}{c^2 E_{LIV}}. \qquad (2.2.22)$$

From Equations (2.2.21) and (2.2.22), and by considering the subliminal case ($S = -1$), we can write

$$\frac{E_\gamma^3}{c^2 E_{LIV}} = 4(m_e c)^2. \qquad (2.2.23)$$

Then, the threshold energy for such interaction can be written as:

$$E_\gamma = (4m_e^2 c^4 E_{LIV})^{\frac{1}{3}}. \qquad (2.2.24)$$

According to many arguments and constraints $E_{LIV} \sim E_P$ (e.g., Liberati & Maccione 2009; Fairbairn et al. 2014; Tavecchio & Bonnoli 2016). From (2.2.24) we can see that a single photon can produce an electron-positron pair, if the photon has energy $E_\gamma \geq 10$ TeV.

A generic approach for calculating the squared probability amplitude for vacuum Cherenkov radiation and the possibility of the photon decay by correcting the QED coupling at first order in LIV parameters is presented in (Martínez-Huerta & Pérez-Lorenzana 2016), where they found that vacuum Cherenkov radiation and photon decay, kinetically forbidden in a Lorentz invariant framework but can be possible under the LIV hypothesis.

2.2.4 Cosmic Gamma Ray Horizon and the Lorentz Invariance Violation Effect

Gamma ray photons with energies greater than the electron-positron pair-production threshold from objects (e.g. blazers) located at a large distance can expected to be affected by their QED interaction with low-energy extrag-alactic diffused photons (Nikishov 1962). The intergalactic gamma-gamma absorption signatures have attracted great interest in astrophysics and cosmology (see Chapter 1). From equation (2.2.10), we can see that the LIV modifies the dispersion relation for gamma rays it could also affect the kinematics in the pair production process. With this modification and the cross-section for interaction that attenuates the VHE-gammaa rays as it travels through the diffuse extragalactic background radiation (see, e.g., Amelino et al. 1998; Bolmont 2016; Tavecchio & Bonnoli 2016; Abdalla & Böttcher 2018).

In Chapter 5 and Chapter 6, detailed calculations considering a subluminal and a superluminal modification of the photons dispersion relation for the LIV effect by considering EBL gamma-gamma absorption and also the impact of the LIV effect on the Compton scattering process are presented.

References

Abdalla, H. & Böttcher, M., ApJ, 865, 159, arXiv: 1809.00477

Amelino-Camelia, G., Ellis, J., Mavromatos, N. E., Nanopoulos, D. V., & Sarkar, S. 1998, Nature, 393, 763

Biteau, J. & Williams D. A. 2015, ApJ, 812, 1

Borowiec, A. and Gupta, Kumar S. and Meljanac, S. and Pachol, A., 2010, EPL, 92, 2, arXiv: 0912.3299

Bolmont, J. 2016, Is the speed of light in vacuum really constant ?. Astrophysics [astro-ph]. UPMC, tel-01388037, https://hal.sorbonne-universite.fr/tel-01388037/document

Colladay, D. and Kostelecký, V. A., 1998, Phys. Rev. D 58 , 116002, arXiv: hep-ph/9809521

Carroll, S. M., et al., 2001, Phys. Rev. Lett. 87 141601

Colladay, D., Kostelecký, V.A., 1997, Phys. Rev. 55 6760

Gross, D. J., 1996, Proc. Natl. Acad. Sci. USA, 93, 4256

Das, A., & Okubo, S., 2014 , Lie Groups and Lie Algebras for Physicists, World Scientific Publishing Co., Inc., River Edge, NJ, USA, ISBN:9814603279 9789814603270

Fairbairn, M., Nilsson, A., Ellis, J., Hinton, J. & White, R. 2014, JCAP, 1406, 005

Fujikawa, K., 1984 Phys. Rev. D 29, 285

Hinchliffe, I. and Kersting, N. and Ma, Y. L., 2004, Int. J. Mod. Phys., A19, 179, arXiv: hep-ph/0205040

Jacobson T. and Mattingly D., 2004, Phys. Rev. D70 024003, arXiv:gr-qc/0402005

Kosinski, P., Lukierski, J., Maslanka, P. & Sobczyk, J., 1995, Mod. Phys. Lett., A10, 2599, arXiv: hep-th/9412114

Liberati, S. & Maccione, L., 2009, Ann. Rev. Nucl. Part. Sci., 245, 59

Lorentz, M. & Brun, P. 2017, Proceedings, 6th Roma International Workshop on Astroparticle Physics (RICAP16): Rome, Italy, June 21-24, 136, 03018

Majid, S. & Ruegg, H., 1994, Phys. Lett., B334, 348, arXiv: hep-th/9405107

Martinetti, P., J., 2015, Phys. Conf. Ser. 634, 1, arXiv: 1510.08348

Martínez-Huerta, H. & Pérez-Lorenzana, A., 2016, J. Phys. Conf. Ser., 761, 012035, arXiv:1609.07185

Nikishov, A. I. 1962, Sov. Phys. JETP, 14, 393

Nibbelink, S. G. and Pospelov, M., 2005 Phys. Rev. Lett. 94, 081601, arXiv:hep-ph/0404271.

Snyder, H. S., 1947, Phys. Rev. 71, 38–41

Tavecchio, F. & Bonnoli, G., 2016, Astron. Astrophys., 585, A25

Weinberg, S., 1995, The Quantum Theory of Fields, Cambridge University Press, Cambridge, doi:10.1017/CBO9781139644167

EBL Inhomogeneity and Hard-Spectrum Gamma Ray Sources

EBL INHOMOGENEITY AND HARD-SPECTRUM GAMMA-RAY SOURCES

Hassan Abdalla [1,2] and Markus Böttcher[1]

[1]Centre for Space Research, North-West University, Potchefstroom 2520, South Africa
[2]Department of Astronomy and Meteorology, Omdurman Islamic University, Omdurman 382, Sudan

ABSTRACT

The unexpectedly hard very-high-energy (VHE; $E > 100$ GeV) γ-ray spectra of a few distant blazars have been interpreted as evidence for reduction of the $\gamma\gamma$ opacity of the Universe due to the interaction of VHE γ-rays with the extragalactic background light (EBL) compared to the expectation from our current knowledge of the density and cosmological evolution of the EBL. One of the suggested solutions to this problem consisted of the inhomogeneity of the EBL. In this paper, we study the effects of such inhomogeneities on the energy density of the EBL (which then also becomes anisotropic) and the resulting $\gamma\gamma$ opacity. Specifically, we investigate the effects of cosmic voids along the line of sight to a distant blazar. We find that the effect of such voids on the $\gamma\gamma$ opacity, for any realistic void size, is only of the order of $\lesssim 1$ % and much smaller than expected from a simple linear scaling of the $\gamma\gamma$ opacity with the line-of-sight galaxy under-density due to a cosmic void.

Keywords: radiation mechanisms: non-thermal — galaxies: active — galaxies: jets — cosmology: miscellaneous

1. INTRODUCTION

Gamma rays from astronomical objects at cosmological distances with energies greater than the threshold energy for electron-positron pair production can be annihilated due to $\gamma\gamma$ absorption by low-energy extragalactic photons. The importance of this process for high-energy astrophysics was first pointed out by Nikishov (1962). In particular, very-high-energy (VHE; $E > 100$ GeV) γ-ray emission from blazars is subject to $\gamma\gamma$ absorption by the extragalactic background light (EBL), resulting in a high-energy cut-off in the γ-ray spectra of blazars (e.g., Stecker 1992). The probability of absorption depends on the photon energy and the distance (redshift) of the source. Studies of intergalactic $\gamma\gamma$ absorption signatures have attracted further interest in astrophysics and cosmology due to their potential use to probe the cluster environments of blazars (Sushch & Böttcher 2015) and to estimate cosmological parameters (Biteau & Williams 2015). However, bright foreground emissions prevent an accurate direct measurement of the EBL (Hauser & Dwek 2001). Studies of the EBL therefore focus on the predicted $\gamma\gamma$ absorption imprints and employ a variety of theoretical and empirical methods (e.g., Stecker 1969, 1992; Aharonian et al. 2006; Franceschini et al. 2008; Razzaque et al. 2009; Finke et al. 2010; Dominguez et al. 2011a; Gilmore et al. 2012). All the cited works agree that the universe should be opaque (i.e., $\tau_{\gamma\gamma} \gtrsim 1$) to VHE γ-rays from extragalactic sources at high redshift ($z \gtrsim 1$).

Observations of distant ($z \gtrsim 0.5$) γ-ray blazars have been interpreted by some authors (e.g., MAGIC Collaboration 2008; Archambault et al. 2014) as evidence that the universe may be more transparent to very high energy γ-rays than expected based on all existing EBL models. Furthermore, several studies have found that, after correction for EBL absorption, the VHE γ-ray spectra of several blazars appear to be unexpectedly hard (photon indices $\Gamma_{\rm ph} \lesssim 1.5$) and/or exhibit marginal hints of spectral upturns towards the highest energies (e.g., Finke et al. 2010; Furniss et al. 2013). These unexpected VHE signatures in the spectra of distant blazars — although present only at marginal significance — are currently the subject of intensive research. Possible solutions include the hypothesis that the EBL density is generally lower than expected from current models (Furniss et al. 2013); the existence of exotic axion like particles (ALPs) into which VHE γ-rays can oscillate in the presence of a magnetic field, thus enabling VHE-photons to avoid $\gamma\gamma$ absorption (Dominguez et al. 2011b); an additional VHE γ-ray emission component due to interactions along the line of sight of extragalactic ultra-high-energy cosmic rays (UHECRs) originating from the blazar (e.g., Essey & Kusenko 2010); and EBL inhomogeneities. The idea of EBL inhomogeneities was considered by Furniss et al. (2015), who found tentative hints for correlations between hard VHE γ-ray sources and under-dense regions along the line of sight. They suggested a direct, linear scaling of the EBL $\gamma\gamma$ opacity with the line-of-sight galaxy number

density. The effect of EBL inhomogeneities on the $\gamma\gamma$ opacity was also investigated by Kudoda & Faltenbacher (2016). However, in that work, EBL inhomogeneities were considered only as a modulation of the redshift dependence of the cosmic star formation rate, without a detailed consideration of the geometrical effects of large-scale structure of the Universe. Both Furniss et al. (2015) and Kudoda & Faltenbacher (2016) concluded that the possible reduction of the EBL $\gamma\gamma$ opacity due to inhomogeneities is likely negligible.

In this paper, we investigate the effect of cosmological inhomogeneities on the energy density of the EBL and the resulting $\gamma\gamma$ opacity with a detailed calculation of the inhomogeneous and anisotropic EBL in a realistic geometrical model setup. Specifically, we will consider the effect of cosmic voids along the line of sight to a distant blazar and investigate the resulting inhomogeneous and anisotropic EBL radiation field. In Section 2, we describe the model setup and the method used to evaluate the EBL characteristics and the resulting $\gamma\gamma$ opacity. The results are presented in Section 3, where we also compare our results to a simple linear scaling of the EBL $\gamma\gamma$ opacity with the line-of-sight galaxy count density for the specific example of PKS 1424+240. We summarize and discuss our results in Section 4.

2. EBL IN THE PRESENCE OF A COSMIC VOID

Our calculations of the inhomogeneous EBL are based on a modified version of the formalism presented in Razzaque et al. (2009), considering only the direct starlight. The effect of re-processing of starlight by dust has been included in Finke et al. (2010) and leads to an additional EBL component in the mid- to far infrared, which is neglected here. Since dust re-processing is a local effect, it will be affected by cosmic inhomogeneities in the same way as the direct starlight contribution considered here.

For the purpose of a generic study of the effects of cosmic voids along the line of sight to a blazar, we start out by considering a single spherical cosmic void located with its center at redshift z_v and radius R between the observer and a γ-ray source at redshift z_s. The geometry is illustrated in Figure 1. We calculate the angle- and photon-energy-dependent EBL energy density at each point between the observer and the source by using co-moving coordinates, converting redshifts z to distances $l(z)$. The cosmic void is represented by setting the star formation rate to 0 within the volume of the void.

For the evaluation of the differential EBL photon number density spectrum at a given redshift z, we modify the expression from Razzaque et al. (2009), based on the direct contribution from stars throughout cosmic history:

$$
\begin{aligned}
\frac{dN(\epsilon, z)}{d\Omega d\epsilon dV} = &\int_{\tilde{z}=z}^{\infty} d\tilde{z} \left| \frac{dt}{d\tilde{z}} \right| \Psi(\tilde{z}) f_{\text{void}}(\Omega, \tilde{z}) \int_{M_{min}}^{M_{max}} dM \left(\frac{dN}{dM} \right) \\
&\times \int_{max\{0, z_d(M, z')\}}^{\tilde{z}} dz' \left| \frac{dt}{dz'} \right| f_{\text{esc}}(\epsilon') \frac{dN(\epsilon', M)}{d\epsilon' dt} (1 + z').
\end{aligned}
\tag{1}
$$

where Ω represents the solid angle with respect to the photon propagation direction, and $f_{\text{void}}(\Omega, \tilde{z})$ is the step function set to zero within the void, as specified below. $\Psi(\tilde{z})$ is the cosmic star formation rate, dN/dM is the stellar mass function, $dN(\epsilon', M)/(d\epsilon' dt)$ is the stellar emissivity function, and $f_{\text{esc}}(\epsilon')$ is the photon escape probability, for which we use the parameterizations of Razzaque et al. (2009). $dt/d\tilde{z}$ is evaluated using a concordance cosmology with $\Omega_m = 0.3$, $\Omega_\Lambda = 0.7$ and $h = 0.7$.

From Figure 1 we can find the distances l_1 and l_2 where the gamma-ray propagation direction Ω crosses the boundaries of the void, as

$$
\ell_{1,2} = \ell_v \, \mu \mp \sqrt{R^2 - \ell_v^2 \sin^2 \theta},
\tag{2}
$$

where $\mu = \cos\theta$ is the cosine of the angle between the line of sight and the gamma-ray propagation direction, $\Omega = (\theta, \phi)$. The maximum angle $\theta_{\max}$ at which the gamma-ray travel direction still crosses the boundary at one point, is given by:

$$
\sin\theta_{\max} = \frac{R}{\ell_v}.
\tag{3}
$$

and the corresponding distance to the tangential point, $\ell_{\max}$, is given by

$$
\ell_{\max} = \ell_v \, \cos\theta_{\max}.
\tag{4}
$$

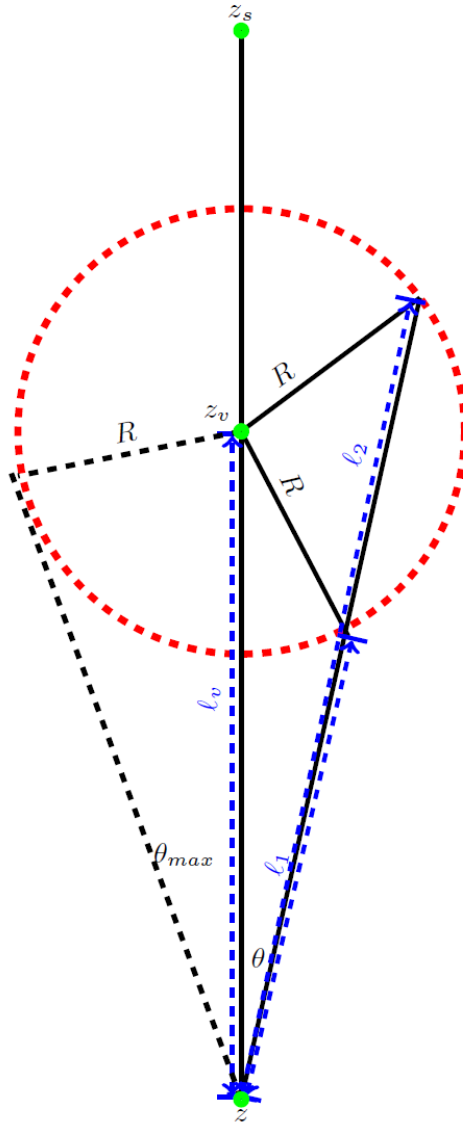The void condition can now be written as

Figure 1. Illustration of an underdense region between the observer at redshift z and source at redshift z_s. We assume that the underdense region has a radius R and the redshift at the center of the underdense region is z_v.

$$f_{\text{void}}^{\text{outside}} = \begin{cases} 0 & \text{if} \quad \ell_1 < \tilde{\ell} < \ell_2 \\ 1 & \text{else} \end{cases}$$

for points z along the line of sight that are located outside the void, and

$$f_{\text{void}}^{\text{inside}} = \begin{cases} 0 & \text{if} \quad \tilde{\ell} < \ell_2 \\ 1 & \text{else} \end{cases}$$

for points z along the line of sight located inside the void. Note that, although the star formation rate has been set to zero inside the void, the EBL is not zero there because of the contribution from the rest of the Universe outside the void.

To calculate the EBL density in comoving cordinates, the photon energy and volume can be transformed as $\epsilon_1 = \epsilon(1 + z_1)$ and $V_1 = V/(1 + z_1)^3$ respectively. Using equation (1), the EBL energy density can then be written as

(Razzaque et al. 2009):

$$\epsilon_1 \mu_{\epsilon_1}(\epsilon_1, z_1, \Omega) = (1+z_1)^4 \; \epsilon^2 \; \frac{dN(\epsilon, z = z_1)}{d\Omega \; d\epsilon \; dV}. \tag{5}$$

With this expression for the EBL energy density, we can calculate the optical depth due to $\gamma\gamma$ absorption for a γ-ray photon from a source at redshift z_s with observed energy E as (Gould & Schréder 1967):

$$\tau_{\gamma\gamma}(E, z_s) = c \; \int_0^{z_s} dz_1 \left| \frac{dt}{dz_1} \right| \oint d\Omega \int_0^\infty d\epsilon_1 \; \frac{\mu_{\epsilon_1}(\epsilon_1, z_1, \Omega)}{\epsilon_1} \; (1-\mu)\sigma_{\gamma\gamma}(s). \tag{6}$$

The $\gamma\,\gamma$ pair-production cross section $\sigma_{\gamma\gamma}(s)$ can be written as:

$$\sigma_{\gamma\gamma}(s) = \frac{1}{2}\pi r_e^2 (1-\beta_{cm}^2) \left[(3-\beta_{cm}^4)\ln\left(\frac{1+\beta_{cm}}{1-\beta_{cm}}\right) - 2\beta_{cm}(2-\beta_{cm}^2) \right] H\left(\frac{(1+z_1)E\epsilon_1(1-\mu)}{2(m_e c^2)^2} - 1 \right) \tag{7}$$

where r_e is the classical electron radius and $\beta_{cm} = (1-\frac{1}{s})^{1/2}$ is the electron-positron velocity in the center-of-momentum (c.m.) frame of the $\gamma\gamma$ interaction, $s = \frac{s_0}{2}(1-\cos\theta)$ is the c.m. frame electron/positron energy squared, $s_0 = \frac{\epsilon E}{m_e^2 c^4}$ and H is the Heaviside function, $H(x) = 1$ if $x \geq 0$ and $H(x) = 0$ otherwise, representing the threshold condition that pair production can only occur if $\frac{(1+z_1)E\epsilon_1(1-\mu)}{2(m_e c^2)^2} > 1$.

In the case of a homogeneous and isotropic EBL (with which we will compare our results for the inhomogeneous EBL case), equation (6) can be simplified using the dimensionless function $\bar{\varphi}$ defined by Gould & Schréder (1967):

$$\bar{\varphi}[s_0(\epsilon)] = \int_1^{s_0(\epsilon)} s\bar{\sigma}(s)ds,$$

where $\bar{\sigma}(s) = \frac{2\sigma(s)}{\pi r_e^2}$ and $s_0(\epsilon) = E(1+z)\epsilon/m_e^2 c^4$, so that equation (6) reduces to equation (17) in Razzaque et al. (2009):

$$\tau_{\gamma\gamma}^{\mathrm{hom}}(E, z) = \; c \; \pi r_e^2 \left(\frac{m_e^2 c^4}{E}\right)^2 \int_0^{z_s} \frac{dz_1}{(1+z_1)^2} \left| \frac{dt}{dz_1} \right| \; \times \; \int_{\frac{m_e^2 c^4}{E(1+z1)}}^\infty d\epsilon_1 \; \frac{\mu_{\epsilon_1}}{\epsilon_1^3} \; \bar{\varphi}[s_0(\epsilon)]. \tag{8}$$

Knowing the optical depth $\tau_{\gamma\gamma}$, we can calculate the attenuation of the intrinsic photon flux F_ν^{int} as:

$$F_\nu^{obs} = F_\nu^{int} e^{-\tau_{\gamma\gamma}(E,z)}, \tag{9}$$

where F_ν^{obs} is the observed spectrum.

3. RESULTS

3.1. General Parameter Study: Single Void

We first investigate the effect of a single cosmic void along the line of sight to a distant γ-ray source on the resulting angle-averaged EBL energy density. Figure 2 (top panels) compares the EBL energy density spectrum (keeping in mind that only the direct starlight contribution is accounted for) in the case of a void (dashed lines), compared to the homogeneous case (solid lines) for a spherical void of radius $R = 50\,h^{-1}$ Mpc (left panels) and $R = 100\,h^{-1}$ Mpc (right panels), at different points (redshifts, as indicated by the labels) along the line of sight. The center of the void is assumed to be located at a redshift of $z_v = 0.5$, considering a source located at redshift $z_s \geq 0.6$. The bottom panels of Figure 2 show the fractional difference between the homogeneous and the inhomogeneous case as a function photon energy for various redshifts along the line of sight, for the same two cases. As expected, the effect of the void is largest right in the center of the void, but even there, it does not exceed a few % (maximum fractional deficit ~ 7 % in the $R = 100\,h^{-1}$ Mpc case). The effect generally increases with photon energy. This is because high-energy photons are produced primarily by high-mass stars and, thus, trace the most recent star-formation history, which, for points within the void, is zero up to the time corresponding to the light travel time to the boundary of the void. As a function of position along the line of sight, the void-induced EBL deficit decreases approximately symmetrically for points in front of and behind the center of the void, with the slight asymmetry being due to the $(1 + z_1)^4$ factor in Equation 5.

Figure 3 illustrates the effect of the void on the differential EBL energy density as a function of distance along the line of sight to the γ-ray source, for two representative EBL photon energies, in the near-IR ($\epsilon = 1$ eV) and near-UV ($\epsilon = 8$ eV). The top panels show the absolute values of the energy densities, while the bottom panels show the fractional
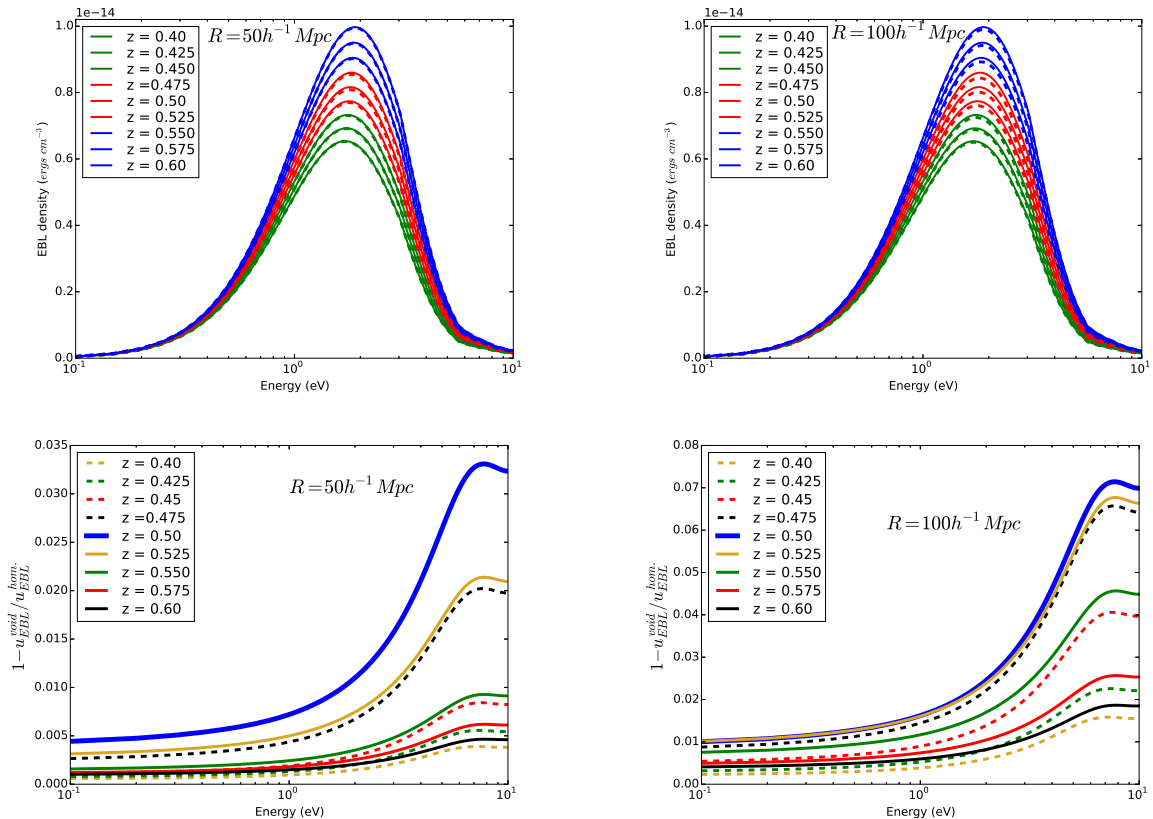
Figure 2. Top panels: Angle-averaged EBL photon energy density spectra for a homogeneous EBL (solid lines) and in the presence of a spherical cosmic void (dahed lines) with its center at redshift $z_v = 0.5$ (comoving distance 1.724 Gpc) and with radius $R = 50\,h^{-1}$ Mpc (left) and $R = 100\,h^{-1}$ (right). Green curves indicate locations in front of the void, red within the void, and blue behind the void. Bottom panels: Relative deficit of the EBL energy density due to the void.

difference between the homogeneous and the inhomogeneous cases. The figure illustrates that the maximum effect (at the center of the void) is approximately proportional to the size of the void, but does not exceed ~ 7 % in the case of the $R = 100\,h^{-1}$ Mpc void.

The relative EBL deficit as a function of distance is plotted for various different photon energies in the case of the $R = 50\,h^{-1}$ Mpc void in the left panel of Figure 4. The right panel of Figure 4 illustrates the angle dependence of the EBL in the presence of a void, compared to the homogeneous case. Right in the center of the void ($z_v = 0.5$ in the example studied here), the EBL is isotropic, due to the assumption of a spherical void, but reduced compared to the homogeneous EBL case. For positions located outside the void, the reduction is present only for EBL photon arrival directions intersecting the void, as expected.

Figure 5 illustrates the effect of a void on the $\gamma\gamma$ opacity for the same two example cases as illustrated in Figure 2, for sources located at various redshifts in front of, within, and behind the void. As expected, the effect is negligible if the source is located in front of the void (as seen by an observer on Earth), and is maximum for source locations right behind the void. However, even in the case of the $R = 100\,h^{-1}$ Mpc void, the maximum effect on the $\gamma\gamma$ opacity is less than 1 %. Note that the effect on the $\gamma\gamma$ opacity is much smaller than the maximum EBL energy density deficit in the center of the void due to the integration over the entire line of sight.

3.2. *Multiple voids along the line of sight*

After investigating the effect of one single cosmic void along the line of sight we now investigate the more realistic case of several voids along (or near) the line of sight. From Figure 3, we notice that the relativie EBL-energy-density-deficit scales approximately proportional to the size of the void. We therefore conclude that the effect of a number n of voids of radius R_1 is aproximately the same as the effect of a large void with radius $R_n = n\,R_1$. As a test case, we therefore consider void sizes up to $R \lesssim 1\,h^{-1}$ Gpc which approximates the effect of $\lesssim 10$ voids with realistic void sizes $R \lesssim 100\,h^{-1}$ Mpc distributed along or very close to the line of sight. The center of the cumulative void is assumed to
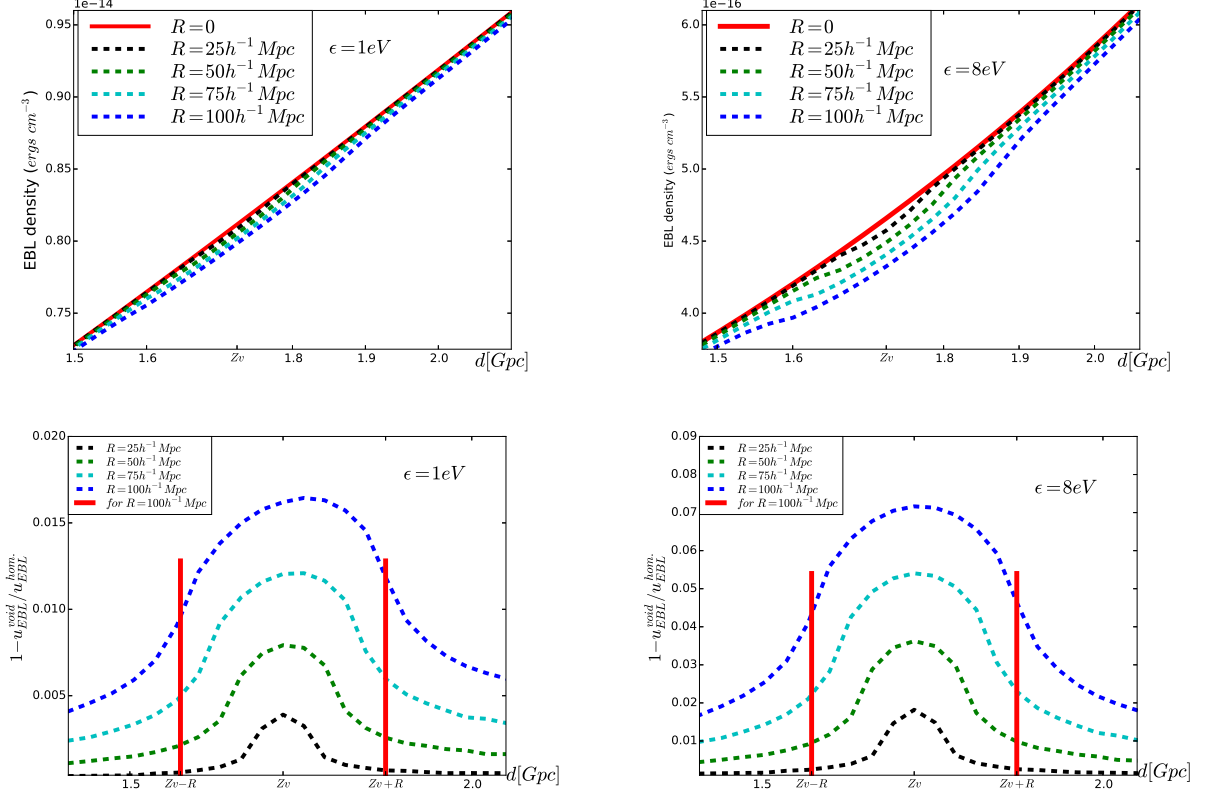
Figure 3. Top panels: Differential EBL photon energy density as a function of distance along the line of sight for various sizes (as indicated by the labels) of a void located at $z_v = 0.5$, at two representative photon energies of $\epsilon = 1$ eV (left) and $\epsilon = 8$ eV (right). The red solid lines ($R = 0$) represent the homogeneous case. The general increase of the EBL energy density with redshift is due to the $(1 + z_1)^4$ factor in Equation 5 and the increasing star formation rate with redshift. Bottom panels: Relativie EBL energy density deficit due to the presence of the void for the same cases as in the top panels. The red vertical lines indicate the boundaries of the void for the $R = 100\,h^{-1}$ Mpc case.
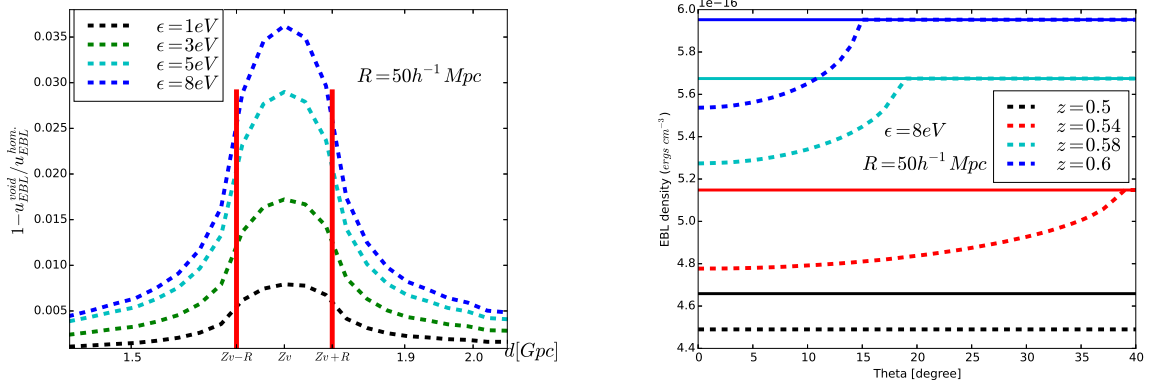

Figure 4. Left panel: Relative differential EBL-energy-density deficit as a function of distance along the line of sight, for various EBL photon energy densities, in the case of a $R = 50\,h^{-1}$ Mpc void located at $z_v = 0.5$. The red vertical lines indicate the boundaries of the void. Right panel: Angle dependence (θ is the angle with respect to the direct line of sight through the center of the void) of the EBL energy density in the presence of a $R = 50\,h^{-1}$ Mpc at $z_v = 0.5$ void (dashed lines), compared to the homogeneous case (solid lines, which does not have any angle dependence), at a representative near-UV photon energy of $\epsilon = 8$ eV, for two positions (redshifts) along the line of sight: at the center of the void (black, lower curves), within the void, but behind its center (red curves), and behind the void (blue and cyan, upper curves).

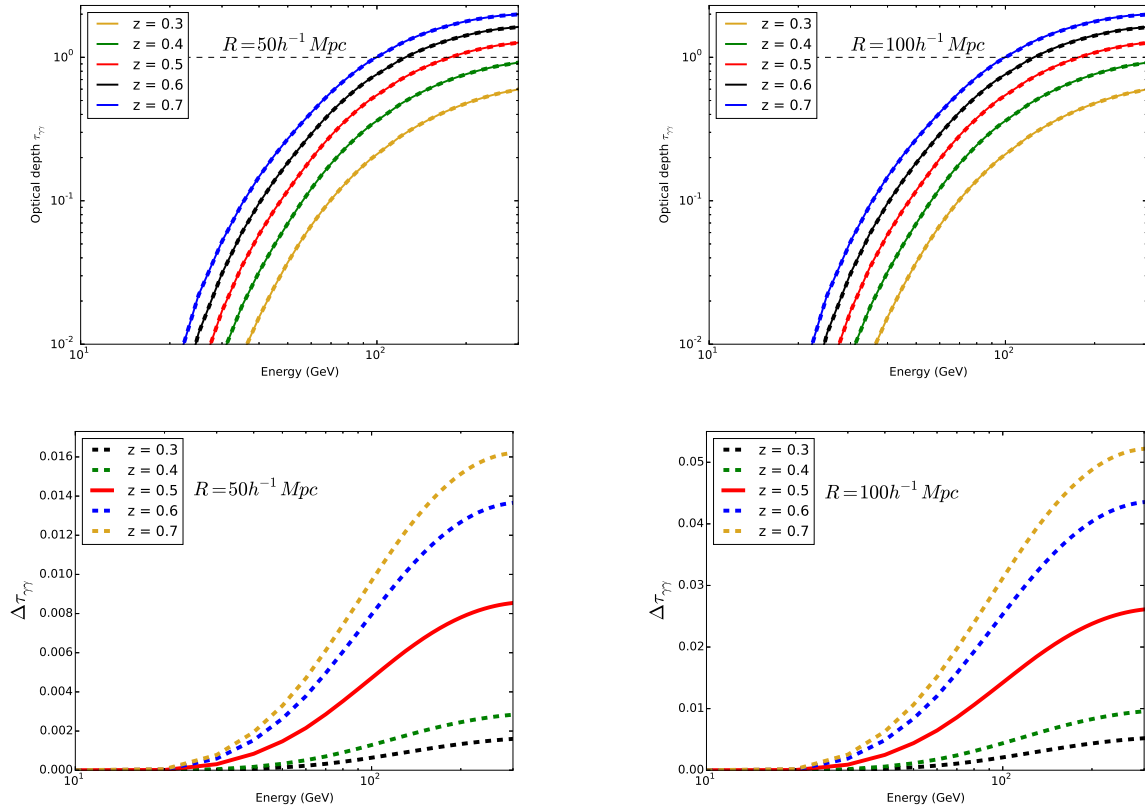be located at a redshift of $z_v = 0.3$, considering a source located at redshift $z_s \geq 0.6$.

Figure 5. Top panels: EBL $\gamma\gamma$ optical depth as a function of γ-ray photon-energy in the presence of a void (dashed), compared to the homogeneous case (solid), for the same example voids as illustrated in Figure 2. Bottom panels: $\gamma\gamma$ optical depth deficit due to the presence of the voids for the same two cases as in the top panels.

Figure 6 (top left panel) compares the EBL energy density spectrum for the case of such an accumulation of voids (dashed lines) to the homogeneous EBL case (solid lines). The top right panel of Figure 6 shows the fractional difference between the homogeneous and the inhomogeneous case as a function of photon energy for various redshifts along the line of sight. In the bottom left panel of Figure 6, we compare the resulting $\gamma\gamma$ opacities for the case of an ensemble of voids (dashed lines) and the homogeneous EBL case (solid lines), and the bottom right panel shows the $\gamma\gamma$ optical depth deficit due to the presence of the voids for the same two cases as in the left panel.

We can notice that for the extreme case of an accumulation of about 10 voids of typical sizes along the line of sight to a blazar, the EBL energy density even at the center of the cumulative void is reduced by around 35 %, and the resulting maximum $\gamma\gamma$ opacity reduced by around 15 %. This is because even if the star-formation rate is set to zero within the void, the EBL density within the void is still substantial due to the contributions from the rest of the Universe outside the void.
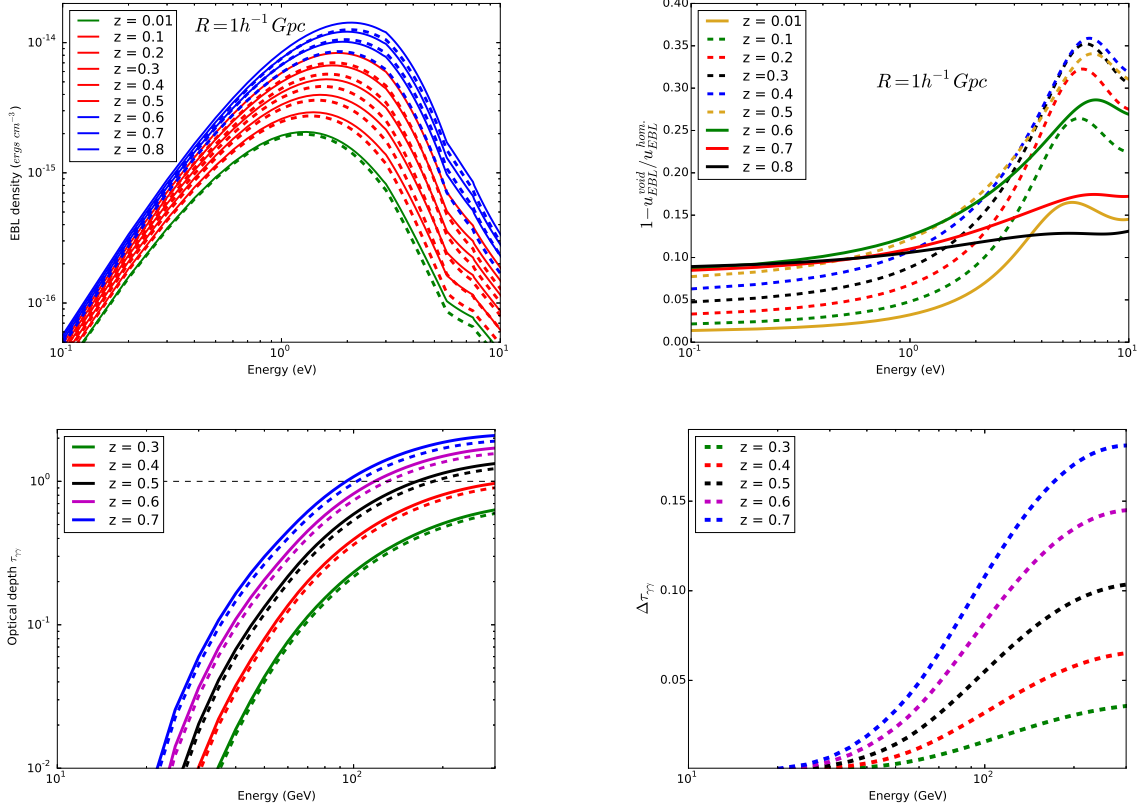
Figure 6. Top left panel: Angle-averaged EBL photon energy density spectra for a homogeneous EBL (solid lines) and in the presence of an accumulation of 10 cosmic voids of radius $R = 100 \, h^{-1}$ Mpc each (dahed lines), whose distribution along the line of sight is centered at redshift $z_v = 0.3$. Green curves indicate locations in front of the ensemble of voids, red within, and blue behind the ensemble of voids. Top right panel: Relative deficit of the EBL energy density due to the voids, dash lines and solid lines represents the effect of voids to the EBL-energy-density inside and outside the ensemble of voids, respectively. Bottom left panels: EBL $\gamma\gamma$ optical depth as a function of γ-ray photon-energy in the presence of voids (dashed), compared to the homogeneous case (solid), for the same example voids as illustrated in the top panels. Bottom right panels: $\gamma\gamma$ optical depth deficit due to the presence of the voids for the same two cases as in the left panel.

3.3. *Application to PKS 1424+240*

Furniss et al. (2015) had investigated the possibility that the unusually hard VHE γ-ray spectra observed in some distant ($z \gtrsim 0.5$) γ-ray blazars might be due to a reduced EBL density caused by galaxy underdensities along the line of sight. Specifically, they investigated a possible correlation between galaxy-count underdensities based on the Sloan Digital Sky Survey (SDSS) and the positions of hard-spectrum VHE blazars, and found a tentative hint for such a correlation (although the small sample size prevented the authors from drawing firm conclusions). Based on this result, as a first estimate of the effect of such underdensities on the EBL, they suggested a linear scaling of the line-of-sight galaxy density with the EBL $\gamma\gamma$ opacity. For the specific case of the distant ($z \geq 0.6$, Furniss et al. 2013) VHE blazar PKS 1424+240, they found that the reduction of the EBL resulting from such a direct linear scaling is not sufficient to remove the apparent spectral hardening of the VHE γ-ray spectrum observed by VERITAS, when correcting for EBL absorption based on state-of-the-art (homogeneous) EBL models (Archambault et al. 2014).

For an assumed redshift of $z = 0.6$ for PKS 1424+240, our example case of $R = 50 \, h^{-1}$ Mpc and $z_v = 0.5$ results in approximately the same galaxy-count underdensity factor as found by Furniss et al. (2015) along the line of sight to this source. In Figure 7, we therefore compare the EBL reduction effect based on the direct linear scaling with galaxy underdensity, with our detailed EBL calculation assuming a void along the line of sight, for the two observing periods presented in Archambault et al. (2014). The left panel illustrates the effect on the actual νF_ν spectra, while the right panel shows the γ-ray spectra normalized to the flux points corrected by the homogeneous Gilmore et al. (2012) EBL-absorption model. The figure illustrates that the EBL-opacity reduction effect due to the void, found in our detailed calculations, is slightly smaller than the effect resulting from a direct linear scaling with galaxy underdensity.
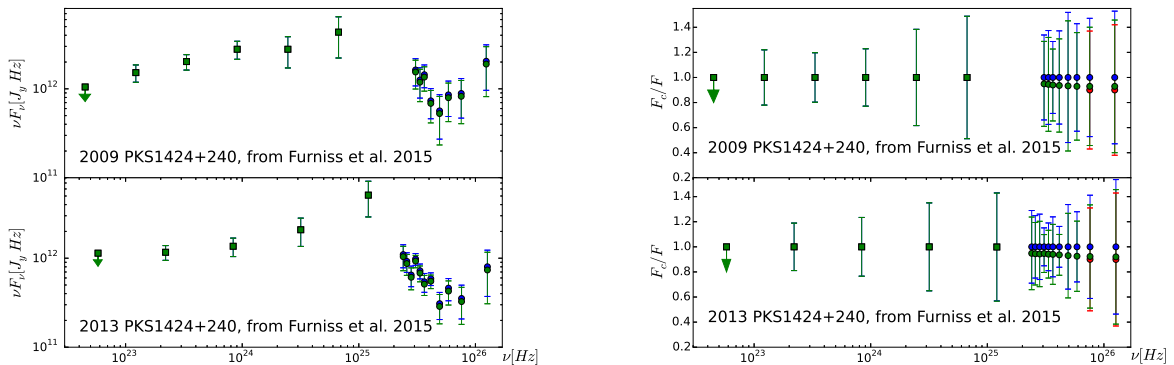
Figure 7. HE – VHE γ-ray spectra of PKS1424+240, from Archambault et al. (2014). The blue points show the EBL-corrected spectrum using the Gilmore et al. (2012) EBL model. The red points represent the reduced EBL correction, using the linear scaling of $\tau_{\gamma\gamma}$ with the line-of-sight galaxy density, as suggested by Furniss et al. (2015). The green points illustrate the reduced EBL correction resulting from our model calculation with a void of radius $R = 50h^{-1}$ Mpc centered at $z_v = 0.5$ (comoving distance 1.724 Gpc), assuming a source redshift of $z_s = 0.6$ (comoving distance 2.056 Gpc), which results in approximately the same perceived line-of-sight galaxy underdensity as used by Furniss et al. (2015). The left panels show the actual νF_ν spectra, while the right panels show the spectra normalized to the EBL-corrected flux points from Archambault et al. (2014).

Thus, we conclude that the tentative spectral hardening of the VHE spectrum of PKS 1424+240 is likely not an artifact of an under-estimate of the EBL opacity due to possible EBL inhomogeneities.

4. SUMMARY AND CONCLUSIONS

We have presented detailed calculations of the effect of cosmic inhomogeneities on the EBL and the resulting $\gamma\gamma$ opacity for VHE γ-ray photons from sources at cosmological distances. Specifically, we have considered the presence of a cosmic void, which, for simplicity, we have represented as a spherical region in which the local star formation rate is zero. We have shown that for realistic void sizes of $R \lesssim 100\,h^{-1}$ Mpc, the EBL energy density even at the center of the void is reduced by less than 10 %. Even if the void is located right in front of the background γ-ray source, the $\gamma\gamma$ opacity is reduced by typically less than 1 %. We found an approximately linear scaling of the EBL deficit effect with the size of the void. Even in the presence of a large number of voids adding up to a total line of sight distance through voids of $\sim 2\,h^{-1}$ Gpc ($= 2\,R_n$), the EBL $\gamma\gamma$ opacity is only reduced by ~ 15 %.

This reduction is smaller than obtained from a direct linear scaling of the $\gamma\gamma$ opacity with galaxy-count underdensities along the line of sight to γ-ray sources. For the specific case of PKS 1424+240, we have illustrated that the inferred (marginal) spectral hardening of the VHE γ-ray spectrum, after correction for EBL absorption, if confirmed by future, more sensitive VHE γ-ray observations, is most likely not an artifact of an over-estimation of the EBL opacity due to cosmic inhomogeneities.

Since we have shown that realistic EBL inhomogeneities do not lead to a significant reduction of the EBL $\gamma\gamma$ opacity, hints for unexpected spectral hardening of the VHE spectra of several blazars remain, for which other explanations would have to be invoked, if they can be confirmed by future observations (e.g., by the Cherenkov Telescope Array, CTA). One possibility is that this hardening is, in fact, a real, intrinsic feature of the γ-ray spectra of these blazars, possibly due to a pion-production induced cascade component in a hadronic blazar model scenario (e.g., Böttcher et al. 2013; Cerruti et al. 2015). If such a spectral hardening is not intrinsic to the source, more exotic explanations, such as ALPs or a cosmic-ray induced secondary radiation component, would need to be invoked.

5. ACKNOWLEDGMENTS

REFERENCES

Aharonian F. et al. 2006, Nature, 440, 1018

MAGIC Collaboration: Albert, J., et al., 2008, Science, 320, 1752

Archambault S. et al. 2014, ApJ, 785, L16

Biteau A. & Williams D. A. 2015, ApJ, 812, 1

Böttcher, M., Reimer, A., Sweeney, K., & Prakash, A., 2013, ApJ, 768, 54

Cerruti, M., Zech, A., Boisson, C., & Inoue, S., 2015, MNRAS, 448, 910

Dominguez, A., et al., 2011a, MNRAS, 410, 2556

Dominguez, A., Sánchez-Conde, M. A., & Prada, F., 2011b, J. Cosmol. Astropart. Phys., 11, 020

Essey W. & Kusenko A. 2010, ApJ, 33, 81

Finke, J. D., Razzaque, S., & Dermer, C. D., 2010, ApJ, 712, 238

Franceschini, A., Rodigheiro, G., & Vaccari, M., 2008, A&A, 487, 837

Furniss A., et al., 2013, ApJ, 768, L31

Furniss A., Stutter, P. M., Primack, J. R., & Dominguez, A., 2015, MNRAS, 446, 2267

Gilmore, R. C., Sommerville, R. S., Primack, J. R., & Dominguez, A., 2012, MNRAS, 422, 3189

Gould, R. J. & Schréder, G. P. 1967, Phys. Rev., 155, 1408

Hauser, M. G. & Dwek, E. 2001, ARA&A, 39, 249

Kudoda, A. M. & Faltenbacher, A., 2016, PoS, HEASA2015, 20

Nikishov, A. I. 1962, Sov. Phys. JETP, 14, 393

Razzaque S., Demer, C. D., & Finke, J. D., 2009, ApJ, 697, 483

Stecker, F. W. 1969, ApJ, 157, 507

Stecker, F. W., de Jager, O. C., & Salamon, M. H., 1992, ApJ, 390, L49

Sushch, I. & Böttcher, M. 2015, A & A, 573, A47

The Effects of EBL Inhomogeneity on the Gamma-Gamma Absorption of VHE Gamma Rays

The effects of EBL inhomogeneity on the gamma-gamma absorption of VHE gamma-rays

Hassan Abdalla *

Centre for Space Research, North-West University, Potchefstroom 2520, South Africa
Department of Astronomy and Meteorology, Omdurman Islamic University, Omdurman 382, Sudan
E-mail: hassanahh@gmail.com

Markus Böttcher

Centre for Space Research, North-West University, Potchefstroom 2520, South Africa
Astrophysical Institute, Department of Physics and Astronomy, Ohio University, Athens, OH 45701, USA
E-mail: Markus.Bottcher@nwu.ac.za

Very High Energy Gamma Rays (VHE; more than 100 GeV) from Cosmological Gamma Ray Sources such as blazars can be absorbed by the Extragalactic Background light (EBL), which leads to a high-energy cut-off in blazar spectral energy distributions. However, recent observations of distant gamma ray sources suggest that the universe is more transparent to VHE gamma rays than expected from our current knowledge of a homogeneous EBL. One of the possible solutions is the hypothesis that a reduced EBL opacity results from inhomogeneities of the EBL density in particular if the line of sight to a blazar is passing through large voids in intergalactic space. We have evaluated the inhomogeneous and anisotropic EBL density and resulting gamma-gamma opacity in such a case. We find that even a sizeable void $R \lesssim 1 h^{-1}$ Gpc or many typical voids $R \lesssim 100 h^{-1}$ Mpc located along the line of sight to a distant blazar leads to a reduction of the EBL opacity only around 15%. EBL inhomogeneities are not expected to reduce the EBL gamma-gamma opacity significantly, and alternative solutions to the problem of hard VHE spectra of blazars may be required.

---

*Speaker.

1. Introduction

Very High Energetic Gamma rays from distant blazars can be annihilated due to $\gamma\gamma$ absorption by low-energy intergalactic photons. The importance of this process for high-energy astrophysics was first pointed out by [1]. Currently the study of $\gamma\gamma$ absorption of VHE photons from high-redshift sources is one of the hot topics in high energy astrophysics due to their potential to study the cluster environments of blazars [2] and estimate cosmological parameters [3]. However, The EBL is very difficult to be measured accurately due to foreground emissions [4]. Studies of the EBL therefore focus on the predicted $\gamma\gamma$ absorption imprints and employ a variety of theoretical and empirical methods [5, 6, 7, 8, 9, 10, 11, 12]. Recent observations of distant ($z \gtrsim 0.5$) γ-ray blazars have been interpreted by some authors [13, 14] that the universe may be more transparent to very high energy γ-rays than expected based on all existing EBL models. Possible solutions include the hypothesis that the EBL density is generally lower than expected from current models [15]; the existence of exotic Axion Like Particles (ALPs) [16]; extragalactic Ultra-high-Energy Cosmic Rays (UHECRs) [17]; and EBL inhomogeneities [18, 19, 20]. Based on a detailed calculation of the opacity due to an inhomogeneous EBL, including cosmic voids of typical sizes between the observer and a distant blazar, we have shown that for realistic void sizes of $R \lesssim 100 h^{-1}$ Mpc, the EBL energy density even at the center of the void is reduced by less than 10 %. Even if the void is located right in front of the background γ-ray source, the $\gamma\gamma$ opacity is reduced by typically less than 1 %. More details regarding to this work can be found in [20]. In the current work we consider an unrealistic extreme void or an equivalent accumulation of about 10 voids of typical sizes, distributed along the line of sight, to investigate whether this could explain the spectral hardening feature in the VHE spectra of some blazars such as PKS 1424+24.

2. EBL in the Presence of a Cosmic Void

Our calculations of the inhomogeneous EBL are based on a modified version of the formalism presented in [9], considering only the direct starlight. The effect of re-processing of starlight by dust has been included in [10] and leads to an additional EBL component in the mid- to far infrared, which is neglected here. Since dust re-processing is a local effect, it will be affected by cosmic inhomogeneities in the same way as the direct starlight contribution considered here.

For the purpose of a generic study of the effects of cosmic voids along the line of sight to a blazar, we assume that a spherical cosmic void is located with its center at redshift z_v and raduis R between the observer and a γ-ray source at redshift z_s. The geometry is illustrated in Figure 1. We calculate the angle- and photon-energy-dependent EBL energy density at each point between the observer at redshift O and the source by using co-moving cordinates, converting redshifts z to distances $l(z)$. The cosmic void is represented by setting the star formation rate to 0 within the volume of the void.

We start out by modifying the expression from [9] for the differential photon number density of the EBL at a given redshift z, based on the direct contribution from stars throughout cosmic history. For more details see [20].

Figure 2 illustrates the effect of the void on the differential EBL energy density as a function of distance along the line of sight to the γ-ray source, for one representative EBL photon energy,
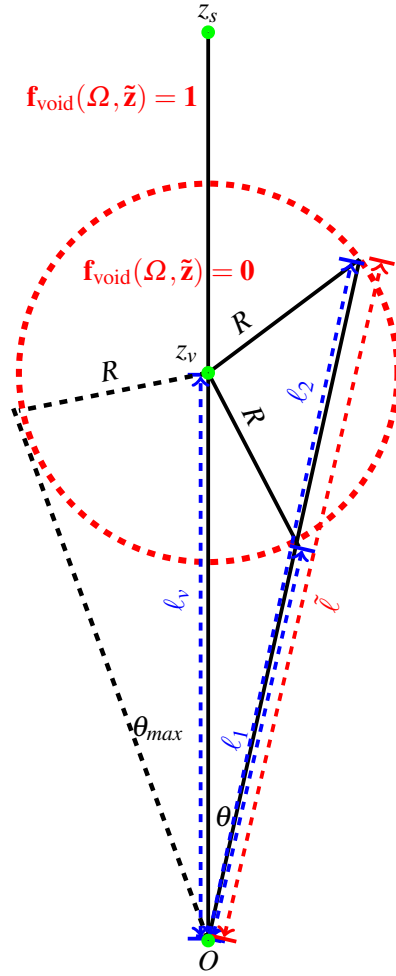
Figure 1: Illustration of the geometry of an underdense region between the observer at redshift O and source at redshift z_s. We assume that the underdense region has a radius R and the redshift at the center of the underdense region is z_v

in near-UV ($\varepsilon = 8$ eV). The figure illustrates that the maximum effect (at the center of the void) is approximately proportional to the size of the void, but does not exceed ~ 7 % in the case of the $R = 100\,h^{-1}$ Mpc void. Also, we can notice that, when we double the void radius, the relativie EBL-energy-density-deficit will double. We can therefore conclude that the effect of a single large void with radius R is approximately equivalent to the effect of a number of smaller voids with radii adding up to R.
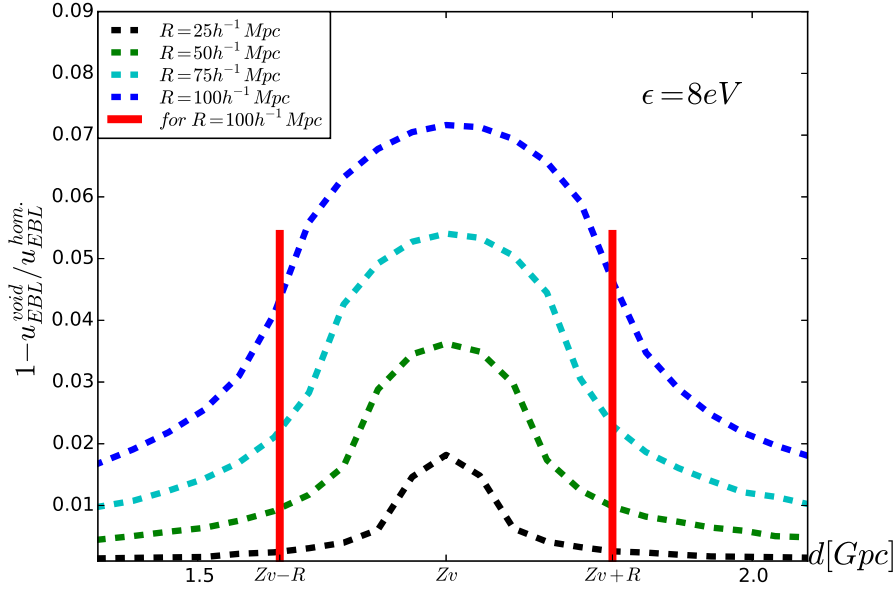
Figure 2: Relativie EBL energy density deficit due to the presence of the void for the same cases as in the top panels. The red vertical lines indicate the boundaries of the void for the $R = 100\,h^{-1}$ Mpc case [20].

3. Gamma-gamma Absorption in the presence of a void

To study the influence of a cosmic void along the line of sight to a distant VHE-γ-rays source on the EBL energy density and resulting $\gamma\gamma$ opacity, we used the formalism described in the previous section (with the geometry illustrated in Figure 1). We consider spherical unrealistically large void sizes $R \lesssim 1\,h^{-1}$ Gpc or equivalently around ten realistic void sizes $R \lesssim 100\,h^{-1}$ Mpc distributed along or very close to the line of sight to a distant blazar. The center of the void is assumed to be located at a redshift of $z_v = 0.3$, considering a source located at redshift $z_s \geq 0.6$.

Figure 3 (left panel) compares the EBL energy density spectrum for the case of a void (dashed lines), compared to the homogeneous case (solid lines). The right panel of Figure 3 shows the fractional difference between the homogeneous and the inhomogeneous case as a function of photon energy for various redshifts along the line of sight. In the left panel of Figure 4, we compare the resulting gamma-gamma opacities for the case of a voide (dashed lines) and the homogeneous case (solid lines), and the right panel shows the gamma-gamma optical depth deficit due to the presence of the voids for the same two cases as in the left panel.

We can notice that for even unrealistically large void sizes or an equivalent accumulation of about 10 voids of typical sizes, most of them distributed excactly along-the line of sight with the remaining ones located very close to the line of sight, the EBL energy density even at the center of the void is reduced by around 35 % and the resulting maximum $\gamma\gamma$ opacity reduced by around 15 %. This is because even if the star-formation rate is set to zero within the void, the EBL density within the void is still substantial due to the contributions from the rest of the Universe outside the void.
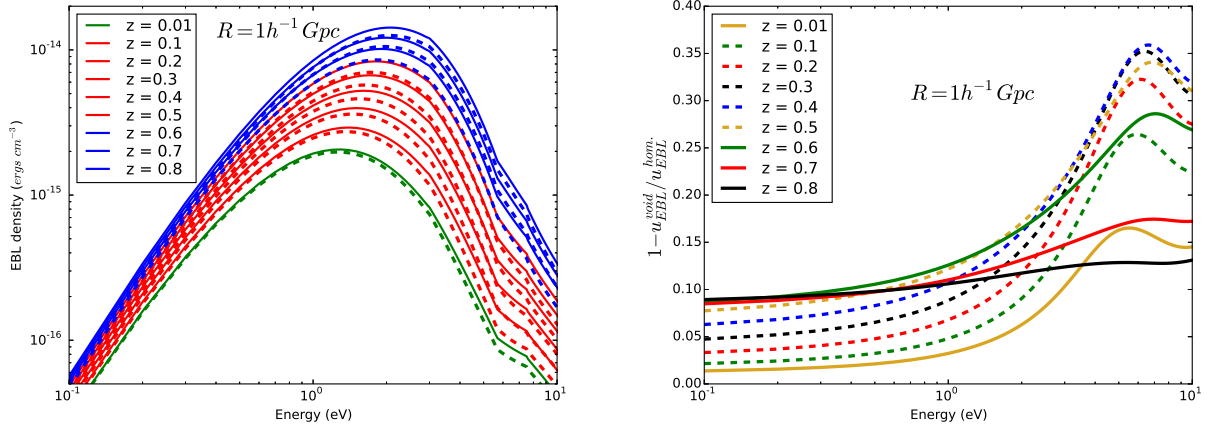
3

Figure 3: Left panel: Angle-averaged EBL photon energy density spectra for a homogeneous EBL (solid lines) and in the presence of a spherical cosmic void (dahed lines) with its center at redshift $z_v = 0.3$ and with radius $R = 1\,h^{-1}$ Gpc. Green curves indicate locations in front of the void, red within the void, and blue behind the void. Right panel: Relative deficit of the EBL energy density due to the void, dash lines and solid lines represents the effect of void to the EBL-energy-density inside and outside the void respectively.
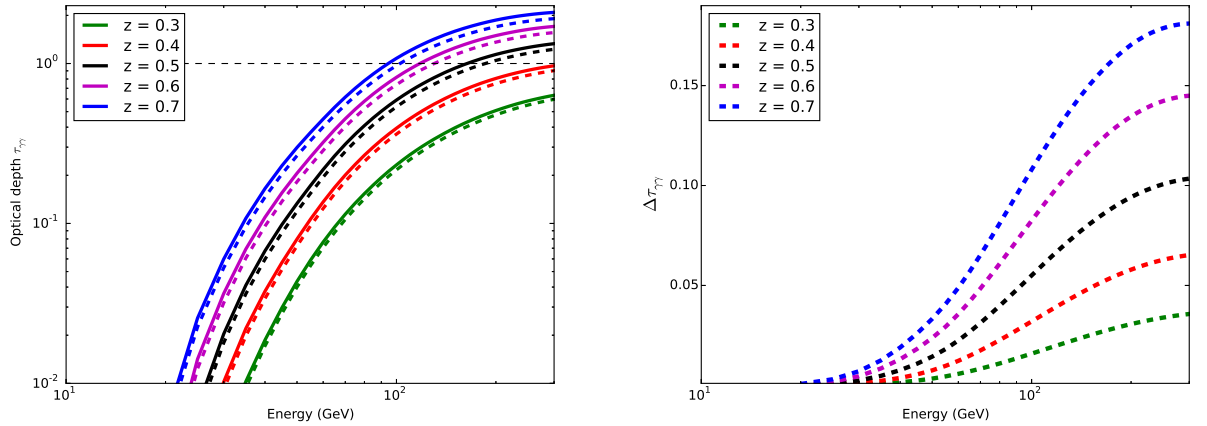

Figure 4: Left panels: EBL $\gamma\gamma$ optical depth as a function of γ-ray photon-energy in the presence of a void (dashed), compared to the homogeneous case (solid), for the same example voids as illustrated in Figure 3. Right panels: $\gamma\gamma$ optical depth deficit due to the presence of the voids for the same two cases as in the left panel.

4. Summary and Conclusions

We have presented detailed calculations of the effect of cosmic inhomogeneities on the EBL and the resulting $\gamma\gamma$ opacity for VHE γ-ray photons from sources at cosmological distances. Specifically, we have considered the presence of a large cosmic void, which, for simplicity, we have represented as a spherical region in which the local star formation rate is zero. We have shown that for unrealistically large void sizes $R \lesssim 1\,h^{-1}$ Gpc or equivalently around ten realistic void sizes $R \lesssim 100\,h^{-1}$ Mpc distributed along or very close to the line of sight to a distant blazar, the EBL

energy density even at the center of the void is reduced by around 35 %. Even if the void is located right in front of the background γ-ray source, the $\gamma\gamma$ opacity is reduced by typically less than 15 %. Specifically, we found that even with an alignment of about 10 realistic voids towards a blazar at z = 0.6 (such as PKS 1424+240), gamma-rays with energies above 130 GeV are expected to be heavily attenuated. In order to suppress the gamma-gamma opacity sufficiently up to energies of 300 GeV, one would need more than 40 voids of typical sizes $R \lesssim 100h^{-1}$ Mpc located exactly along or very close to the line of sight. This is clearly unrealistic and in conflict with observational constraints.

As with our current knowledge of the EBL, the spectral hardening feature in PKS 1424+240 and a few other VHE γ-ray blazars remains even when considering possible EBL inhomogeneities. Thus, other explanations for such hardening must be invoked. One possibility is that this hardening is, in fact, a real, intrinsic feature of the γ-ray spectra of these blazars, possibly due to a pion-production induced cascade component in a hadronic blazar model scenario [21, 22]. If such a spectral hardening is not intrinsic to the source, more exotic explanations, such as ALPs or a cosmic-ray induced secondary radiation component, would need to be invoked.

5. Acknowledgments

References

[1] Nikishov, A. I. 1962, Sov. Phys. JETP, 14, 393

[2] Sushch, I. & Böttcher, M. 2015, A & A, 573, A47

[3] Biteau A. & Williams D. A. 2015, ApJ, 812, 1

[4] Hauser, M. G. & Dwek, E. 2001, ARA&A,, 39, 249

[5] Stecker, F. W. 1969, ApJ, 157, 507

[6] Stecker, F. W., de Jager, O. C., & Salamon, M. H., 1992, ApJ, 390, L49

[7] Aharonian F. et al. 2006, Nature, 440, 1018

[8] Franceschini, A., Rodigheiro, G., & Vaccari, M., 2008, A&A, 487, 837

[9] Razzaque S., Demer, C. D., & Finke, J. D., 2009, ApJ, 697, 483

[10] Finke, J. D., Razzaque, S., & Dermer, C. D., 2010, ApJ, 712, 238

[11] Dominguez, A., et a., 2011a, MNRAS, 410, 2556

[12] Gilmore, R. C., Sommerville, R. S., Primack, J. R., & Dominguez, A., 2012, MNRAS, 422, 3189

[13] MAGIC Collaboration: Albert, J., et al., 2008, Science, 320, 1752

[14] Archambault S. et al. 2014, ApJ, 785, L16

[15] Furniss A., et al., 2013, ApJ, 768, L31

[16] Dominguez, A., Sánchez-Conde, M. A., & Prada, F., 2011b, J. Cosmol. Astropart. Phys., 11, 020

[17] Essey W. & Kusenko A. 2010, ApJ, 33, 81

[18] Furniss A., Stutter, P. M., Primack, J. R., & Dominguez, A., 2015, MNRAS, 446, 2267

[19] Kudoda, A. M. & Faltenbacher, A., 2016, PoS, HEASA2015, 20

[20] Abdalla, H. & Böttcher, M., (2016, ApJ, submitted).

[21] Böttcher, M., Reimer, A., Sweeney, K., & Prakash, A., 2013, ApJ, 768, 54

[22] Cerruti, M., Zech, A., Boisson, C., & Inoue, S., 2015, MNRAS, 448, 910

Why the Universe is Unexpectedly Transparent to Very High Energy Gamma Rays

Why the universe is unexpectedly transparent to very high energy gamma-rays

Hassan Abdalla *

Centre for Space Research, North-West University, Potchefstroom 2520, South Africa
Department of Astronomy and Meteorology, Omdurman Islamic University, Omdurman 382,
Sudan
E-mail: hassanahh@gmail.com

Markus Böttcher

Centre for Space Research, North-West University, Potchefstroom 2520, South Africa
E-mail: Markus.Bottcher@nwu.ac.za

Recent observations of distant gamma ray sources indicate that the universe may be more transparent to VHE-gamma-rays than expected. In this paper we study the reduction of the EBL gamma-gamma opacity due to the existence of underdense regions along the line of sight to VHE gamma-ray sources and the possibility of a Lorentz Invariance Violation (LIV) signature. Therefore, we study whether one or both of these effects could be suitable to explain the spectral hardening observed in a few VHE gamma-ray sources. We found that, although the cosmic opacity for VHE gamma rays with energy more than 10 TeV can be strongly reduced, the spectral hardening feature observed in some VHE gamma-ray blazars with energy from 300 GeV up to few TeVs (e.g. PKS 1424+240) still remains puzzling.

---

*Speaker.

1. Introduction

The extragalactic Very High Energetic (VHE) photons from distant gamma-ray sources (e.g. blazars) can be absorbed due to $\gamma\gamma$ absorption by low-energy extragalactic background light (EBL) photons. The photon flux attenuation due to this process and its importance in high-energy astrophysics was first pointed out by Nishikov in 1962 [1], which has shown that the probability of conversion of TeV gamma ray traversing a length comparable to the Hubble distance into an electron-positron pair due to it is interaction with soft EBL photons, is appreciable. Currently, the study of the opacity or transparency of the Universe to VHE photons coming from high redshift astronomical objects due to their interaction with intergalactic EBL photons is a very active area of high-energy astrophysics, because of its potential to study the cluster environments of blazars [2] and estimate some cosmological parameters [3]. However, the EBL is very difficult to measure directly because of the strong foreground emissions within our galaxy and solar system (e.g. atmosphere and zodiacal light) [4].
Several important studies have been carried out to estimate the average EBL energy density and its cosmological evolution, and to calculate the predicted $\gamma\gamma$ absorption imprints, by employing a variety of theoretical and empirical research methods [5, 6, 7, 8, 9, 10, 11, 12, 13].

Recent observations of some distant VHE-gamma rays sources (e.g. blazars) seem to indicate hard VHE gamma-ray spectra which have been interpreted by several authors as a hint that the Universe might be more transparent to VHE gamma-rays than expected from current EBL models. [14, 15, 16]. There have been many attempts to find possible explanations for this VHE-gamma ray signature in some distant blazar spectra. Possible solutions include the hypothesis that the EBL density is generally lower than expected from current models [17]; the existence of exotic Axion Like Particles (ALPs) [14, 18]; photo-pion-production interactions of extragalactic Ultra-high-Energy Cosmic Rays (UHECRs) along the line of sight [19]; and EBL inhomogeneities [20, 21, 22].
In a previous paper [22] we investigated the effects of inhomogeneities of the EBL on the gamma-gamma opacity using the prescription of Razzaque et al. (2014) [9].
In this paper, to include the additional EBL component from mid- to far infrared, by re-processing of starlight, we used the model of Finke et al. (2015) [10]. To calculate the resulting $\gamma\gamma$ opacity for VHE γ-ray photons from sources at cosmological distances, due to their interaction with intergalactic radiation fields (EBL) through electron-positron pair production, we assumed a VHE-gamma ray source located at redshift 0.6. Then, we investigate the effect of cosmic voids along the line of sight to the VHE-γ-rays source, and the effect of LIV, to compare the two effects, and discuss in which energy band each is dominant.

2. Cosmic Voids Along the Line of Sight

To study the impact of an under-dense region, a generic study of the effects of cosmic voids along the line of sight to a blazar has been done [22], in which we assumed that a spherical cosmic void with radius R is located with its center at redshift z_v, between the observer and the VHE γ-ray source located at redshift z_s. We calculate the angle- and photon-energy-dependent EBL energy density at each point between the observer at redshift zero and the source by using co-moving cordinates, converting redshifts z to distances $l(z)$. The cosmic void is represented by setting the star formation rate to 0 within the volume of the void. Following Razzaque et al. (2014), only the direct starlight contribution to the EBL was considered in [22]. From figure (1), we notice that the
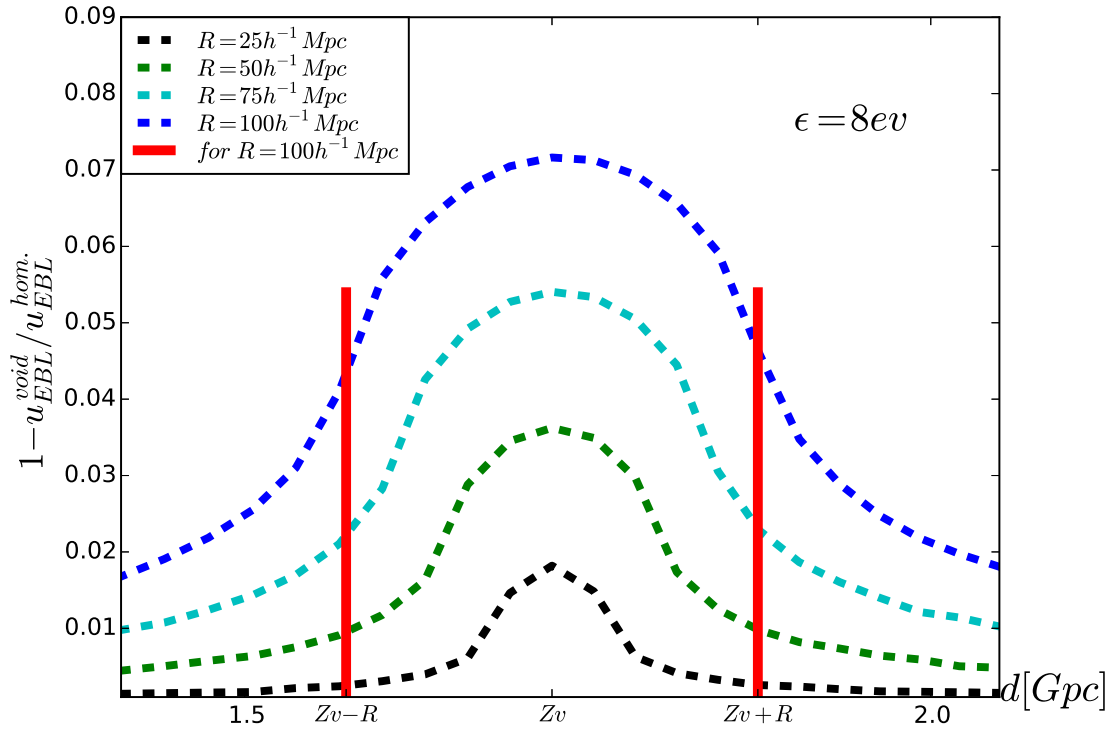
Figure 1: The relative EBL photon energy density deficit due to the presence of a void of various sizes (as indicated by the labels) as a function of distance along the line of sight of a void located at $z_v = 0.5$, at a representative photon energy of $\varepsilon = 8$ eV . The red vertical lines indicate the boundaries of the void for the $R = 100 h^{-1}$ Mpc case [22].

EBL deficit is proportional to the size of the void. Therefore, the effect of a number n of voids of radius R_1 is aproximately the same as the effect of a large void with radius $R_n = nR_1$. Detailed calculations, which assume voids along the line of sight using the Razzaque. et al. (2009) [9] EBL model, can be found in [22].

In this work we calculate the impact of cosmic voids along our line of sight to a distant VHE gamma-ray source, by using the model developed by by Finke, et al. (2015) [10]. In this model,

the full EBL spectrum (from far infrared through visible and extending into the ultraviolet) is calculated, by considering the stars that evolved off the main sequence and re-emission of absorbed starlight by dust. More details can be found in [10]. We investigate the impact of the existence of an accumulation of about 10 voids of typical sizes with radius $R = 100 h^{-1}$ Mpc centered at redshift $z_v = 0.3$ along the line of sight to an object (e.g. ablazar) located at redshift $z_v = 0.6$, which is presented in figure (2).
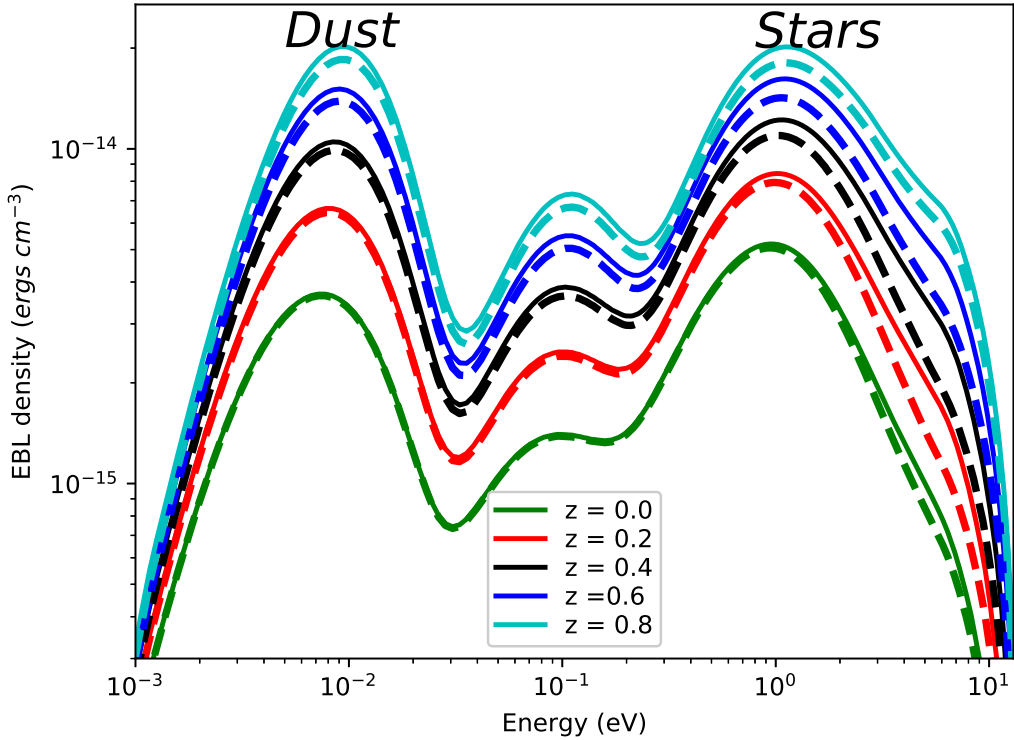
Figure 2: Differential EBL photon energy density as a function of distance along the line of sight. The solid lines ($R = 0$) represent the homogeneous case, and the dashed lines represent the EBL energy density considering an accumulation of about 10 voids of typical sizes with radius $R = 100 h^{-1}$ Mpc centered at redshift $z_v = 0.3$. The general increase of the EBL energy density with redshift is due to the increasing star formation rate with redshift.

In figure (2) we present the EBL energy density spectrum (the full spectrum from 0.001 to 10 eV including the direct emission, and absorption and reradiation by dust) for the case of a void (dashed lines), compared to the homogeneous case (solid lines) at different points (redshifts, as indicated by the labels) along the line of sight. To represent the difference between the homogeneous
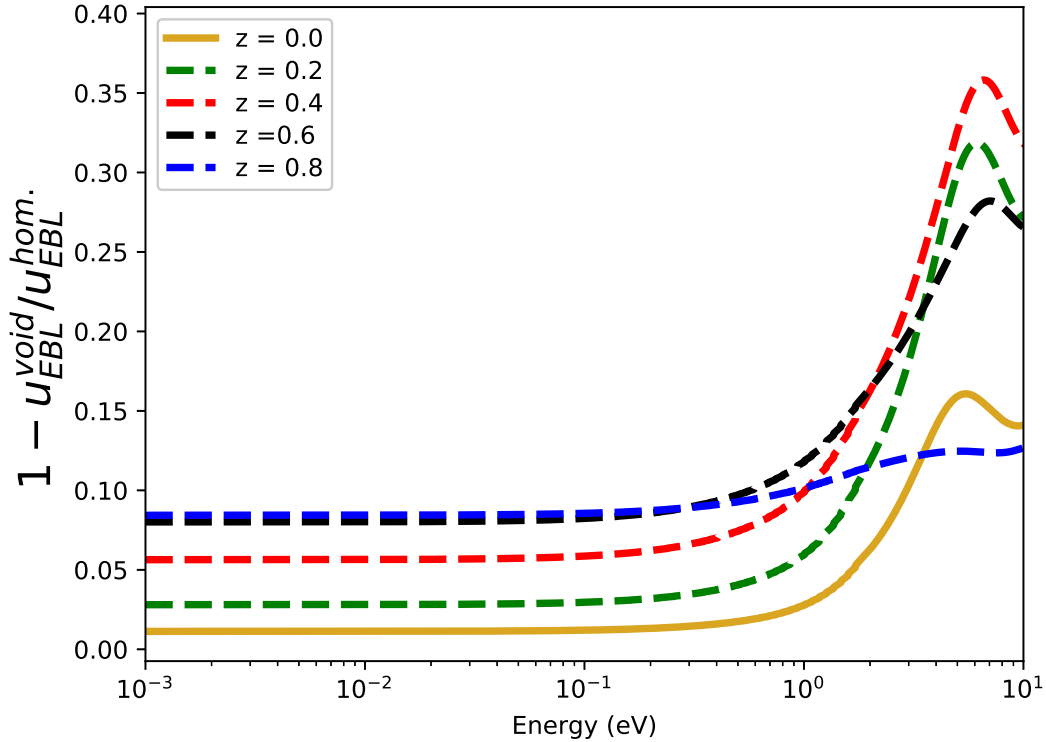

Figure 3: Relativie EBL energy density deficit due to the presence of a void for the same cases as represented in figure (2). The fraction between the homogeneous and inhomogeneous cases for different redshifts presented in this figure.

and inhomogeneous cases clearly, we calculated the fractional difference between the homogeneous and the inhomogeneous case as a function of photon energy for various redshifts along the line of sight. The result is plotted in figure (3). Figure (3) illustrates that the EBL deficit is smaller for low-energy (IR) photons than for optical - ultraviolet photons. This is because the UV EBL is dominated by hot, young stars, thus more strongly reflecting the local effect of the void.

Since in this work we set only the star formation rate inside the void equal to zero, some dust reprocessing still takes place inside the void.

From figure (3), we can notice that the relative EBL energy density deficit due to the presence of voids is quite significant only at (and around) the center of the voids but the deficit close to the edge of the void or just outside of the void is very small. Therefore the reduction of the gamma-gamma opacity due to the cosmic voids is expected to be insignificant; the optical depth deficit for the VHE-gamma rays due to the possibility of cosmic voids is investigated in Sections (3) and (4).

4

3. Lorentz Invariance Violation

Lorentz invariance (or Lorentz symmetry) is one of the fundamental concepts in the Special Theory of Relativity. But recently, several quantum-gravity theories predict that familiar concepts such as Lorentz symmetry can be broken at energies approaching the Planck energy scale ($E_{LIV} \sim 1.2 \times 10^{19} GeV$). While such extreme energies are currently unreachable by experiments, tiny residual effects at attainable energies can be measured when VHE photos propagate over sufficiently large distances. Thus, for photons traveling over cosmological distances, the accumulated deviations from the Lorentz symmetry might be large enough to be measured. The deviation from Lorentz symmetry can be described by a modification of the dispersion relation as follows [23, 24, 25, 26, 27]:

$$E^2 = p^2 c^2 + m^2 c^4 \pm E^2 \left(\frac{E}{\zeta_n E_{LIV}} \right)^n, \tag{3.1}$$

where c is the conventional speed of light, the dimensionless parameter ζ_n and the order of the leading correction n are depending on particle type and theoretical framework. The values $n = 1, 2$ are the cases most often considered. The" $-$ sign" represents a subluminal scenario (decreasing photon speed with increasing energy), and the "+ sign" represents the superluminal case (increasing photon speed with increasing energy) [23, 28]. The violation of Lorentz invariance leads to a modification of the threshold energy and cross section of the gamma-gamma pair production process. This can lead to an energy-dependent refractive index for light in vaccum, with higher energy photons propagating more slowly than their lower-energy counterparts [28]. The modified pair-production threshold energy ε_{min}, can be obtained solely on the minimal assumption that the standard energy-momentum conservation still holds in the Lorentz violation framework (Note: this may not be true in some LIV schemes). To lowest non-trivial order in E/E_{LIV}, the modified pair-production threshold energy ε_{min} by considering the subluminal case only, can be written as [29]:

$$\varepsilon_{min} = \frac{m^2 c^4}{E_\gamma} + \left(\frac{E^2}{4 E_{LIV}} \right), \tag{3.2}$$

where E is the considered VHE-photon energy and E_{LIV} is the relevant energy scale, which is commonly assumed to be of the order of the Planck energy. For energies $E \ll E_{LIV}$, any deviation from Lorentz symmetry is expected to be very small. The resulting threshold energy ε_{min} of a target photon as a function of its VHE gamma-ray energy is shown in figure (4). In this figure we represented the standard quantum electrodynamics case by a black solid line and the dashed-lines indicate the modified threshold energy for different E_{LIV} values (in units of 10^{19} GeV). The standard relation for optical depth at the energy E_γ and for a source at redshift z_s is modified as [29]:

$$\tau_{\gamma\gamma}(E_\gamma, z_s) = \frac{c}{8E_\gamma^2} \int_0^{z_s} \frac{dz}{H(z)(1+z)^3} \int_{\varepsilon_{min}}^{\infty} \frac{n(\varepsilon, z)}{\varepsilon^2} \int_{s_{min}}^{s_{max(z)}} \left(s - \frac{E_\gamma^3}{E_{LIV}} \right) \sigma_{\gamma\gamma}(s) ds, \tag{3.3}$$

where $H(z) = H_0 \sqrt{[\Omega_m (1+z)^3 + \Omega_\Lambda]}$, $n(\varepsilon, z)$ is the EBL photon number density as a fuction of redshift z and energy ε, and $\sigma_{\gamma\gamma}(s)$ is the total pair production cross section as a function of the modified square of the center of mass energy $s = -\frac{E^3}{E_{LIV}} + 2\varepsilon E_\gamma (1 - cos(\theta))$, where θ is the angle between the soft EBL photon of energy ε and the VHE gamma ray photon. The limits of the last
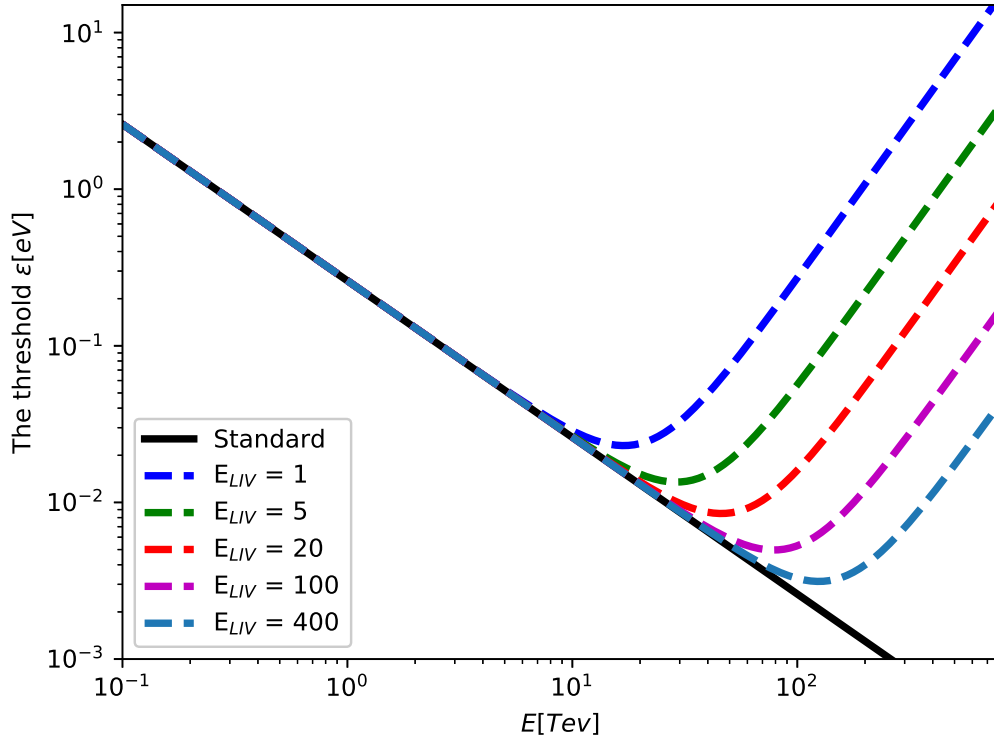
Figure 4: This figure (reproduced from [29]), gamma-gamma pair production threshold energy as a function of VHE gamma-ray photon energy (Equation (3.2)). The black solid-line shows the standard case and the dashed lines indicate the modified threshold due to the effect of LIV, for different values of the parameter E_{LIV} (in the units of 10^{19} GeV).

integral can be written as $s_{min} = 4m_e^2c^4$ and $s_{max} = 4\varepsilon E_\gamma(1+z) - \frac{E_\gamma^3}{E_{LIV}}$. Note that the kinematics outlined above take into account the modified dispersion relation only for photons, but not for electrons. From equation 3.3, it is obvious that when $E_{LIV} \longrightarrow \infty$, the standard relations are recovered. In the following, it is assumed that the expression for the cross section as a function of s remains unchanged.

4. Cosmic Voids and LIV

We compare the effects of inhomogeneities due to the presence of cosmic voids to those of LIV in figure (5). For comparison purposes, to study the effect of cosmic voids along the line of sight and/or of LIV, in figure (6) we plot the relativie optical depth $\tau_{\gamma\gamma}$ deficit as a function of energy for VHE-gamma rays that propagate from a source located at redshift $z = 0.6$. The effect of a cosmic void along the line of sight is presented by the black dot-dashed line. As already elaborated in [22], the effect of a plausible EBL inhomogeneity on the gamma-gamma opacity is not sufficient to explain the unexpected spectral hardening of, e.g., the blazar PKS 1424+240. We also notice that the optical depth $\tau_{\gamma\gamma}$ deficit decreases with energy and is very small for VHE
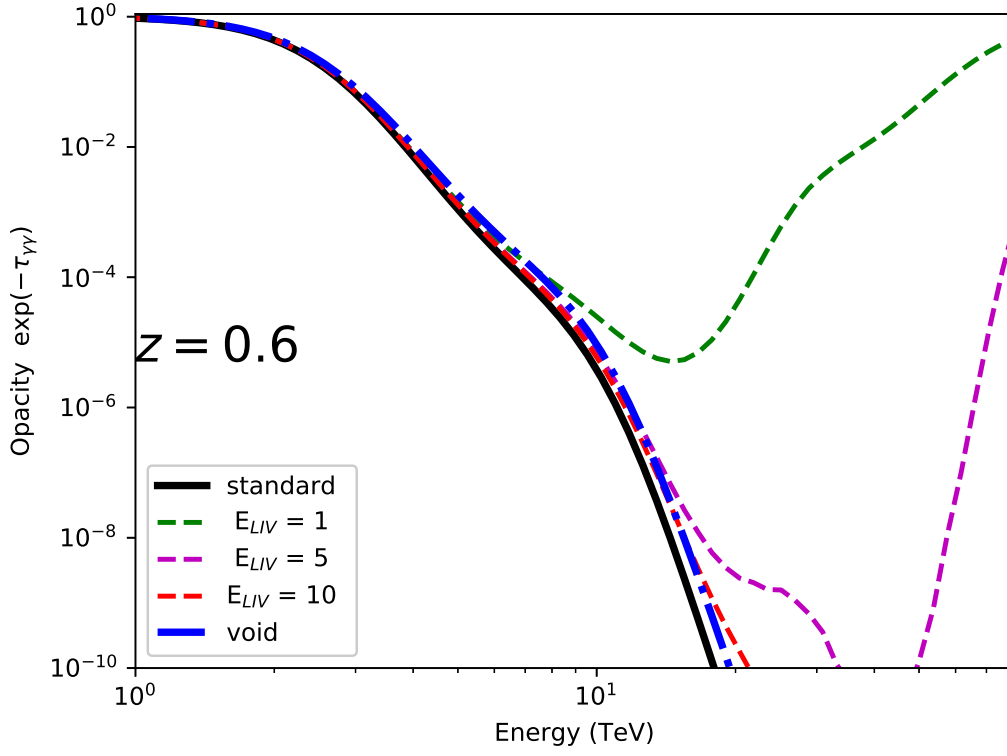
Figure 5: Absorption coefficient $\exp(-\tau_{\gamma\gamma})$ as a function of energy for VHE-gamma rays that propagate from a source located at redshift $z = 0.6$, using the EBL model devoloped by Finke, et al. (2015) [10]. The black solid line represents the case of standard quantum electrodynamics (QED) physics and using the homogeneous EBL energy density distribution, and the blue dot-dashed line represents the case of standard QED and EBL energy density calculated by considering an accumulation of 10 voids of typical sizes with radius $R = 100 h^{-1}$ Mpc centered at redshift $z_v = 0.3$. The dashed-lines show the modified coefficient for different values of E_{LIV} in the unit of Planck energy scale ($1.2 \times 10^{19} GeV$).

gamma-ray photons above ~ 10 TeV. To study the effects of LIV, we again use the EBL model of Finke, et al. (2015) [10], and calculate both the effect of LIV alone, as well as the combined effect of LIV and a cosmic void. In figure (6), the green, blue and red lines represent the deficit due to the LIV modification, for different values of E_{LIV} and the violet dashed line due to both effects. We can notice that the LIV effect is very small for energies below about 5 TeV, but very significant at higher energy $E \approx 10$ TeV or higher.

Our results show that, due to LIV, one may expect VHE gamma-ray photons beyond 10 TeV to be observable from cosmological sources, but even the combination of LIV and cosmic voids is insufficient to explain the spectral hardening in the TeV regime seen in several blazars.
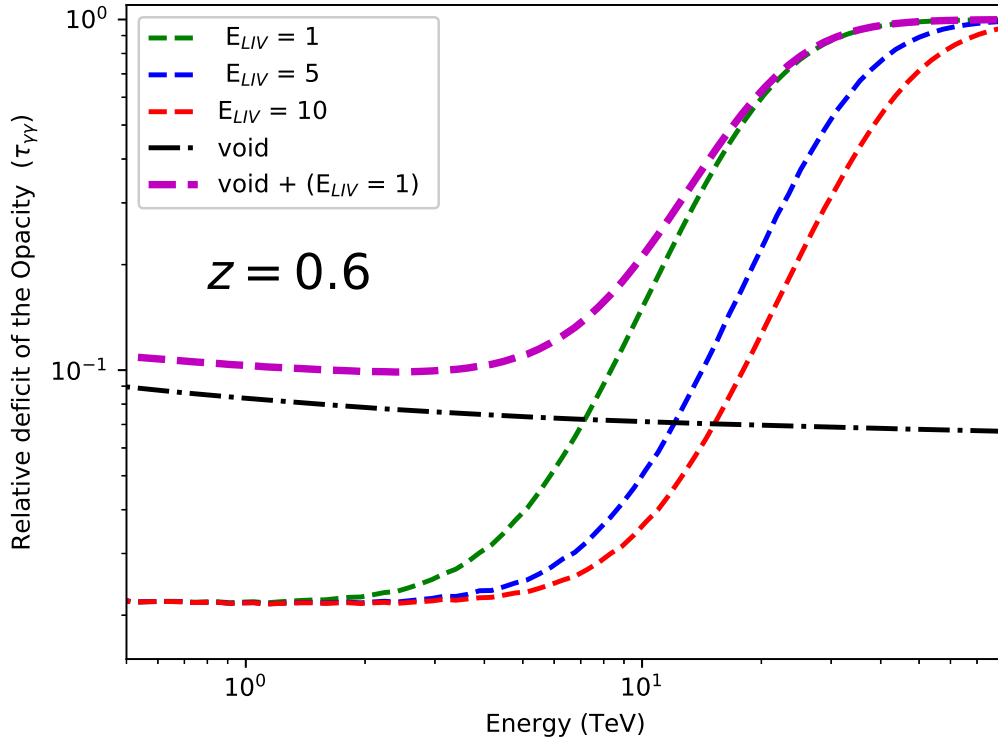
Figure 6: Relativie optical depth $\tau_{\gamma\gamma}$ deficit as a function of energy for VHE-gamma rays that propagate from a source located at redshift $z = 0.6$, using Finke, et al. (2015) [10] EBL model. The black-dashed line represent the case that, the deficit due to that the EBL energy density calculated by considering an accumulation of about 10 voids of typical sizes with radius $R = 100\,h^{-1}$ Mpc centered at redshift $z_v = 0.3$. The green, blue, red lines represent that, the deficit due to the correction from LIV for different values of E_{LIV} in the unit of Planck energy scale ($1.2 \times 10^{19}\,GeV$) and the top dashed line due to the both effects.

5. Summary and Conclusions

We have presented calculations of modifications of the gamma-gamma opacity for VHE γ-ray photons from sources at cosmological distances, due to their interaction with intergalactic radiation fields (EBL) through electron-positron pair production. We evaluated both the effects of cosmic voids along the line of sight and of Lorentz-invariance violating extensions of the standard model. We found that the optical depth deficit for VHE-gamma rays due to the existence of cosmic voids along our line of sight to distant blazars is not enough to explain the unexpected spectral hardening of the VHE spectra of several blazars (e.g. PKS 1424+240).

We found that the optical depth $\tau_{\gamma\gamma}$ deficit due to voids decreases with energy and becomes negligible for VHE gamma-ray photons above ~ 10 TeV. We confirm previous results that the effect of LIV becomes important only at VHE energies above ~ 10 TeV. Even if we consider the combination of both effects (cosmic void along the line of sight and LIV) the reduction of the EBL gamma-gamma opacity is too small to explain the unexpectedly hard VHE gamma-ray spectra of

some blazars. More detailed calculations considering a subluminal and a superluminal modification of the dispersion relation for photons for the LIV effect, by considering $\gamma\gamma$ absorption and also the impact of LIV effect on the Compton scattering process are presented in [30].

The future Cherenkov Telescope Array with its significant sensitivity above 10 TeV will offer the opportunity to test LIV extensions of the standard model due to the resulting reduction of the EBL opacity at those energies, and thus offer an exciting window on fundamental physics [28]. However, the spectral hardening of several observed VHE gamma-ray sources (e.g. blazars) with energy from 300 GeV up to few TeVs (e.g. PKS 1424+240) still remains puzzling. Therefore, other explanations for such hardening must be invoked. One possibility is that this hardening is, in fact, a real, intrinsic feature of the γ-ray spectra of these blazars, possibly due to a pion-production induced cascade component in a hadronic blazar model scenario [31, 32]. If such a spectral hardening is not intrinsic to the source, more exotic explanations, such as ALPs or a cosmic-ray induced secondary radiation component, would need to be invoked.

References

[1] Nikishov, A. I. 1962, Sov. Phys. JETP, 14, 393

[2] Sushch, I. & Böttcher, M. 2015, A & A, 573, A47

[3] Biteau A. & Williams D. A. 2015, ApJ, 812, 1

[4] Hauser, M. G. & Dwek, E. 2001, ARA&A,, 39, 249

[5] Stecker, F. W. 1969, ApJ, 157, 507

[6] Stecker, F. W., de Jager, O. C., & Salamon, M. H., 1992, ApJ, 390, L49

[7] Aharonian F. et al. 2006, Nature, 440, 1018

[8] Franceschini, A., Rodigheiro, G., & Vaccari, M., 2008, A&A, 487, 837

[9] Razzaque S., Demer, C. D., & Finke, J. D., 2009, ApJ, 697, 483

[10] Finke, J. D., Razzaque, S., & Dermer, C. D., 2010, ApJ, 712, 238

[11] Dominguez, A., et a., 2011a, MNRAS, 410, 2556

[12] Gilmore, R. C., Sommerville, R. S., Primack, J. R., & Dominguez, A., 2012, MNRAS, 422, 3189

[13] H.E.S.S. Collaboration: Abdalla, H., et al. 2017 , Astron. Astrophys., 606, A59

[14] Dzhatdoev T.A., et al. 2017, Astron. Astrophys., 603, A59

[15] MAGIC Collaboration: Albert, J., et al., 2008, Science, 320, 1752

[16] Archambault S. et al. 2014, ApJ, 785, L16

[17] Furniss A., et al., 2013, ApJ, 768, L31

[18] Dominguez, A., Sánchez-Conde, M. A., & Prada, F., 2011b, J. Cosmol. Astropart. Phys., 11, 020

[19] Essey W. & Kusenko A. 2010, ApJ, 33, 81

[20] Furniss A., Stutter, P. M., Primack, J. R., & Dominguez, A., 2015, MNRAS, 446, 2267

[21] Kudoda, A. M. & Faltenbacher, A., 2016, PoS, HEASA2015, 20

[22] Abdalla, H. & Böttcher, M., 2017, ApJ, 835, 237

[23] Amelino-Camelia, G., et al. 1998, Nature, 393, 763

[24] Garay, L., J. 1995, Int. J. Mod. Phys. A, 10, 145

[25] Mattingly, D. 2005, Liv. Rev. Relat., 8, 5

[26] Martínez-Huerta, H. & Pẽrez-Lorenzana, A., 2017, Phys. Rev. D95, 063001

[27] Chrétien, M., Bolmont, J., Jacholkowski, A. 2016, ICRC 2015, 34, 764, arXiv: 1509.03545

[28] Fairbairn M. et al. 2014, JCAP, 06, 005

[29] Tavecchio, F. & Bonnoli, G., 2016, Astron. Astrophys., 585, A25

[30] Abdalla, H. & Böttcher, M., 2018, ApJ, 865, 159, arXiv: 1809.00477v1

[31] Böttcher, M., Reimer, A., Sweeney, K., & Prakash, A., 2013, ApJ, 768, 54

[32] Cerruti, M., Zech, A., Boisson, C., & Inoue, S., 2015, MNRAS, 448, 910

Lorentz Invariance Violation Effects on Gamma-Gamma Absorption and Compton scattering

LORENTZ INVARIANCE VIOLATION EFFECTS ON GAMMA-GAMMA ABSORPTION AND COMPTON SCATTERING

Hassan Abdalla[1,2][a] and Markus Böttcher[1][b]

[1]Centre for Space Research, North-West University, Potchefstroom 2520, South Africa

[2]Department of Astronomy and Meteorology, Omdurman Islamic University, Omdurman 382, Sudan

ABSTRACT

In this paper, we consider the impact of Lorentz Invariance Violation (LIV) on the $\gamma - \gamma$ opacity of the Universe to VHE-gamma rays, compared to the effect of local under-densities (voids) of the Extragalactic Background Light, and on the Compton scattering process. Both subluminal and super-luminal modifications of the photon dispersion relation are considered. In the subluminal case, LIV effects may result in a significant reduction of the $\gamma - \gamma$ opacity for photons with energies $\gtrsim 10$ TeV. However, the effect is not expected to be sufficient to explain the apparent spectral hardening of several observed VHE γ-ray sources in the energy range from 100 GeV – a few TeV, even when including effects of plausible inhomogeneities in the cosmic structure. Superluminal modifications of the photon dispersion relation lead to a further enhancement of the EBL $\gamma\gamma$ opacity. We consider, for the first time, the influence of LIV on the Compton scattering process. We find that this effect becomes relevant only for photons at ultra-high energies, $E \gtrsim 1$ PeV. In the case of a superluminal modification of the photon dispersion relation, both the kinematic recoil effect and the Klein-Nishina suppression of the cross section are reduced. However, we argue that the effect is unlikely to be of astrophysical significance.

Keywords: radiation mechanisms: non-thermal — galaxies: active — galaxies: jets — cosmology: miscellaneous — quantum-gravity: Lorentz Invariance Violation (LIV)

1. INTRODUCTION

Recent astronomical observations and laboratory experiments appear to show hints that several phenomena in physics, astrophysics and cosmology oppose a traditional view of standard-model physics (e.g., Riess et al. 1998; Furniss et al. 2013). This has motivated developments of modified or alternative theories of quantum physics and gravitation (e.g., Capozziello et al. 2013; Wanas & Hassan 2014; Nashed & El Hanafy 2014; Arbab 2015; Sami et al. 2018), generally termed *physics beyond the standard model* (e.g., Sushkov 2011; Abdallah et al. 2013; El-Zant 2015).

The special theory of relativity postulates that physical phenomena are identical in all inertial frames. Lorentz invariance is one of the pillars of modern physics and is considered to be a fundamental symmetry in Quantum Field Theory. However, several quantum-gravity theories postulate that familiar concepts such as Lorentz invariance may be broken at energies approaching the Planck energy scale, $E_P \sim 1.2 \times 10^{19} GeV$ (e.g., Amelino et al. 1998; Jacob & Piran 2008; Liberati & Maccione 2009; Amelino 2013; Tavecchio & Bonnoli 2016). Currently such extreme energies are unreachable by experiments on Earth, but for photons traveling over cosmological distances the accumulated deviations from Lorentz invariance may be measurable using Imaging Atmospheric Cherenkov Telescope facilities, in particular the future Cherenkov Telescope Array (CTA) (e.g., Fairbairn et al. 2014; Lorentz & Brun 2017).

[a] hassanahh@gmail.com

[b] Markus.Bottcher@nwu.ac.za

A deviation from Lorentz invariance can be described by a modification of the dispersion relation of photons and elementary particles such as electrons (e.g., Amelino et al. 1998; Tavecchio & Bonnoli 2016). It is well known that the speed of light in a refractive medium depends on its wavelength, with shorter wavelength (high momentum) modes traveling more slowly than long wavelength (low momentum) photons. This effect is due to the sensitivity of light waves to the microscopic structure of the refractive medium. Similarly, in quantum gravity theories, very high energy photons could be sensitive to the microscopic structure of spacetime, leading to a violation of strict Lorentz symmetry. In that case, γ-rays with higher energy are expected to propagate more slowly than their lower-energy counterparts (e.g., Amelino et al. 1998; Fairbairn et al. 2014; Tavecchio & Bonnoli 2016; Lorentz & Brun 2017). This would lead to an energy-dependent refractive index for light in vacuum. Therefore, the deviation from Lorentz symmetry can be measured by comparing the arrival time of photons at different energies originating from the same astrophysical source (e.g., Amelino et al. 1998; Azzam 2009; Tavecchio & Bonnoli 2016; Wei 2017; Lorentz & Brun 2017).

Gamma rays from objects located at a cosmological distance with energies greater than the threshold energy for electron-positron pair production can be annihilated due to $\gamma - \gamma$ absorption by low-energy extragalactic background photons (Nikishov 1962). The intergalactic $\gamma - \gamma$ absorption signatures have attracted great interest in astrophysics and cosmology due to their potential to indirectly measure the Extragalactic Background Light (EBL) and thereby probe the cosmic star-formation history (e.g., Biteau & Williams 2015). The predicted $\gamma - \gamma$ absorption imprints have been studied employing a variety of theoretical and empirical methods (e.g., Stecker 1969, 1902; Hauser & Dwek 2001; Primack et al. 2005; Aharonian et al. 2006; Franceschini et al. 2008; Razzaque et al. 2009; Finke et al. 2010; Dominguez et al. 2011a; Gilmore et al. 2012).

Recent observations indicate that the very-high-energy (VHE; $E > 100$ GeV) spectra of some distant ($z \gtrsim 0.5$) blazars, after correction for $\gamma - \gamma$ absorption by the EBL, appear harder than physically plausible (e.g., Furniss et al. 2013), although systematic studies of the residuals of spectral fits with standard EBL absorption on large samples of VHE blazars (e.g., Biteau & Williams 2015; Mazin et al. 2017) reveal no significant, systematic anomalies on the entire samples. Nevertheless, the unexpected VHE-γ-ray signatures seen in a few individual blazars are currently the subject of intensive research. Possible explanations of this spectral hardening include the hypothesis that the EBL density could be lower than expected from current EBL models (Furniss et al. 2013), an additional γ-ray emission component due to interactions along the line of sight of extragalactic Ultra-high-Energy Cosmic Rays (UHECRs) originating from the blazar (e.g., Essey & Kusenko 2010; Dzhatdoev 2015), the existence of exotic Axion-Like Particles (ALPs) into which VHE γ-rays can oscillate in the presence of a magnetic field, thus enabling VHE-photons to avoid $\gamma - \gamma$ absorption (e.g., Dominguez et al. 2011b; Dzhatdoev et al. 2017), EBL inhomogeneities (e.g., Furniss et al. 2015; Kudoda & Faltenbacher 2016; Abdalla & Böttcher 2017) and the impact of LIV, which can lead to an increase of the $\gamma\gamma$ interaction threshold and thus to a reduction of cosmic opacity (especially at energies beyond ~ 10 TeV), thus allowing high-energy photons to avoid $\gamma - \gamma$ absorption (e.g., Tavecchio & Bonnoli 2016; Abdalla & Böttcher 2018).

In this paper, we discuss the reduction of the EBL $\gamma - \gamma$ opacity due to the existence of underdense regions along the line of sight to VHE gamma-ray sources (including contributions of both the direct star light and re-processed emission to the EBL) and compare the results with the LIV effect on cosmological photon propagation. We consider the LIV effect only for photons, but not for electrons, since the high-energy synchrotron spectrum of the Crab Nebula imposes a stringent constraint on any deviation of the electron dispersion relation from Lorentz invariance (e.g., Jacobson et al. 2003).

LIV may also effect the process of Compton scattering, which is likely to be an important γ-ray production process in many astrophysical high-energy sources, such as accreting black hole binaries, pulsar wind nebulae, the jets from active galactic nuclei, and supernova remnants. In this paper, we discuss, to our knowledge for the first time, the impact of LIV on the Compton scattering process, both on energy-momentum conservation and on the Compton cross section.

In Section 2 we investigate the impact of the existence of cosmic voids along the line of sight to a distant VHE γ-ray source, by using the EBL model devoloped by Finke et al. (2010). In Section 3 we review the impact of LIV on the EBL $\gamma\gamma$ opacity. In Section 4 we investigate LIV effects on the Compton scattering process, starting with

basic conservation of energy and momentum, using the LIV-deformed dispersion relation for photons. The results are presented in Section 5, where we compare our results with predictions from standard quantum electrodynamics (QED). We summarize and discuss our results in Section 6. Throughout this paper the following cosmological parameters are assumed: $H_0 = 70$ km s^{-1} Mpc^{-1}, $\Omega_m = 0.3$, $\Omega_\Lambda = 0.7$.

2. THE IMPACT OF A COSMIC VOID ON THE EBL ENERGY DENSITY DISTRIBUTION

A generic study of the effects of cosmic voids along the line of sight to a distant astronomical object (e.g. blazar) on the EBL $\gamma - \gamma$ opacity has been done in (Abdalla & Böttcher 2017). In that paper, the EBL was represented using the prescription of Razzaque et al. (2009), taking into account only the direct starlight contribution to the EBL. Assuming that a spherical cosmic void with radius R is located with its center at redshift z_v, between an observer and a VHE γ-ray source located at redshift z_s, the angle- and photon-energy-dependent EBL energy density at each point between the observer at redshift zero and the source was calculated. The cosmic void was represented by setting the star formation rate to 0 within the volume of the void. We found that the EBL deficit is proportional to the size of the void. Therefore, the effect of a number n of voids of radius R_1 is aproximately the same as the effect of a large void with radius $R_n = nR_1$.

Since in the Razzaque et al. (2009) prescription, only the direct starlight contribution to the EBL is considered, the work of (Abdalla & Böttcher 2017) under-predicts the EBL $\gamma - \gamma$ opacity for VHE γ-rays with energies of $E \gtrsim 1$ TeV. Such VHE photons preferentially interact with longer-wavelength (IR – FIR) EBL photons, which are dominated by dust re-processing of starlight, which is neglected in Razzaque et al. (2009). To study the impact of a cosmic void on the full EBL spectrum, from far infrared through visible and extending into the ultraviolet, we used the EBL model of Finke et al. (2010), in which stars that evolved off the main sequence and re-emission of absorbed starlight by dust are considered. In all other aspects, we follow the formalism of Abdalla & Böttcher (2017).

One of the most complete public catalogues of cosmic voids Sutter et al. (2012) is based on data from the Sloan Digital Sky Survey (SDSS), with effective radii of voids spanning the range $5 - 135 h^{-1}$ Mpc. Also, there is evidence for a $300 h^{-1}$ Mpc under-dense region in the local galaxy distribution (e.g., Keenan et al. 2013). Recent measurements of optical and NIR anisotropies (e.g., Matsuura et al. 2017), at 1.1 and 1.6 μm, indicate that the resulting amplitude of relative EBL fluctuations is typically in the range of 10 to 30% Zemcov et al. (2014).

The impact of an accumulation of cosmic voids amounting to a total size of radius $R = 1 h^{-1}$ Gpc (where $h = H_0/(100$ km s^{-1} Mpc$^{-1})$) centered at redshift $z_v = 0.3$, is illustrated in Figure 1. The EBL energy density spectrum in the presence of voids (dashed lines) is compared to the homogeneous case (solid lines) at different points (redshifts, as indicated by the labels) along the line of sight in the left panel of Figure 1. The fractional difference between the homogeneous and the inhomogeneous case as a function of photon energy for various redshifts along the line of sight is presented in the right panel of Figure 1. We notice that the EBL deficit is smaller for low-energy (IR) photons than for optical – ultraviolet photons. This is because the UV EBL is dominated by hot, young stars, thus more strongly reflecting the local effect of the void. Since in this work we set only the star formation rate inside the void equal to zero, dust re-processing of star light produced outside the void, still takes place inside the void. As can be seen from Figure 1, with our choice of a void configuration, the impact of underdense regions is comparable to the measured optical and NIR anisotropy Zemcov et al. (2014). The impact of the EBL deficit due to the cosmic voids on the EBL $\gamma - \gamma$ opacity will be presented in Section 5.1.

3. LORENTZ INVARIANCE VIOLATION: COSMIC OPACITY

In this Section we review the imprints of LIV on the cosmic $\gamma - \gamma$ opacity, primarily based on the work by Tavecchio & Bonnoli (2016). The results will be compared to the imprints of EBL inhomogeneities discussed in the previous section. The deviation from Lorentz symmetry can be described by a modification of the dispersion relation of photons and electrons (e.g., Amelino et al. 1998; Tavecchio & Bonnoli 2016):

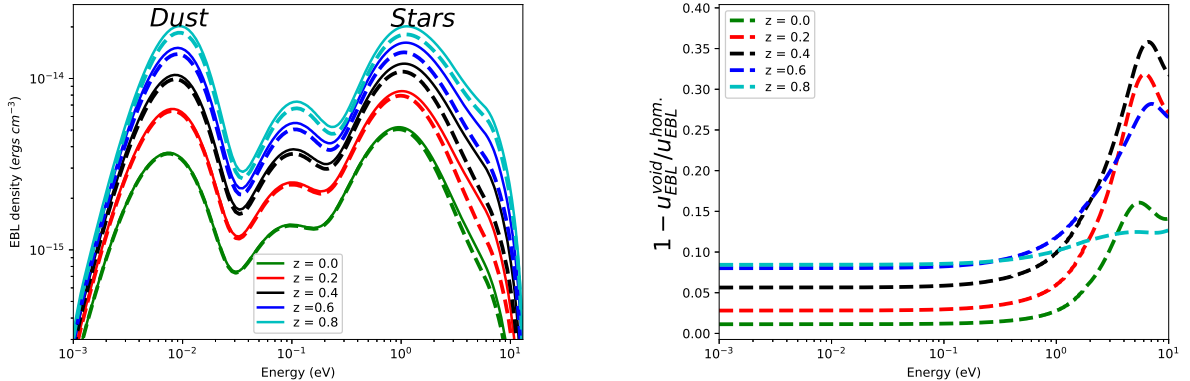$$E^2 = p^2c^2 + m^2c^4 + S\,E^2\left(\frac{E}{E_{LIV}}\right)^n,\tag{1}$$

Figure 1. Left panel: Differential EBL photon energy density as a function of distance (redshift) along the line of sight. The solid lines represent the homogeneous case ($R = 0$), and the dashed lines represent the EBL energy density considering an accumulation of about 10 voids of typical sizes with radius $R = 100\,h^{-1}$ Mpc centered at redshift $z_v = 0.3$. The EBL energy density increases with redshift because of the star formation rate increasing with redshift at low redshifts (e.g., Cole et al. 2001) Right panel: Relativie EBL energy density deficit due to the presence of a void for the same cases as represented in the left panel. U_{EBL}^{void} and U_{EBL}^{hom} are the EBL energy densities considering the cosmic void case and the homogeneous case, respectively. As expected, the maximum EBL energy density deficit occurs around the center of the voids ($z = 0.3$), and the EBL energy density deficit beyond the center of the cosmic voids is greater than the deficit in front of it, comparing points at the same distance from the voids center, due to the star formation rate increasing with redshift.

where c is the conventional speed of light in vacuum, "$S = -1$" represents a subluminal scenario (decreasing photon speed with increasing energy), and "$S = +1$" represents the superluminal case (increasing photon speed with increasing energy). The characteristic energy E_{LIV} is parameterized as a fraction of the Planck energy, $E_{\mathrm{LIV}} = E_P/\xi_n$, where the dimensionless parameter ξ_n and the order of the leading correction n depend on particle type and theoretical framework (e.g., Amelino et al. 1998; Tavecchio & Bonnoli 2016). A value of $E_{LIV} \sim E_P$ (i.e., $\xi_1 = 1$) has been considered to be the physically best motivated choice (e.g., Liberati & Maccione 2009; Fairbairn et al. 2014; Tavecchio & Bonnoli 2016) This is consistent with the results of Biteau & Williams (2015) which constrained $E_{LIV} > 0.65\,E_P$. Some authors (e.g., Schaefer 1998; Billers et al. 1999) argue that the best constraint from current data is $\xi_1 \leq O(1000)$.

In the literature (e.g., Tavecchio & Bonnoli 2016), usually only the subluminal case is considered for the LIV effect on $\gamma\gamma$ absorption, as this is the case that could lead to an increase of the $\gamma\gamma$ interaction threshold and consequently, a decrease of the opacity. In this work, for completeness, we consider both the subluminal and superluminal cases.

Based on the revised dispersion relation (1) with $n = 1$, the modified pair-production threshold energy ϵ_{min} can be written as (e.g., Tavecchio & Bonnoli 2016):

$$\epsilon_{min} = \frac{m^2 c^4}{E_\gamma} - S\,\frac{E_\gamma^2}{4E_{LIV}}. \tag{2}$$

Using equation (2), the target photon energy threshold for pair-production as a function of the γ-ray photon energy for the subluminal and the superluminal cases is illustrated in Figure 2.

Also from equation (1), an effective mass term for photons can be defined as (e.g., Liberati & Maccione 2009; Tavecchio & Bonnoli 2016):

$$(m_\gamma\,c^2)^2 \equiv S\,\frac{E^3(1+z)^3}{E_{LIV}}. \tag{3}$$

Following (Fairbairn et al. 2014; Tavecchio & Bonnoli 2016), we assume that the functional form of the $\gamma - \gamma$ cross section (as a function of the center-of-momentum energy squared s) remains unchanged by the LIV effect, and only the expression for s is modified. The optical depth at the energy E_γ and for γ-ray photons from a source at redshift
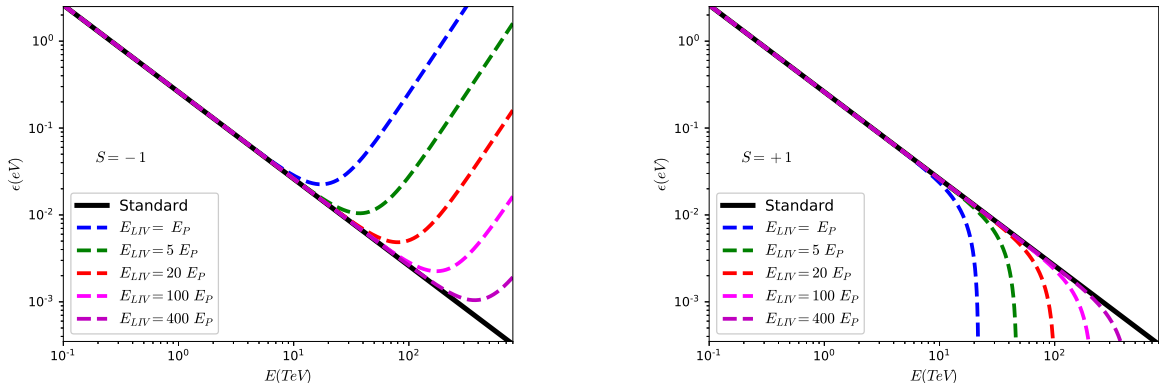
Figure 2. Left panel: Photon target energy at threshold for pair-production as a function of γ-ray photon energy, for the subluminal case. The black solid line represents the case of standard QED and the dashed lines show the LIV-modified threshold for different values of E_{LIV}. Right panel: Same as the left panel, but for the superluminal case.

z_s can thus be evaluated as (Fairbairn et al. 2014; Tavecchio & Bonnoli 2016):

$$\tau_{\gamma\gamma}(E_\gamma, z_s) = \frac{c}{8E_\gamma^2} \int_0^{z_s} \frac{dz}{H(z)(1+z)^3} \int_{\epsilon_{min}}^\infty \frac{n(\epsilon, z)}{\epsilon^2} \int_{s_{min}}^{s(z)_{max}} [s - (m_\gamma c^2)^2]\sigma_{\gamma\gamma}(s)ds, \tag{4}$$

where $H(z) = H_0\sqrt{[\Omega_m(1+z)^3 + \Omega_\Lambda]}$, $s_{min} = 4(m_e c^2)^2$ and $s(z)_{max} = 4\epsilon E_\gamma(1+z) + (m_\gamma c^2)^2$. $n(\epsilon, z)$ is the EBL photon energy density as a function of redshift z and energy ϵ, and $\sigma_{\gamma\gamma}(s)$ is the total pair production cross-section as a function of the modified square of the center of mass energy $s = (m_\gamma c^2)^2 + 2\epsilon E_\gamma(1 - \cos(\theta))$, where θ is the angle between the soft EBL photon of energy ϵ and the VHE γ-ray photon. Obviously, when $E_{LIV} \longrightarrow \infty$, the standard relations are recovered.

By using equation (4) with the EBL model by Finke et al. (2010), we calculate the optical depth for VHE γ-ray photons from a source at redshift 0.6. The comparison with the standard case (homogeneous EBL, no LIV) and with the effect of EBL inhomogeneities (as discused in Section 2) is presented in Section 5.1.

4. LORENTZ INVARIANCE VIOLATION: COMPTON SCATTERING

One of the most important fundamental high-energy radiation mechanisms is Compton scattering, the process by which photons gain or lose energy from collisions with electrons. In the Compton scattering processes, the energy of a scattered photon $E_{\gamma f}$ follows from momentum and energy conservation:

$$\left(E_{\gamma i}/c, \overrightarrow{P}_{\gamma i}\right) + \left(E_{ei}/c, \overrightarrow{P}_{ei}\right) = \left(E_{\gamma f}/c, \overrightarrow{P}_{\gamma f}\right) + \left(E_{ef}/c, \overrightarrow{P}_{ef}\right), \tag{5}$$

which is assumed to still hold even in a Lorentz-invariance violating framework. In Equ. (5), $E_{\gamma i}$, $E_{\gamma f}$ and E_{ei}, E_{ef} are initial and final energies for the photon and electron respectively, and $\overrightarrow{P}_{\gamma i}$, $\overrightarrow{P}_{\gamma f}$ and $\overrightarrow{P}_{ei}$, $\overrightarrow{P}_{ef}$ are initial and final momenta for the photon and electron, respectively. To consider the LIV effect, we consider the first order correction $n = 1$ in the modified dispersion relation (1):

$$E_\gamma^2 = p_\gamma^2 c^2 + S \frac{E_\gamma^3}{E_{LIV}}, \tag{6}$$

As motivated in the introduction, and consistent with our treatment of LIV on the EBL opacity in Section 3, we consider LIV only for photons, not for electrons. Substituting for E_{ef} using the standard electron dispersion relation and momentum conservation (considering that in the electron rest frame, $p_{e,i} = 0$), the energy conservation part of

Equ. (5) can be written as:

$$E_{\gamma f} = E_{\gamma i} + E_{ei} - \sqrt{c^2(p_{\gamma i} - p_{\gamma f})^2 + (m_e c^2)^2}. \tag{7}$$

Squaring and rearranging Equ. (7), expressing all photon momenta in terms of energies using the dispersion relation (6) yields

$$2E_{\gamma i}E_{\gamma f} + 2(E_{\gamma f} - E_{\gamma i})m_e c^2 = S\left(\frac{E_{\gamma i}^3}{E_{LIV}} + \frac{E_{\gamma f}^3}{E_{LIV}}\right) + 2\mu\sqrt{E_{\gamma i}^2 - S\frac{E_{\gamma i}^3}{E_{LIV}}}\sqrt{E_{\gamma f}^2 - S\frac{E_{\gamma f}^3}{E_{LIV}}}. \tag{8}$$

where $\mu = \cos\theta$ is the cosine of the scattering angle in the electron rest frame. In the limit $E_{LIV} \gg E_\gamma$, the square-root expressions in Equ. (8) can be simplified to

$$\sqrt{E_\gamma^2 - S\frac{E_\gamma^3}{E_{LIV}}} \approx E_\gamma\left(1 - S\frac{E_\gamma}{2E_{LIV}}\right). \tag{9}$$

Thus, to lowest order in E_γ/E_{LIV}, Equ. (8) can be written as:

$$2E_{\gamma i}E_{\gamma f} + 2(E_{\gamma f} - E_{\gamma i})m_e c^2 = S\left(\frac{E_{\gamma i}^3}{E_{LIV}} + \frac{E_{\gamma f}^3}{E_{LIV}}\right) + 2\mu E_{\gamma i}E_{\gamma f}\left(1 - S\frac{E_{\gamma i}}{2E_{LIV}} - S\frac{E_{\gamma f}}{2E_{LIV}}\right). \tag{10}$$

Equ. (10) is solved numerically to find the scattered photon energy $E_{\gamma f}$ as a function of initial photon energy $E_{\gamma i}$ and scattering angle $\theta = \cos^{-1}\mu$. Results are presented in Section 5.2.

From QED, the Klein-Nishina cross-section σ_{KN} can be written as:

$$\sigma_{KN} = \int \frac{d\sigma_{KN}}{d\Omega}d\Omega = \int \frac{r_e^2}{2}\left(\frac{E_{\gamma f}}{E_{\gamma i}}\right)^2\left(\frac{E_{\gamma i}}{E_{\gamma f}} + \frac{E_{\gamma f}}{E_{\gamma i}} - \sin^2\theta\right)d\Omega, \tag{11}$$

where $\frac{d\sigma_{KN}}{d\Omega}$ is the differential Klein-Nishina cross section and $d\Omega$ is the solid angle, and r_e is the classical electron radius.

As for our considerations of the LIV effect on the $\gamma - \gamma$ opacity, we assume that the functional dependence of the Klein-Nishina cross section on the incoming and scattered photon energies remains unaffected. Thus, in order to modify the Klein-Nishina cross-section considering the LIV effect, we use the scattered photon $E_{\gamma f}$ from the solution of Equ. (10) in the Klein-Nishina formula (11) and integrate numerically. The results of this integration compared with the standard QED case are presented in Section 5.2.

5. RESULTS AND DISCUSSION

In this section, we present the results for representative test cases for the LIV effect on the cosmic $\gamma - \gamma$ opacity, compared standard Lorentz-invariance case and the suppression of the opacity due to EBL inhomogeneities, and on the Compton scattering process, compared to the standard-model case.

5.1. *EBL Absorption*

To study the opacity or transparency of the Universe to VHE γ-ray photons from distant sources (e.g. blazars) due to their interaction with intergalactic EBL photons, we compare the effects of the EBL inhomogeneities due to the presence of cosmic voids to those of the LIV effect. Figure (3) shows the absorption coefficient $\exp(-\tau_{\gamma\gamma})$ as a function of energy for VHE-gamma rays from a source at redshift $z_s = 0.6$. The standard-model QED case is represented by the black solid line. The impact of an EBL underdensity (for parameters as used in Fig. 1) is illustrated by dot-dashed lines and the LIV effect is represented by dashed lines for different values of the chracteristic LIV energy scale $E_{LIV} = E_P/\xi_1$. Note that the standard case without LIV is recovered for $E_{LIV} \longmapsto \infty$.

The reduction of the EBL $\gamma - \gamma$ opacity due to plausible EBL inhomogeneities is only of the order of $\lesssim 10$ % and decreases with energy. The LIV effect is negligibly small for energies below about 5 TeV, but the cosmic opacity for
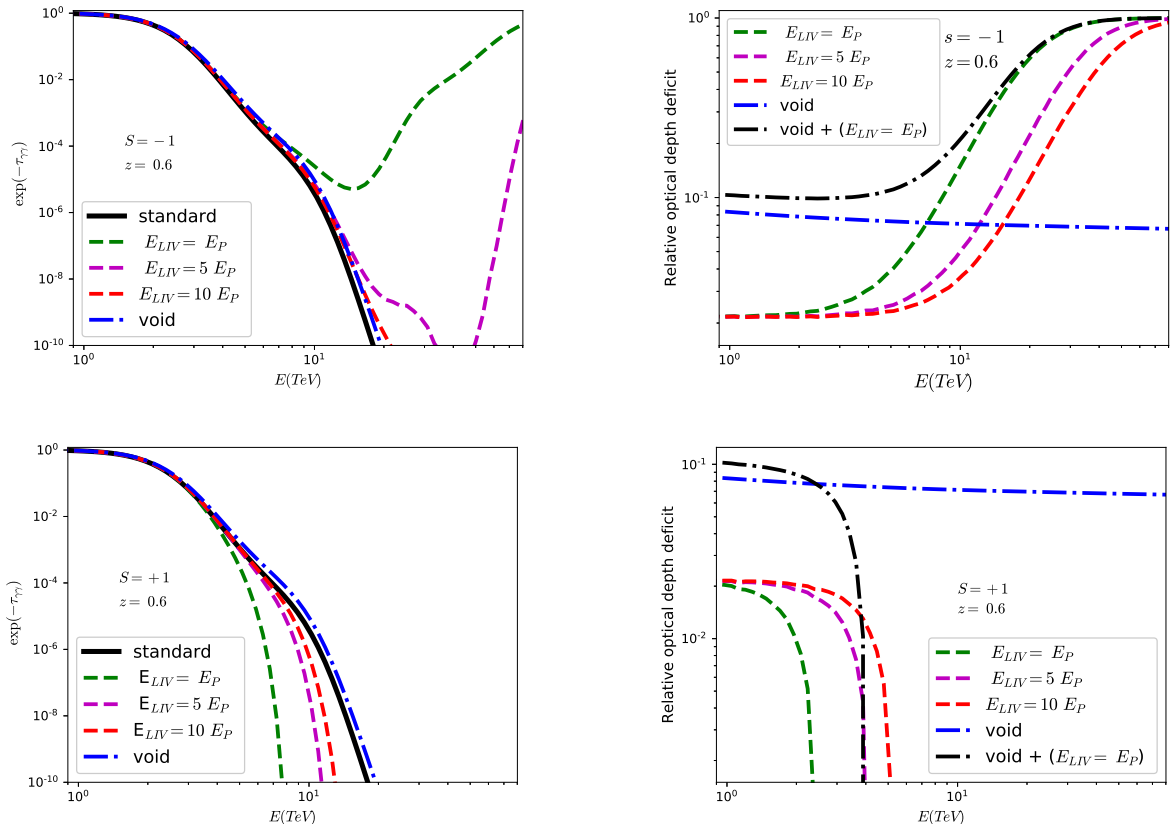
Figure 3. Left panels: Absorption coefficient $\exp(-\tau_{\gamma\gamma})$ as a function of energy for VHE γ-rays from a source at redshift $z_s = 0.6$, using the EBL model of Finke et al. (2010). The black solid line represents the case of standard QED; the dashed lines show the LIV-modified coefficient for different values of E_{LIV}, for the subluminal case (top panel) and the superluminal case (bottom panel). The blue dot-dashed line represents the case of standard QED and EBL energy density calculated by considering an accumulation of 10 voids of typical sizes with radius $R = 100 \, h^{-1}$ Mpc along the line of sight, centered at redshift $z_v = 0.3$. Right panels: Relative optical depth deficit as a function of energy for VHE γ-rays for the same cases as in the left panel. The Relative optical depth deficit is defined as $(1 - \tau_{\gamma\gamma}^{DFS}/\tau_{\gamma\gamma}^{Stand.})$, where $\tau_{\gamma\gamma}^{Stand.}$ represents the optical depth calculated in standard QED and using the homogeneous EBL energy density distribution, and $\tau_{\gamma\gamma}^{DFS}$ represents the optical depth calculated including the effects of cosmic voids (blue dashed-dot line) or of LIV (dashed lines). The black dot-dashed line represents the relativie optical depth deficit due to the combined effect of LIV and EBL inhomogeneities.

VHE γ-rays with energies $\gtrsim 10$ TeV can be strongly reduced for the subluminal case and increased for the superluminal case. Therefore, if LIV is described by the subluminal dispersion relation ($S = -1$), one may expect VHE γ-ray photons beyond 10 TeV to be observable even from distant astrophysical sources.

However, the spectral hardening of several observed VHE gamma-ray sources with energy from 100 GeV up to a few TeV (e.g. PKS 1424+240) still remains puzzling. Compared to the Finke et al. (2010) EBL absorption model for an object at a redshift of $z_s \sim 0.6$, the opacity would have to be reduced by $\gtrsim 60$ % in order to explain the spectral hardening of the VHE spectrum of PKS 1424+240 with standard emission mechanisms. Even if we consider the combined effects of EBL underdensities and LIV, as represented by the solid line in the right panel of Figure (3), the relative optical depth $\tau\gamma\gamma$ deficit is only around 10 % in the energy range from hundred of GeV to a few TeV.
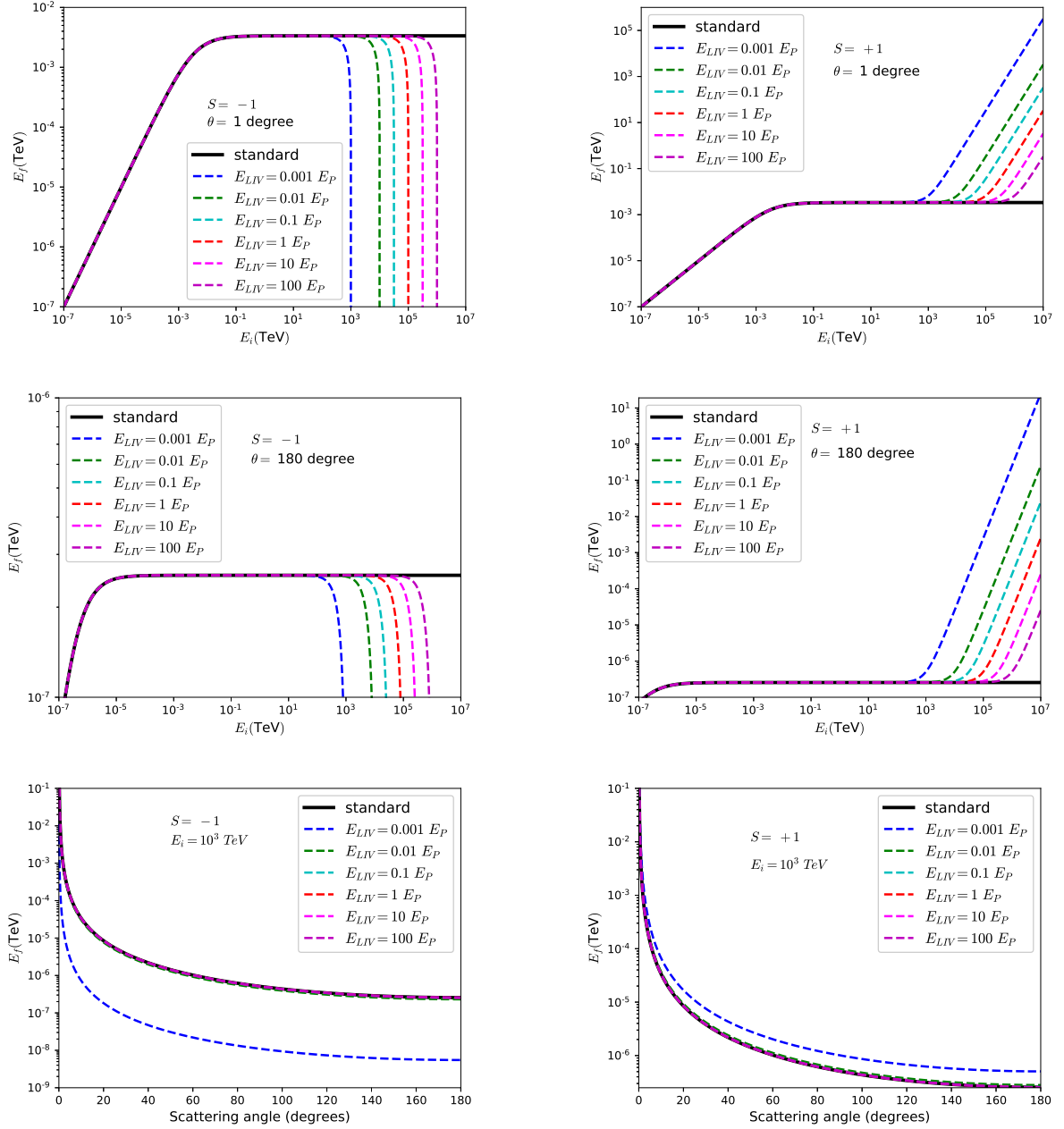
5.2. Compton scattering

Figure 4. Top and middle panels: Scattered photon energies $E_{\gamma,f}$ as a function of incoming photon energy $E_{\gamma,i}$, for scattering angles of 1 and 180 degrees, respectively. The black solid line represents the case of standard QED; the dashed lines show the LIV effect for different values of E_{LIV}, for a subluminal case (left) and superluminal case (right). Bottom panels: Scattered photons energies E_f vs. scattering angle, for an incoming photon energy of $E_i = 1$ PeV in the subluminal case (left) and superluminal case (right). The black solid line represents the case QED; the dashed lines illustrate the LIV effect for different values of E_{LIV}.

The LIV effect on the Compton scattering process has been evaluated as described in Section 4. To assess the importance of LIV signatures, we have evaluated this effect for a large range of values of E_{LIV}. All calculations are done in the electron rest frame.

Figure 4 illustrates the effect of LIV on the scattered photon energies as a function of the incoming photon energies E_i for two representative scattering angles (1 and 180 degrees — top and middle panels) for different values of E_{LIV}, as well as the scattered photon energies as a function of the scattering angle θ for one representative incoming photon energy (10^3 TeV — bottom panels). The subluminal cases are illustrated in the left, the superluminal cases in the right panels. In the standard QED case (black solid curves), the kinematic constraints (recoil) lead to the well-known levelling-off of the scattered photon energies at a value of $E_{\gamma,f} \sim m_e c^2/(1 - \cos\theta)$. In Figure 5 we illustrate the LIV
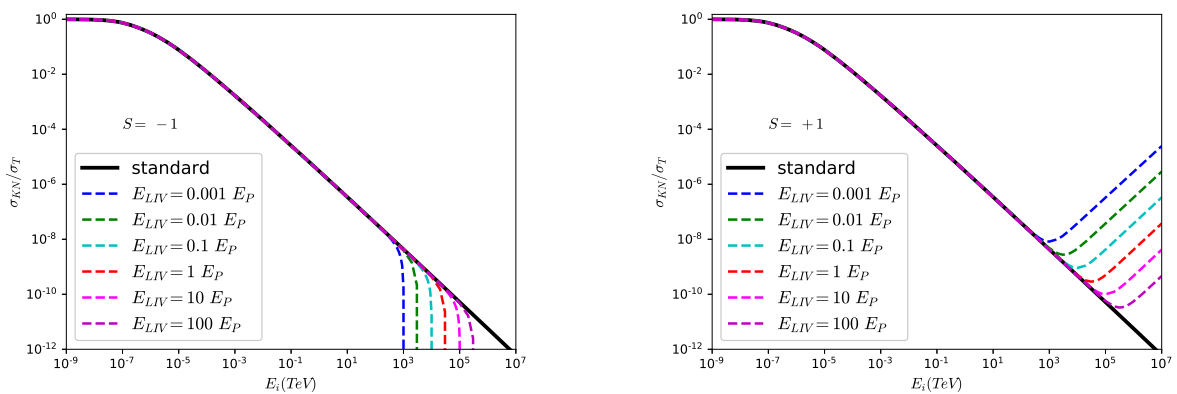

Figure 5. Total Klein-Nishina cross-section σ_{KN} (in the units of σ_T) as a function of the incoming photon energy $E_{\gamma,i}$. The black solid line represents the case of QED; the dashed lines show the LIV-modified Klein-Nishina cross-section for different values of E_{LIV}, for the subluminal (left panel) and superluminal case (right panel).

effect on the total Klein-Nishina cross-section σ_{KN} (in units of σ_T), plotted as a function of the incoming photon energy $E_{\gamma,i}$. The black solid line represents the case of standard QED and the dashed lines show the modified Klein-Nishina cross-section for different values of E_{LIV}, calculated as described in Section 4. Again, the subluminal and superluminal cases are illustrated in the left and right panel, respectively.

From Figures (4) and (5) we see that LIV signatures in the Compton scattering processes are expected to be important only for very large incoming photon energies, $E_{\gamma,i} \gtrsim 1$ PeV. In the superluminal case, the scattered photon energies are larger than expected in the standard case, while in the subluminal case, the scattered photon energies are further reduced. Although the impact of this effect on the scattered photon energy is large for photons with energy $E_{\gamma,i} > 10$ PeV, even in the superluminal case the scattered photon energy $E_{\gamma,f}$ is still much smaller than the incoming photon energy $E_{\gamma,i}$. This indicates that the electron recoil effect is still substantial, as expected, but strongly reduced/increased compared to standard-model kinematics, in the superluminal/subluminal case, respectively. Equally, at energies $E_{\gamma,i} \gtrsim 1$ PeV the Klein-Nishina cross section gradually recovers from the standard-model Klein-Nishina suppression (which sets in at $E_{\gamma,i} \sim m_e c^2$) in the superluminal case, but is expected to remain suppressed to $\sigma_{KN} \lesssim 10^{-6} \sigma_T$ for photon energies below ~ 1 EeV (in the electron rest frame) for any plausible choice of E_{LIV}. In the subluminal case, Compton scattering of photons at energies $E_{\gamma,i} \gtrsim 1$ PeV is expected to be strongly suppressed, far beyond the standard-QED Klein-Nishina suppression.

6. SUMMARY AND CONCLUSIONS

We have presented calculations of the modification of the EBL $\gamma - \gamma$ opacity for VHE γ-ray photons from sources at cosmological distances, by considering two effects: the impact of under-densities (voids) along the line of sight to the source and the LIV effect. For the LIV effect, we considered both a subluminal and a superluminal modification of the dispersion relation for photons. We found that the reduction of the optical depth due to the existence of cosmic voids is insignificant for realistic parameters of the void and is thus insufficient to explain the unexpected spectral hardening of the VHE spectra of several blazars. The effect of LIV becomes important only at γ-ray energies above ~ 10 TeV, where the $\gamma\gamma$ interaction threshold is increased and consequently, the EBL opacity is reduced in the subluminal case. The opposite effect (reduced pair production threshold and increased EBL opacity) results in the superluminal case. The effect is negligible for VHE spectra in the range ~ 100 GeV – a few TeV. However, these results suggest that, if LIV is manifested by a subluminal modification by the photon dispersion relation, VHE γ-ray sources may be detectable at cosmological redshifts $z \gtrsim 1$ at energies $E \gtrsim 10$ TeV, as the EBL opacity at those energies may be greatly reduced compared to standard-model predictions. Observations with the small-size telescopes of the future Cherenkov Telescope Array (CTA: Acharya et al. 2013) — and its predecessors, such as the ASTRI (Astrofisica con Specchi a Technologia Replicante Italiana: Vercellone 2016) array — will provide excellent opportunities to test this hypothesis.

We have presented, to the authors' knowledge for the first time, detailed calculations of the effect of LIV on the Compton scattering process. As for $\gamma\gamma$ absorption, we considered both subluminal and superluminal modifications to the photon dispersion relation. In the superluminal case, we find that for incoming photon energies of $E_{\gamma,i} \gtrsim 1$ PeV in the electron rest frame, both the electron recoil effect and the Klein-Nishina suppression of the scattering cross section are reduced compared to standard-model expectations. This may suggest that Compton scattering at ultra-high energies may overcome the suppression due to the standard Klein-Nishina effect and possibly lead to the production of $>> 1$ PeV photons through inverse Compton scattering. However, it is unlikely that this effect is of relevance to realistic astrophysical environments. Such scattering would require electrons of energies $E_e \gg 1$ PeV. In spite of the recovery at ultra-high energies, the Compton cross section is still suppressed by several orders of magnitude compared to the Thomson cross section. Hence, for any realistic magnetic field value in an astrophysical source, if electrons are actually accelerated to $E_e \gg 1$ PeV, or produced as secondaries in ultra-high-energy muon decay processes, they are likely to lose their energy radiatively via synchrotron radiation rather than Compton scattering. In the subluminal case, both the reduction of scattered photon energies and the Klein-Nishina cut-off of the cross section are further enhanced by the LIV effect, rendering Compton scattering at ultra-high energies even less efficient than due to the standard Klein-Nishina effects.

7. ACKNOWLEDGMENTS

REFERENCES

Abdalla, H. & Böttcher, M., 2017, ApJ, 835, 237

Abdalla, H. & Böttcher, M., 2018, PoS(HEASA2017),028

Acharya, B. S., et al., 2013, Astropart. Phys., 43, 3

Abdallah, W., Delepine, D., Khalil, S., et al. 2013, Phys. Lett., B725, 361

Aharonian, F., Akhperjanian, A. G., Bazer-Bachi, A. R., et al. 2006, Nature, 440, 1018

Amelino-Camelia, G., Ellis, J., Mavromatos, N. E., Nanopoulos, D. V., & Sarkar, S. 1998, Nature, 393, 763

Amelino-Camelia, G. 2013, Living Rev. Rel., 16, 05

Arbab, A.I. 2015, strophys Space Sci, 355, 343

Azzam, W.J., Alothman, M. J., Guessoum, N, 2009, Advances in Space Research, 44, 1354

Biller, S. D., Breslin, A. C, Buckley, J., Catanese, M. & Carson, M. 1999, Phys. Rev. Lett., 83, 2108

Biteau, J. & Williams D. A. 2015, ApJ, 812, 1

Böttcher, M., Reimer, A., Sweeney, K., & Prakash, A., 2013, ApJ, 768, 54

Capozziello, S., Gonzlez, P. A., Saridakis, E. N., & Vsquez, Y. 2013, JHEP, 039, 02

Cerruti, M., Zech, A., Boisson, C., & Inoue, S., 2015, MNRAS, 448, 910

Cole, S., Norberg, P.& Baugh, C., et al. 2001, MNRAS, 326, 255

Dominguez, A., Primack, J. R., Rosario, D. J., et al., 2011a, MNRAS, 410, 2556

Dominguez, A., Sánchez-Conde, M. A., & Prada, F., 2011b, J. Cosmol. Astropart. Phys., 11, 020

Dzhatdoev, T. A., 2015, J. Phys. Conf. Ser, 632, 01

Dzhatdoev, T. A., Khalikov, E. V., Kircheva, A. P. & Lyukshin, A. A., 2017, Astron. Astrophys., 603, A59

El-Zant A., Khalil, S. & Sil, A. 2015, Phys. Rev., D91, 03

Essey W. & Kusenko, A. 2010, ApJ, 33, 81

Fairbairn, M., Nilsson, A., Ellis, J., Hinton, J. & White, R. 2014, JCAP, 1406, 005

February, S., Clarkson, C. & Maartens, R. 2013, JCAP, 1303, 23

Finke, J. D., Razzaque, S., & Dermer, C. D., 2010, ApJ, 712, 238

Franceschini, A., Rodigheiro, G., & Vaccari, M., 2008, A&A, 487, 837

Furniss, A., Williams, D. A., Danforth, C., et al., 2013, ApJ, 768, L31

Furniss A., Stutter, P. M., Primack, J. R., & Dominguez, A., 2015, MNRAS, 446, 2267

Gilmore, R. C., Sommerville, R. S., Primack, J. R., & Dominguez, A., 2012, MNRAS, 422, 3189

Gould, R. J. & Schréder, G. P. 1967, Phys. Rev., 155, 1408

Hauser, M. G. & Dwek, E. 2001, ARA&A, 39, 249

Jacob, U. and Piran, T. 2008, PhRvD, D78, 12

Jacobson, T., Liberati. S. & Mattingly, D. 2003, Nature, 424, 1019

Jones, F. C., 1968, Phys. Rev., 167, 1159

Keenan, R., C., Barger, A., J. and Cowie, L., L. 2013, ApJ, 775, 62

Kudoda, A. M. & Faltenbacher, A., 2016, PoS, HEASA2015, 20

Liberati, S. & Maccione, L., 2009, Ann. Rev. Nucl. Part. Sci., 245, 59

Lorentz, M. & Brun, P. 2017, Proceedings, 6th Roma International Workshop on Astroparticle Physics (RICAP16): Rome, Italy, June 21-24, 136, 03018

Matsuura, S., Arai, T. & Bock, J. J., et al., 2017,ApJ, 839, 7

Mazin, D., Domnguez, A., Fallah, R., V., et al., 2017, AIP Conf. Proc., 1792, 1

Nashed, G. L. & El Hanafy, W., 2014, Eur. Phys. J., C74, 3099

Nikishov, A. I. 1962, Sov. Phys. JETP, 14, 393

Primack, J. R., Bullock, J. S. & Somerville, R. S, 2005, AIP Conf. Proc., 745, 23

Razzaque S., Demer, C. D., & Finke, J. D., 2009, ApJ, 697, 483

Riess, A. G., Filippenko, A. V., Challis, P., et al 1998, Astron. J., 116, 1009

Schaefer, B. E., 1998, Phys. Rev. Lett., 82, 4964

Sami, H., Namane, N., Ntahompagaze, J., Elmardi, M. & Abebe, A. 2018, Int. J. Geom. Meth. Mod. Phys., 15 02

Stecker, F. W. 1969, ApJ, 157, 507

Stecker, F. W., de Jager, O. C., & Salamon, M. H., 1992,ApJ, 390, L49

Sushkov, A. O., Kim, W. J., Dalvit, D. A. R. & Lamoreaux, S. K 2011, Phys. Rev. Lett., 107, 171101

Sutter, P., M., Lavaux, G., Wandelt, B., D. and Weinberg, D., H. 2012, ApJ, 761, 44

Tavecchio, F. & Bonnoli, G., 2016, Astron. Astrophys., 585, A25

Vercellone, S., 2016, in proc. of "Roma International Conference on Astroparticle Physics 2014", EpJ Web of Conf., Vol. 121, id. 04006

Wei, J., Zhang, B., Shao, L., et al. 2017, ApJ, 834, L13

Wanas, M.I. & Hassan, H.A. 2014, Int J Theor Phys, 53, 3901

Zemcov, M., Smidt, J. & Arai, T., et al. 2014, Science, 346, 732

Summary and Conclusions

The propagation of VHE gamma ray photons (VHE; $E > 100$ GeV) over cosmological distances is suppressed by electron-positron pair-production processes with the diffuse EBL. There are many authors who, by using the observation of several blazars, indicated that there is an anomalous transparency for VHE gamma ray photons coming from these blazars.

In this thesis, detailed calculations for the effect of the EBL inhomogeneities and the resulting EBL gamma-gamma absorption for VHE gamma ray photons from objects at cosmological distances are presented in Chapter 3 and Chapter 4. First, we considered the presence of a cosmic void, and for simplicity, we assumed a spherical region in which the local star formation rate is equal to zero. We have used/assumed possible realistic void sizes of $R \lesssim 100 \, h^{-1}$ Mpc (by realistic we mean that there are such possible voids with such sizes available in catalogs, such as the Sloan Digital Sky Survey (SDSS) catalog). The EBL energy density even at the centre of the under-dense region (void) is reduced by less than 10%. We found that even if the void is located right in front of the gamma ray source, the gamma-gamma opacity is reduced by typically less than 1%. By comparing with linear scaling of the EBL gamma-gamma opacity with the line of sight galaxy number density suggested by Furniss et al. (2015) for the specific case of PKS 1424+240 using the same size of the void ($R = 50 \, h^{-1}$ Mpc), we found that this reduction is quite smaller than that obtained by Furniss et al. (2015). After that, we investigated the effect of the existence of multiple voids instead of one single void, and specifically we assumed an accumulation of about 10 voids with typical radii $R = 100 \, h^{-1}$ Mpc centred at redshift $z_v = 0.3$ along the line of sight to an object (e.g. a blazar) located at redshift

$z_v = 0.6$. A more detailed discussion regarding the possibility of multiple voids was presented in Chapter 4. In Chapter 3 and Chapter 4 we illustrated that the inferred spectral hardening of the VHE gamma ray spectrum for blazars (e.g. PKS 1424+240), after correction for the EBL gamma gamma absorption, is most likely not an artifact of an over-estimation of the EBL gamma-gamma opacity due to the possible cosmic inhomogeneities. The calculations of the inhomogeneous EBL energy density in Chapter 3 and Chapter 4 are based on a modified version of the formalism presented in (Razzaque et al. 2009) considering only the direct starlight.

In the paper presented in Chapter 5 we considered the possibility of a Lorentz Invariance Violation (LIV) signature compared with the possibility of the reduction of the EBL gamma-gamma absorption due to the existence of voids along the line of sight to distant VHE gamma ray sources. By using the full EBL spectrum which is proposed by Finke et al. (2010) instead of only the stellar light EBL component (Razzaque et al. 2009) and because we are interested in the VHE gamma ray photons around and beyond TeV energies, photons with energy $\gtrsim 500$ GeV are expected to annihilate due to their interaction with the far infra-red photons. Therefore, gamma-gamma opacity calculations using only the stellar component of EBL are less reliable (Razzaque et al. 2009). By using the full EBL spectrum, we have presented calculations of the modification of the EBL gamma-gamma opacity for VHE gamma ray photons from sources at high red-shift, considering two effects: the effect of under-dense EBL energy density distribution (voids) along the line of sight to the source and the impact of the LIV effect. For the LIV effect, we confirmed previous results that the effect of the LIV becomes important only at energies above ~ 10 TeV and we found that the optical depth deficit due to voids decreases with energy and becomes negligible for VHE gamma ray photons above ~ 10 TeV. Even considering the combination of both effects, cosmic voids along the line of sight and the LIV effect, the reduction of the EBL gamma-gamma opacity is too small to explain the unexpectedly hard VHE gamma ray photons of several blazars.

In the paper presented in Chapter 6, for completeness, we assumed both a subluminal and a superluminal modification for the photons dispersion relation and for the first time, we presented detailed calculations by considering the LIV effect on the Compton scattering process. As for gamma-gamma opacity, we assumed both subluminal and superluminal cases. We found that the impact of the LIV effect becomes important only at gamma ray photons with energies above ~ 10 TeV, where the gamma-gamma interaction threshold is increased and consequently, the absorption due to the EBL is reduced in the subluminal scenario. The opposite effect (reduced pair production threshold and opacity due to increased EBL) results in the superluminal scenario. However, these results suggest that, if the LIV effect is manifested by a subluminal modification, VHE gamma ray sources may be detectable at high redshifts and energies $E \gtrsim 10$ TeV, as the EBL opacity at those energies may be greatly reduced compared to standard QED predictions. Therefore, observations with the future Cherenkov Telescope Array

(see e.g., Acharya et al. 2013) and its predecessors, such as the ASTRI (Astrofisica con Specchi a Technologia Replicante Italiana Vercellone, 2016) array could provide excellent opportunities to test this hypothesis.

For the Compton scattering process, we found that for incoming photon with energies $E_{\gamma,i} \gtrsim$ 1 PeV in the electron rest frame, both the electron recoil effect and the Klein-Nishina cross-section suppression are reduced compared to standard QED, which may suggest that Compton scattering at ultra-high energies may overcome the suppression due to the standard Klein-Nishina effect and may lead to the production of $>>$ 1 PeV photons due to the inverse Compton scattering process. However, it is unlikely for this effect to be compatible with realistic astrophysical environments, since such scattering would require electrons with energies $E_e \gg$ 1 PeV. In spite of the recovery at ultra-high energies, the Compton scattering cross-section is still suppressed by many orders of magnitude compared to the Thomson scattering cross-section. Hence, for any possible realistic magnetic field value in an astrophysical object, if the electrons can be accelerated to $E_e \gg$ 1 PeV, or produced as secondaries (e.g. muon decay processes at ultra-high-energy), they are likely to lose their energy radiatively via synchrotron emission rather than due to the Compton scattering process. In the subluminal case, both the reduction of scattered photon energies and the Klein-Nishina cut-off of the cross-section are further enhanced by the impact of the LIV effect, rendering the Compton effect at ultra-high energies even less efficient than the case of the standard Klein-Nishina effects.

Overall, we can conclude that the spectral hardening feature in PKS 1424+240 and a few other VHE gamma ray blazars (with photon energies $\sim$ 100 GeV up to a few TeV) remain, even by jointly considering possible EBL inhomogeneities and the LIV effect. Therefore, other explanations for such hardening must be found. One possibility is that this hardening is a real, intrinsic feature of the gamma ray spectra of these blazars, possibly due to a pion-production induced cascade component in a hadronic blazar scenario (see e.g., Böttcher et al. 2013; Cerruti et al. 2015). If a spectral hardening for such energies is not intrinsic to the source, more exotic explanations, such as Axion Like Particles (ALPs) or the possibility of a cosmic-ray-induced secondary radiation component, would need to be found.

References

Acharya, B. S., et al., 2013, Astropart. Phys., 43, 3

Böttcher, M., Reimer, A., Sweeney, K., & Prakash,A., 2013, ApJ, 768, 54, arXiv: 1304.0605

Cerruti, M., Zech, A., Boisson, C., & Inoue, S., 2015, MNRAS, 448, 910

Furniss A., Stutter, P. M., Primack, J. R., & Dominguez, A., 2015, MNRAS, 446, 2267

Razzaque S., Demer, C. D., & Finke, J. D., 2009, ApJ, 697, 483

Vercellone, S., 2016, in proc. of Roma International Conference on Astroparticle Physics 2014, EpJ Web of Conf., Vol. 121, id. 04006

Appendix

UNIVERSITEIT VAN DIE VRYSTAAT
UNIVERSITY OF THE FREE STATE
YUNIVESITHI YA FREISTATA
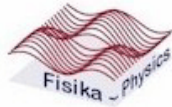
Department of Physics

⊠ P.O. Box 339, Bloemfontein 9300, Republic of South Africa
▣ http://www.ufs.ac.za/
▤ +27(0)51 401 3507 Tel: 051-4012321

Proceedings of HEASA2017   3 November 2018

To whom it may concern

This letter serves to confirm that the Proceedings of the **5th Annual Conference on High Energy Astrophysics in Southern Africa (HEASA2017)**, which took place at the University of the Witwatersrand (Wits) in Johannesburg (South Africa) during 4-6 October 2017 will be published in the online journal **Proceedings of Science** (ISSN 1824-8039) at https://pos.sissa.it. The papers to be published in the proceedings have been subjected to a blind-fold review process by peers and as a result these papers should be considered as **"refereed conference proceedings publications."**

Yours sincerely

Prof P.J. Meintjes
Chief Editor: HEASA2017 Proceedings
University of the Free State
Tel: +2751 401 2191
Fax:+2751 401 3507
e-mail: MeintjPJ@ufs.ac.za

On behalf of the Editorial Board of the HEASA 2017 Proceedings

Prof. Markus Boettcher (Northwest University)
Prof. Soebur Razzaque (University of Johannesburg)
Dr. David Buckley (South African Astronomical Observatory)
Prof. Sergio Colafrancesco (University of the Witwatersrand)
Prof. Andrew Chen (University of the Witwatersrand)
Prof. Nukri Komin (University of the Witwatersrand)